Measurements using top quark pairs with CMS at the LHC

D. Cano Fernández[1], A Castro[2], C Ciocca[2], J Cuevas Maestro[3], M Davids[4], J D'Hondt[5], M Duda[4], I. González Caballero[1], J Heyninck[5], S Kasselmann[4], S Lowette[5], F Palla[6], D Tornier[4], R Vilar[1], J Vizán[3], M Vos[6]

[1] IFCA (CSIC-U. Cantabria), Spain
[2] Dipartimento di Fisica, Universitá degli Studi di Bologna, Italy
[3] University of Oviedo, Spain
[4] RWTH Aachen, III Physikalisches Institut B, Physikzentrum-RWTH Aachen, D-52056 Aachen, Germany
[5] Vrije Universiteit Brussel (IIHE-VUB), Pleinlaan 2, B-1050 Brussels, Belgium
[6] INFN Sezione di Pisa, Italy

E-mail: jodhondt@vub.ac.be

Abstract.

This note describes the selection and reconstruction of top-quark pair events with the CMS detector at the LHC, and the determination of the top-quark mass. All three main channels, classified by the decay of the W boson arising in top-quark decay, are considered here: di-leptonic, semi-leptonic and fully hadronic $t\bar{t}$ events. The performance of the selections, the resulting cross section measurements, and the mass reconstruction accuracy are evaluated based on a detailed simulation of the CMS detector.

1. Introduction

At the Large Hadron Collider (LHC) protons will be collided to obtain a centre-of-mass energy of 14 TeV. Relative to the Tevatron proton-anti-proton collisions at 1.96 TeV the production cross-section of $t\bar{t}$ events in Next-to-Leading Order at the LHC is significantly increased to about 800 pb [1]. The larger cross section, together with the foreseen increased instantaneous luminosity, results in a much larger sample of $t\bar{t}$ events will be collected at the LHC. During the first year of running an integrated luminosity of 10 fb^{-1} will be collected and result in the production of about 8 million $t\bar{t}$ events. Therefore the LHC experiment can be considered as a real top-quark factory compared to the few hundreds of events collected at the Tevatron.

This note describes the selection and reconstruction of top-quark pair events with the CMS detector at the LHC, and the determination of the top-quark mass. All three main channels, classified by the decay of the W boson arising in top-quark decay, are considered here: di-leptonic, semi-leptonic and fully hadronic $t\bar{t}$ events. The performance of the selections, the resulting cross section measurements, and the mass reconstruction accuracy are evaluated based on a detailed simulation of the CMS detector, based on the GEANT-4 program [9, 10, 11].

The simulated events used in this note were generated using PYTHIA 6.2. Additional events were generated with the AlpGen program, and passed through a fast detector simulation [12]. The studies presented in this note are focused on the low-luminosity phase of LHC ($2 \cdot 10^{33} cm^{-2} s^{-1}$); during this phase an average of 3.5 minumum bias events are expected to be superimposed to the main collision (*pile-up*). These events were added to the main process following a Poisson distribution.

The leading-order cross section for $t\bar{t}$ production at the LHC is 488 pb, while the next-to-leading order including the resummation of Sudakov logarithms is 830 pb. Since the simulation of both signal and background event samples is to leading order, the corresponding leading-order cross sections are used throughout. Luminosities in a range of up to several tens of 1 fb^{-1} are considered.

The following sections present the details on cross section and mass estimators applied in the di-lepton channel (Section 2), the semileptonic channel (Section 3) and the fully hadronic channel (Section 4). Summary and conclusions are given in Section 5.

2. Di-Leptonic Top-Pair Events

The di-lepton decay channel denotes the case where the two W bosons from the decaying top-quark pair both decay to final states containing an electron or a muon, accounting for about 5% of all $t\bar{t}$ SM decays. Measuring the rate of the reaction $pp \to t\bar{t} \to b\ell^+\nu_\ell \bar{b}\ell'^-\bar{\nu}_{\ell'}$ tests both the production and decay mechanisms of the top quark.

These events are characterised by two high-energy leptons, two jets from the hadronisation of the b quarks, and large missing energy from the two unobserved neutrinos. Additional jets are often produced by initial-state and final-state radiation.

In general, the reconstruction and selection of di-lepton $t\bar{t}$ events is based on reconstructing the directions and energies or momenta of isolated electrons, muons and jets, and on reconstructing the missing transverse energy $\not{E}_{\mathrm{T}}$ from the transverse momentum balance in the event. The purity of the event samples is enhanced by identifying jets that originated from a b quark (b tagging), since in the Standard Model every $t\bar{t}$ event contains two b jets.

2.1. Simulated samples

Samples of simulated events, for the signal and main backgrounds, were produced using the full CMS software chain. It starts by generating events with `CMKIN` using `PYTHIA` 6.2, followed by detector simulation `OSCAR` [10] and reconstruction [11]. Low-luminosity pile-up collisions (with an instantaneous luminosity of $2 \cdot 10^{33}$ cm^{-2}s^{-1}) from minimum bias events were added to each of the events and were simulated and reconstructed using the same chain. The signal sample consists of about one million simulated $t\bar{t}$ di-lepton events. A sample of about three million $t\bar{t}$ inclusive events was also used. Background samples of diboson (WW, WZ, and ZZ) + jets of about 10^5 events were considered. Finally samples of size varying between 10^5 and 4×10^5 of Z+jets events simulated in different bins of p_T of the Z boson were used.

2.2. Event Selection

In this section we present a di-lepton selection optimized for high luminosities, of the order of 10 fb^{-1}. The selection of events in this channel requires after trigger selection the presence of two oppositely charged leptons with $E_{\mathrm{T}} > 20$ GeV in the pseudorapitity ranges $|\eta| < 2.4$ and $|\eta| < 2.5$ for muons and electrons, respectively, if a third lepton pass these selection criteria, the two with highest E_{T} are kept.

The main backgrounds with a final state mimicking the signal are Z production accompanied by jets and di-boson production with jets. Misidentified leptons and leptons from b-jets in $t\bar{t}$ events represent another important and, after cuts, dominating background. Here, dilepton events with W bosons decaying into τ-leptons are considered signal events if the τ's decay leptonically.

This work uses muons from the CMS "Global Muon Reconstructor" [4]. Muon reconstruction is seeded by the four candidates found by the Level 1 muon trigger.

A "forward" Kalman-filter technique is used, moving from the inner muon chambers to the outer muon chambers, followed by a "backward" Kalman-filter (moving outside to inside). The track is extrapolated to the nominal interaction point and a vertex constrained fit is performed. Next, the track is extrapolated to include hits in the silicon and pixel trackers. The list of final muon candidates is then made by cutting on the χ^2 of each trajectory. The selected candidates are then refitted, excluding hits with high residual values in muon stations with high occupancy. More details may be found in [4]. Cosmic-ray muons are removed by timing cuts.

A primary electron in CMS is composed of a single track emerging from the interaction vertex and matched to an electromagnetic supercluster. Electron and photon showers deposit their energy in several crystals in the ECAL. Approximately 94% of the incident energy of a single electron or photon is contained in 33 crystals, and 97% in 55 crystals. Summing the energy measured in such fixed arrays gives the best performance for unconverted photons, or for electrons. Because of the strong magnetic field the energy reaching the calorimeter is spread in ϕ. The spread energy is clustered by building a cluster of clusters, a "supercluster," which is extended in ϕ [22].

Electrons are required to have a ratio between the energies in the hadronic and electromagnetic calorimeter below 0.05, and a ratio between the energy in the electromagnetic calorimeter and the track momentum has to be in the range $(0.8, 3)$. The HLT trigger [23] is based on the presence of $\mathbf{1}\mu$ **or** $\mathbf{1}e$ which cover with high efficiency all the possible final states in this channel. Selection thresholds used in HLT are tightened in the offline lepton selection. Figure 1 shows the muon and electron spectra after applying these selections, comparing the generated and reconstructed distributions. The reconstruction efficiency is good, both for muons and electrons. More than 97% of the generated muons are correctly reconstructed in the considered range, as well as 90% of the electrons with p_{T} above 20 GeV/c.

An electron is considered isolated if the total measured E_{T} of the jets within a cone $\Delta R \leq 0.3$, minus the lepton E_{T}, is $< 30\%$ of the lepton E_{T}. In a similar way a muon is considered isolated, if the sum of the p_{T} of all the tracks present in a cone of $\Delta R \leq 0.3$ minus p_{T} of the μ is less than 2 GeV/c. Figure 2 shows the distribution of these variables for muon and electrons. Here, negative values occur due to the different resolutions of the subdetectors involved in measuring electrons and tracks.

Candidate events must have $\not\!\!E_{\mathrm{T}} > 40$ GeV. The analysis requires at least two jets with uncorrected $E_{\mathrm{T}} > 20$ GeV detected within $|\eta| < 2.5$, where a jet is defined as a fixed-cone cluster with a cone size of $R = 0.5$. Jets produced by electrons are discarded before applying the previous selection by removing those which have an electromagnetic supercluster within $\Delta R = 0.2$ with a ratio between the electromagnetic energy of that supercluster and the uncorrected jet energy above 0.75.

Using these selection cuts, the efficiency at generator level is about 20% and a similar value is obtained at reconstruction level as shown in table 1.

	Signal	τ	WW	WZ	ZZ	Z+jets	other $t\bar{t}$
Before selection	24.3	30.4	7.74	0.89	0.11	3912	438
L1 + HLT	19.4	15.1	4.4	0.37	0.07	657	92
2 jets $E_{\mathrm{T}} > 20$ GeV	11.5	9.8	0.6	0.012	0.006	23.9	73.1
$\not\!\!E_{\mathrm{T}} > 40$ GeV	9.6	8.1	0.5	0.01	0.003	5.8	53.6
2 opposite charged leptons	3.2	0.42	0.04	0.001	0.001	1.17	0.12
b-tag of 2 highest E_{T} jets	1.12	0.15	0.002	$\sim 10^{-4}$	$\sim 10^{-5}$	0	0.05

Table 1. Cumulative effect of the different selection criteria applied to the simulated $t\bar{t}$ e-μ di-lepton sample and simulated backgrounds. The column denoted as τ corresponds to a $t\bar{t}$ dilepton sample in which at least one W decays into a τ lepton. Numbers correspond to **LO** accepted cross-sections in pb.

2.2.1. Background estimation The dominant backgrounds to dilepton $t\bar{t}$ events can be divided into two main categories:

a) Physics backgrounds, i.e. , those who have real leptons, real $\not\!\!E_{\mathrm{T}}$ and jets originating from initial or final state radiation, arising mainly from diboson (WW, WZ, and ZZ) + jets production. This category also contains the background coming from top quark decays, either from the semileptonic channel or from tau decays. This kind of backgrounds are expected to be determined using MC simulation.

b) Instrumental backgrounds, characterized in general by their large cross-sections but not having significant $\not\!\!E_{\mathrm{T}}$, among them are: Drell-Yan ($Z/\gamma^{\star} \to \ell^{+}\ell^{-}$) production, "fake" leptons in $W \to \ell\nu$ + jet events where a jet is falsely reconstructed as a lepton candidate. It is harder to estimate their contribution to the final sample using MC simulation, then it will be estimated using real data.

2.2.2. b-tagging In a $t\bar{t}$ event two genuine jets arise from the hadronisation of b quarks. Thus b-tagging techniques are used to further suppress backgrounds in which no jets from b-quarks are present. The technique used is based on the explicit reconstruction of a secondary vertex (SV) in a jet [2]. Several variables, like the mass of the charged particles associated to the vertex and the distance between the positions of primary and secondary vertices, are combined into a single quantity computed for every jets in an event. The distribution of this variable for the three possible types of jet categories, no reconstructed SV, pseudo SV (tracks with significant impact parameter but no reconstructed SV), and reconstructed SV, as defined in [2], is used to tag jets as coming from a b-quark. Candidate events must have at least a value of 1 in each of the two jets selected.

2.2.3. Selection efficiency and cross-section determination After this selection an efficiency of 5% is obtained, with a very high rejection of all the backgrounds considered at the level of 10^{-3} or better, as shown in table 1. A S/B value of 5 is obtained, the

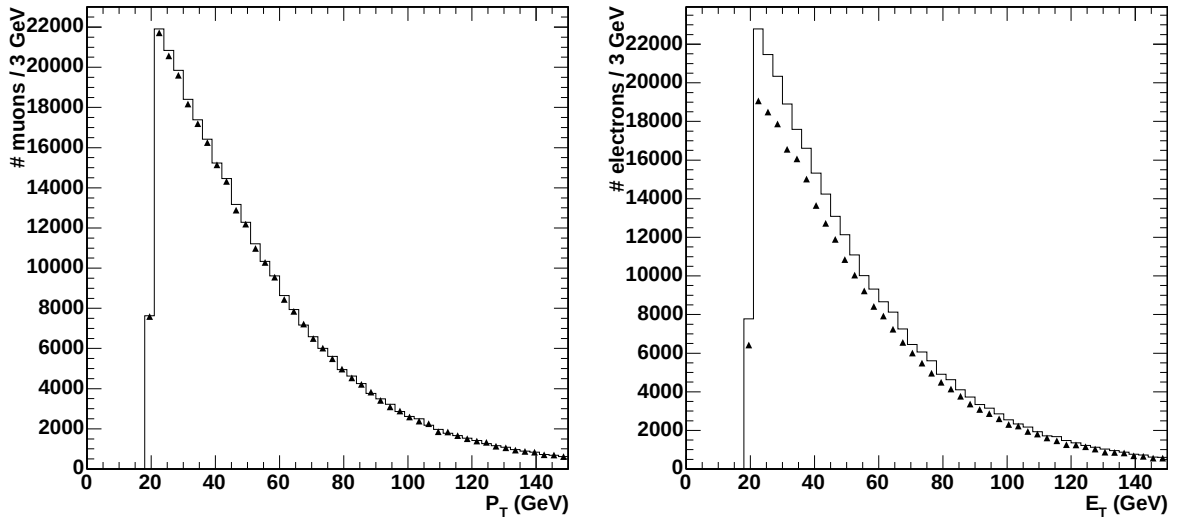

Figure 1. Left: distribution of reconstructed μ p_{T} (dots) in signal events compared with respect to the generated values (solid histogram) for μ selected after a p_{T} cut of 20 GeV/c. Right: distribution of reconstructed electron p_{T} (dots) in signal events compared with respect to the generated values (solid histogram) for electron selected after a p_{T} cut of 20 GeV/c.

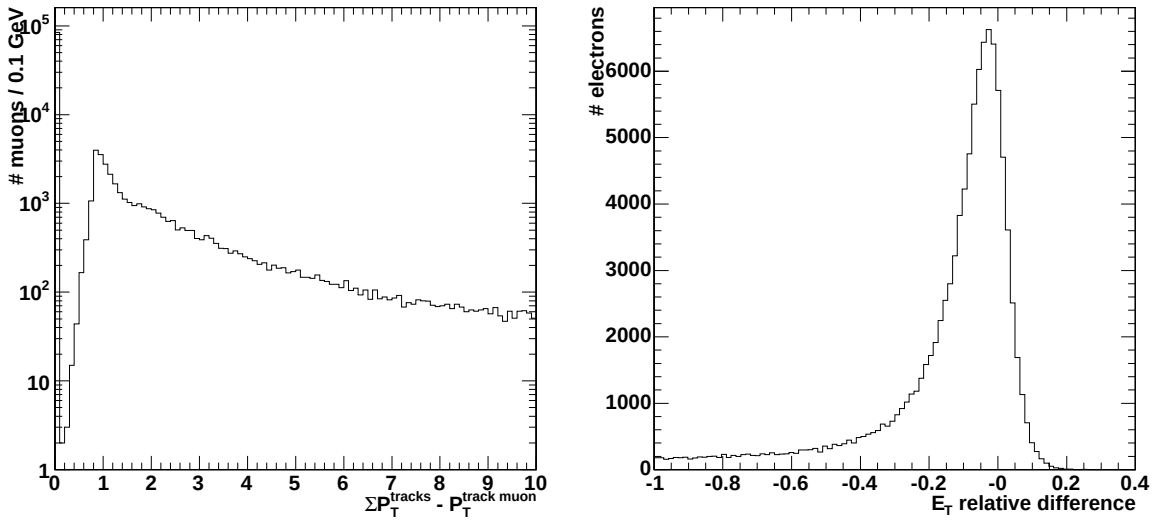

Figure 2. Distribution of variables used in μ (left) and e (right) isolation as described in the text.

main background being the one arising from the dilepton channel in which at least one of the W decays into $\tau\nu_\tau$ and the τ decays leptonically. Events selected in this way are used to determine the total $t\bar{t}$ cross-section.

2.2.4. Systematic uncertainties Different sources of systematic uncertainties are identified that affect event selection and background determination and thus the cross-

section measurement: ISR, FSR, parton distribution functions, b-quark fragmentation, jet energy calibration, lepton identification and isolation, b-tagging efficiency, etc. Detailed studies of these sources have been done based mainly on the results of the studies performed in [4] and [3]. The uncertainty in the amount of initial and final state radiation has been estimated using samples generated with Pythia and simulated and reconstructed with the CMS fast simulation and reconstruction program. Different samples of 2×10^5 events were simulated and reconstructed. In those samples Λ_{QCD} and Q^2_{max} were varied in their recommended range. Their values were controlled by the Pythia parameters $PARP(61)$, $PARP(72)$ and $PARJ(81)$, which were varied in the ranges 0.15 to 0.35 and $PARP(67)$ and $PARP(71)$ which were modified in the ranges 0.25 to 0.4 and 1 to 16 respectively. The uncertainty in the cross-section was taken as coming from the difference in the number of observed events in the samples with the largest difference in the parameters, leading to a 2.5% relative uncertainty in the final value of the cross-section. The uncertainty in the jet energy scale is one of the most important contributions to the determination of the $t\bar{t}$ cross-section determination. The heavy quark jet energy scale has been varied by a value of $\alpha = 3\%$ modifying the reconstructed momenta using the formula $p^{\mu,jet}_{scaled,\pm\alpha} = (1 \pm \alpha)\ p^{\mu,jet}_{unscaled,\pm\alpha}$ for values of the reconstructed p_{T} higher than 50 GeV/c, and varying linearly from 10% to 3% for p_{T} values ranging from 20 to 50 GeV/c. The relative uncertainty in the cross-section due to this effect has been estimated to be a 3.6% relative value. The effect due to the systematics on $\not\!\!E_{\mathrm{T}}$ has been estimated using a 5% uncertainty in this quantity, that leads to a relative 1.1% uncertainty in the cross-section estimation. The effect due to the uncertainty in b-tag efficiency has been estimated by varying the values of the jet b-tag combined variable by a value of 4% and 5% in the barrel ($|\eta| < 1.5$) and endcaps ($|\eta| > 1.5$) according to the estimations given in [4] for an integrated luminosity of 10 fb^{-1} leading to a 3.8% relative uncertainty in the cross-section estimation. Values of 1% and 0.5% have been conservatively taken as uncertainties coming from electron and muon reconstruction and identification, leading to a 1.6% relative uncertainty in the cross-section estimation. Most of the estimations above are statistically dominated. Checks have been done on events selected with looser selection criteria to increase the confidence on these estimations. Other systematic effects have been studied, as in the case of ISR and FSR mainly using samples generated with the CMS fast simulation program, according to the suggestions given in [3]. Among them, we have considered the following effects. Taking a 30% difference between samples with and without in-time pile-up for the low luminosity regime ($\mathcal{L} = 2 \times 10^{33}$ cm^{-2} s^{-1}) leads to a 3.6% relative uncertainty in the cross-section value. The Underlying Event description has been studied by simulating samples with different values of the color screening cut-off parameter, that correspond to the $PARP(82)$ value in the Pythia generator. This value has been varied in the range 2.4 to 3.4 leading to a 4.1% relative uncertainty in the cross-section. The uncertainty coming from hadronization and fragmentation was estimated by varying the Lund b parameter and σ_q. Samples were simulated with values of $PARJ(42)$ and $PARJ(21)$ within 2σ values of the OPAL central data,

leading to a relative uncertainty in the cross-section of 5.1%. Uncertainties arising from PDFs were studied with CTEQ 6M using a reweighting routine that leads to a 5.2% uncertainty in the cross-section determination. The statistical uncertainty in the cross-section determination is about 0.9% for 10 fb^{-1} integrated luminosity. Finally the uncertainty in the cross-section coming from the luminosity estimation was taken as 3% as expected for 10 fb^{-1} integrated luminosity. These numbers lead to

$$\Delta\sigma_{t\bar{t}\ dil\ e/\mu}/\sigma_{t\bar{t}\ dil\ e/\mu} = 11\%\ \text{(syst.)} \pm 0.9\%\ \text{(stat.)} \pm 3\%\ \text{(luminosity)}$$

and are summarized in table 2.

Effect	$\Delta\sigma_{t\bar{t}\ dil\ e/\mu}/\sigma_{t\bar{t}\ dil\ e/\mu}$
ISR and FSR	2.5%
Jet Energy Scale	3.6%
b-tag efficiency	3.8%
lepton reconstruction	1.6%
$\not{E}_{\text{T}}$	1.1%
Pile-Up	3.6%
Underlying Event	4.1%
heavy quark fragmentation	5.1%
PDF uncertainties	5.2%
Statistical uncertainty	0.9%
Integrated luminosity	3%

Table 2. Uncertainties in the $t\bar{t}$ dilepton cross-section determination

2.3. Event Selection for 1 fb^{-1}

For an integrated luminosity of 1 fb^{-1} about 54000 signal events are expected according to the leading-order estimate of PYTHIA.

Events are required to pass the Level-1 and High Level Trigger, in particular the single and di-lepton subtriggers. In addition to trigger criteria, events must contain at least two jets and two oppositely charged leptons. Electrons are identified using an electron likelihood method combining various electromagnetic shower variables, i.e. the energy distribution in the electromagnetic calorimeter cells and the ratio of deposited energy in the electromagnetic and hadronic calorimeter, and track-energy matching criteria. After this preselection about 15000 signal events are left with a signal over background ratio of $S : B = 1 : 10$. The most important background at this stage consists of Z+jets production with an accepted cross section of about 120 pb and similar final state.

Further cuts are applied to specifically reduce the number of Z+jets events as well as the contribution of the other $t\bar{t}$ channels. To reduce the background from misidentified

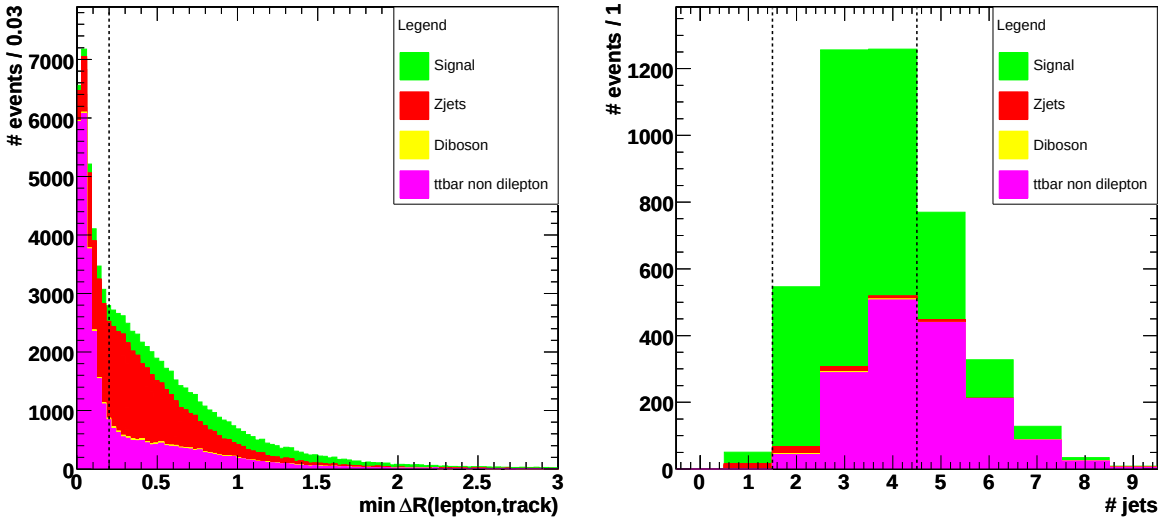

Figure 3. Left: Cut on the minimal distance in ΔR between the lepton candidate and the closest nearby track. Right: All cuts applied, except a cut on the number of jets with p_{T} greater than 30 GeV/c. Both plots are scaled to 1 fb^{-1}

leptons and leptons in b-jets, a lepton will be rejected if it does not satisfy track or calorimeter isolation criteria. The track isolation, as illustrated in figure 3 requires no tracks with significant transverse momentum (more than 10% if the lepton p_{T}) in a $\Delta R < 0.2$ cone around the lepton candidate. The required two charged leptons are then chosen with a discriminant based on the likelihood ratio in case of an electron, the energy deposited in a cone of $\Delta R = 0.2$ around the lepton axis and the p_{T} of the lepton.

Both b-jets are selected with a discriminator based on the jet p_{T}, the invariant mass of tracks inside the jet and the btag-value [2]. Using this scheme both the jets and leptons of the signal are selected with a purity (in case there is an object reconstructed) of more than 90%. It has been shown in reference [2] that, during the *first data taking phases* of the LHC, the degradation in b-tagging performance is still acceptable. This implies that the b-tagging results presented here remain essentially correct.

The Z mass peak of the invariant mass distribution of two same type leptons is used to remove the contamination due to Z+jet events, as is the requirement for positive btag discriminator values of the two selected jets. The non-dilepton $t\bar{t}$ events usually contain more jets with a p_{T} greater than 30 GeV/c but do not contain two high p_{T} leptons. The second lepton candidate is considerably softer than the corresponding lepton from the signal decay channel. So a cut on the lower transverse momentum lepton is imposed with $p_{\mathrm{T}} > 20$ GeV/c. These cuts are illustrated in the right hand plot of figure 3 and in the plots of figure 4.

The two neutrinos in the decay of the Ws lead to significant missing transverse energy (MET) whereas the decay of Zs into electrons or muons does not generate MET. So a cut on MET to be greater than 40 GeV improves the signal to background ratio.

After cuts about 1800 signal events are left with a signal over background ratio of

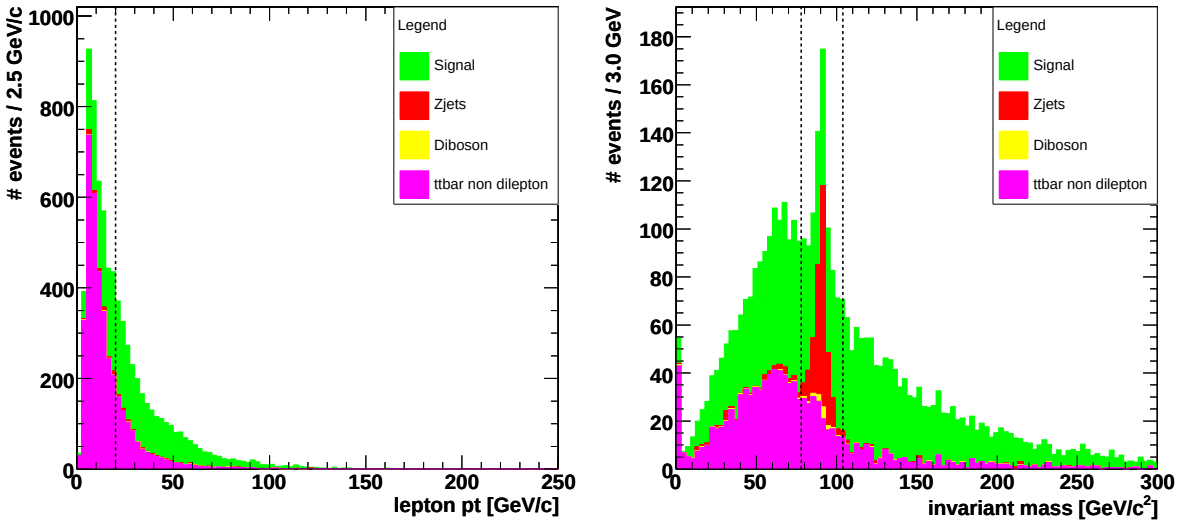

Figure 4. Left: Distribution of the lepton p_T after applying all cuts but the second (lower) lepton p_T cut. Right: Distribution of the invariant mass of the two selected leptons. Vertical lines indicate the window where the Z mass veto is applied.

	$t\bar{t}$ dilept	other $t\bar{t}$	Z + jets	ZZ	ZW	WW	$S:B$
Before selection	54.22	433.78	11055.30	11.10	0.89	7.74	0.005
L1	45.06	302.34	2967.13	3.09	0.49	6.06	0.014
HLT	36.41	184.43	2007.67	1.55	0.39	4.96	0.017
2 jets	25.92	151.23	194.73	0.45	0.04	0.91	0.075
2 leptons	14.96	24.95	123.26	0.20	0.02	0.24	0.101
isolated leptons	9.60	4.22	48.33	0.10	0.01	0.13	0.182
2 bjets	5.30	3.13	2.55	0.02	0.0005	0.01	0.928
lepton inv. mass	4.46	2.88	0.55	0.004	0.0001	0.01	1.292
lepton pt cut	3.07	0.62	0.34	0.003	0.0001	0.01	3.151
$\not{E}_{\mathrm{T}}$ cut	2.30	0.43	0.05	0.001	0.0001	0.01	4.748
# high p_{T} jet cut	1.85	0.21	0.03	0.001	0.00004	0.007	7.332
kinematical reco.	0.66	0.05	0.002	< 0.001	< 0.00004	< 0.007	12.167

Table 3. Selection cuts for the signal and considered background samples. All numbers represent the cumulative accepted cross sections in pb and can be scaled with a factor of 1000 to get the expected number of events in 1/fb.

7.33 : 1 as shown in table 3.

The kinematics of the $t\bar{t}$ dilepton events yield an underconstrained equation system due to the two undetected neutrinos in the final state. However if all other kinematic quantities have been measured it is possible to make a fit imposing m_W and assuming a top mass parameter in the range of 100 to 300 GeV/c^2. A weight can then be assigned to the different solutions obtained (see section 2.4). The event topology of most of the background events passing the previous cuts does not satisfy the dilepton kinematical

constraints. Therefore the actual computation of a mass estimate in the range of 100 to 300 GeV/c^2 further reduces the background and raises the signal over background ratio to about $S : B = 12.2 : 1$ as can be seen in the last line of table 3 and in figure 5.

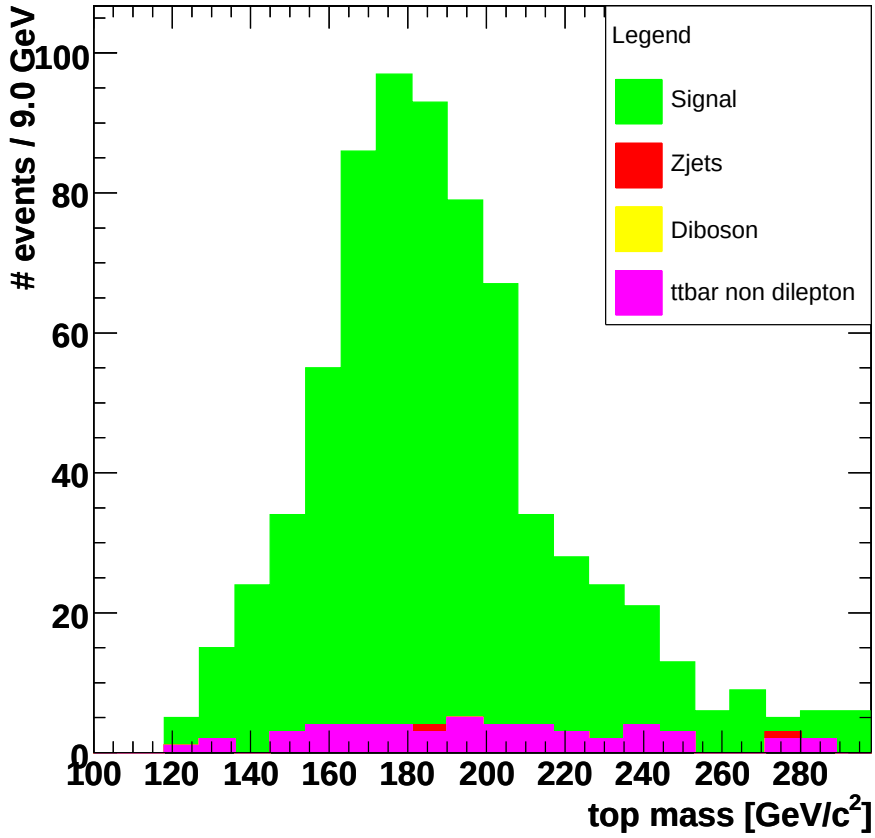

Figure 5. Most Likely top mass after selection for 1 fb^{-1}.

2.4. Kinematical event reconstruction

The $t\bar{t}$-system can be reconstructed from the visible final state particles and either the predicted standard model neutrino energy spectrum or the knowledge of the top mass itself. The event kinematics consist of four equations from the invariant masses of the decaying top quarks (eq. 1 and eq. 2) and W-bosons (eq. 3 and eq. 4). Assuming momentum conservation in the transverse plane neglecting ISR or initial transverse momentum of the partons two more equations can be added to the equation system (eq. 5 and eq. 6).

$$m_t^2 = (E^{l^+} + E^{\nu} + E^{b})^2 - \sum_i (p_i^{l^+} + p_i^{\nu} + p_i^{b})^2 \quad (1)$$

$$m_{\bar{t}}^2 = (E^{l^-} + E^{\bar{\nu}} + E^{\bar{b}})^2 - \sum_i (p_i^{l^-} + p_i^{\bar{\nu}} + p_i^{\bar{b}})^2 \quad (2)$$

$$m_{W^+}^2 = (E^{l^+} + E^{\nu})^2 - \sum_i (p_i^{l^+} + p_i^{\nu})^2 \quad (3)$$

$$m_{W^-}^2 = (E^{l^-} + E^{\bar{\nu}})^2 - \sum_i (p_i^{l^-} + p_i^{\bar{\nu}})^2 \quad (4)$$

$$0 = p_x^{l^+} + p_x^{l^-} + p_x^{b} + p_x^{\bar{b}} + p_x^{\nu} + p_x^{\bar{\nu}} \quad (5)$$

$$0 = p_y^{l^+} + p_y^{l^-} + p_y^{b} + p_y^{\bar{b}} + p_y^{\nu} + p_y^{\bar{\nu}} \quad (6)$$

Six components of the neutrino momenta are unknown and likewise the top mass in case of a top mass measurement. Nevertheless the equation system can be simplified to a single fourth order polynomial in one of the unknown neutrino components (eq. 7). Its coefficients depend on the visible particles momenta and the top mass.

$$0 = \sum_{i=0}^{4} c_i(M_t, p^{l\pm}, p^{b}, p^{\bar{b}})(p_x^{\bar{\nu}})^i \quad (7)$$

Assuming a value for the top mass as a parameter of the polynomial it can be solved up to a fourfold ambiguity. All other values can then be computed from one of the solutions.

With the knowledge of the top mass and perfect choice, i.e. direct comparison of the up to four different solutions with the MC generator neutrino four momenta, the correlation between generated MC data and the kinematical reconstruction is about 95% (see left hand plot in figure 6). The correlation is not 100% due to neglected ISR and top width effects.

To measure the top mass the event can be kinematically reconstructed by varying the top mass parameter in the polynomial in an interval, e.g. stepping through an interval from 100 GeV to 300 GeV/c^2 in 1 GeV/c^2 steps and weighting of the different (up to four times two hundred) solutions. The solvability, i.e. the probability normalised to the number of events to find at least one real solution to the polynomial depends on the assumed top mass parameter (see right hand side of figure 6). Below a value equal to the W mass the solvability equals zero, since the equation system assumes a real W boson from the top decay.

2.5. Mass determination

The different kinematically possible neutrino solutions from the kinematical equation system are weighted using Standard Model predictions for the energy spectra of the neutrino and antineutrino. These spectra have been computed for every top mass parameter in the range of 100 GeV/c^2 to 300 GeV/c^2 in 1 GeV/c^2 steps corresponding

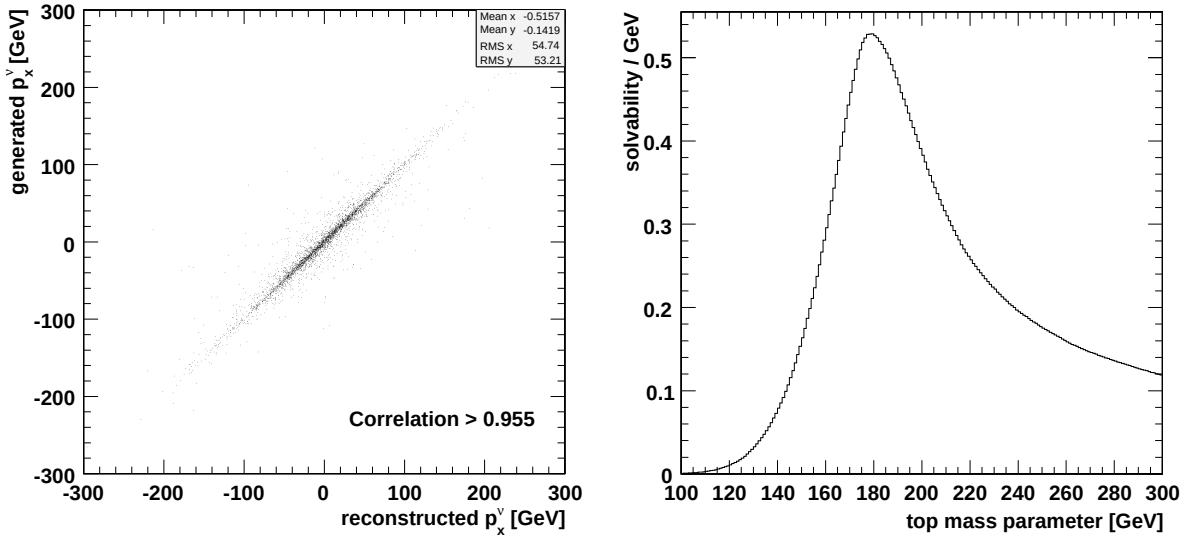

Figure 6. Left: generated neutrino p_x versus reconstructed neutrino p_x. Right: Solvability of the kinematic equation system (both plots use generator level data with $m_t = 175$ GeV/c^2).

to the parameter choices when stepping through the interval. The neutrino solution with the highest weight is chosen and the appropriate top mass of this solution is then the most probable top mass for the examined event.

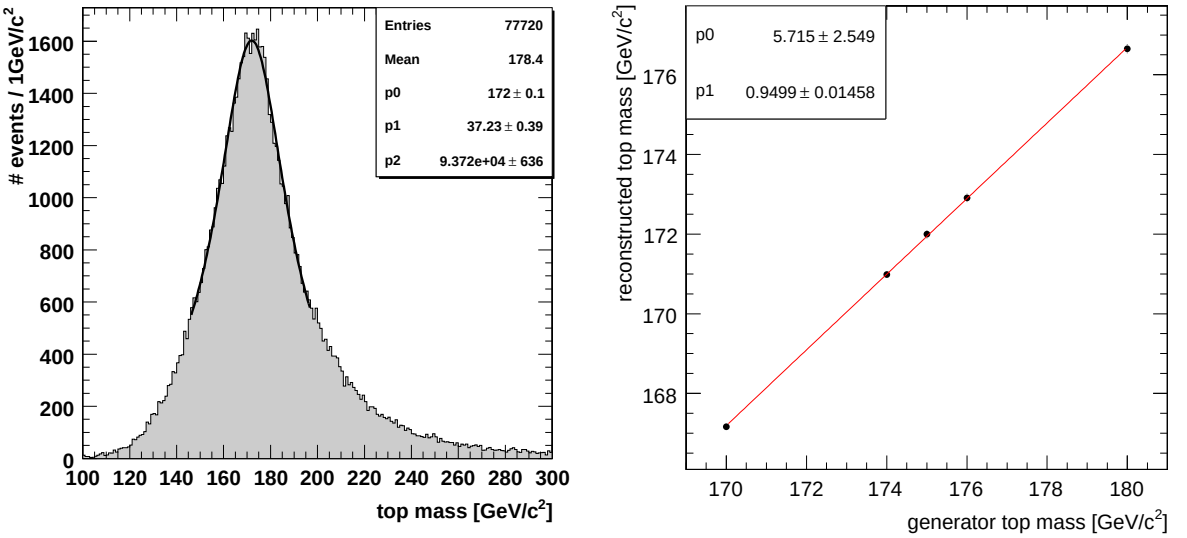

Figure 7. Left: Most likely top mass (generator level; the fit parameter $p0$ corresponds to the mean value whereas $p1$ is the full width at half maximum). Right: Correlation between MC top mass and most likely top mass (generator level)

The distribution of these most probable top masses for a sample of generated top pair decays yields the most likely top mass (see figure 7 left). Using samples generated with a different top mass the correlation between the reconstructed mass and

the generator mass can be plotted (see figure 7 right) resulting in a linear correlation.

Applying the same method for detector simulated and reconstructed events selected with the cuts from section **??** gives an estimator for the top mass in the dilepton channel. For 1 fb^{-1} a Gaussian fit to the signal in a range corresponding to bins with contents above 40% of the maximum yields

$$m_t = (178.5 \pm 1.5)\ \mathrm{GeV}/c^2$$

as illustrated in figure 8 for an input top mass of 175 GeV/c^2. The remaining background is essentially flat as shown in figure 5 and does not affect the mass determination significantly.

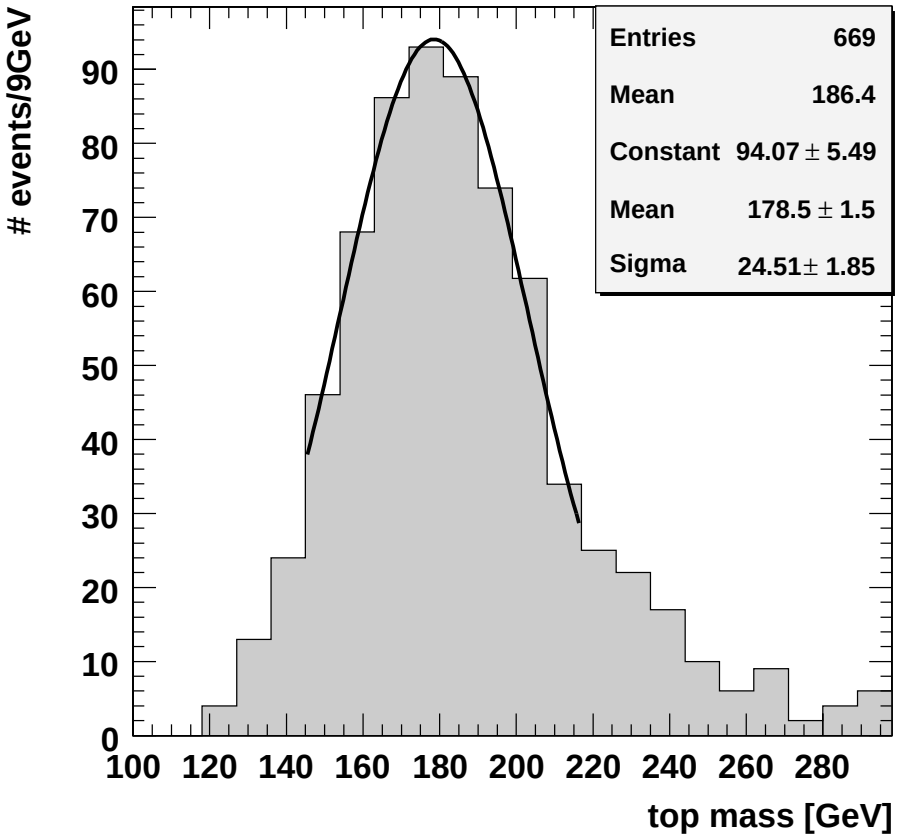

Figure 8. Most Likely top mass after full simulation, reconstruction and selection for 1 fb^{-1} (signal only).

2.5.1. Systematics The main systematic uncertainties on the mass determination in the dilepton channel are due to the approximations used in the kinematic fit and detector effects.

Initial and final state radiation effects modify the kinematics of the process, e.g. the transverse momentum of the $t\bar{t}$ system. This has a direct influence on the solvability of

the equation system described in section 2.4 and on the neutrino solutions obtained from it. We estimate a systematic shift on the top mass of $\Delta m_t = 0.3$ GeV/c^2, following the suggestions of reference [3]. The zero width approximation for both the W bosons and the top quarks in the equation system gives rise to another shift of about 0.1 GeV/c^2.

The most important source of systematic uncertainty arises from uncertainties on the jet energy scale. The expected error after startup (using source calibration and test beam data) is a shift of 15% independent of jet p_{T}. The corresponding top mass shift amounts to $\Delta m_t = 4.2$ GeV/c^2 for integrated luminosities up to 1 fb^{-1}. With better calibration (γ+jet and W fit from the other $t\bar{t}$ channels, see section 2.2.4) this error does reduce to 2.9 GeV/c^2 in a $1 - 10$ fb^{-1} measurement. Further improvements in the knowledge of the jet energy scale (e.g. Z+jet calibration) are expected to lead to a shift of about 1 GeV/c^2 after 10 fb^{-1} integrated luminosity.

In summary, an early top mass measurement in the dilepton channel will be dominated by jet energy scale uncertainties. Already for an integrated luminosity of 1 fb^{-1} the statistical error will be half of the systematic one.

2.6. Top decays in tau leptons

Final states with τ leptons were the subject of dedicated studies. In about 21% of the $t\bar{t}$ events, at least one W boson decays into a τ final state. Depending on its decay, the τ lepton can be identified as a narrow jet, an isolated track, or an electron or muon. Two high-energy b jets, missing transverse energy, and the decay products from the second W boson complete the event topology. Di-leptonic $t\bar{t}$ decays with one tau lepton decaying into hadrons in the final state are considered here $t\bar{t} \rightarrow \mathrm{b\bar{b}}\tau\nu_\tau\ell\nu_\ell$, $(\ell = \mathrm{e}, \mu)$. The primary aim of the analysis is to make a first observation of the final state, containing at least a τ lepton. This will allow lepton universality in the whole top decay process to be tested. Measuring the ratio $BR(t\bar{t} \rightarrow \ell\tau)/BR(t\bar{t} \rightarrow \ell\ell)$ will allow new limits on the presence of non-standard physics in this process to be set. This channel has a special relevance for being not only a source of background for Supersymmetry and Higgs searches, but also for the other dileptonic top channels.

Top candidates with τ are selected and identified following the method described in ref [5], adapting the different selection criteria to the momentum range in which τ candidates are expected to be produced in top decays. All tracks with $p_{\mathrm{T}} > 5$ GeV/c are taken as seed tracks except those corresponding to reconstructed electrons. These tracks are marked as seeds if a jet is within the matching cone of $\Delta R = 0.1$ Then, centered on the seed track all tracks with $p_{\mathrm{T}} > 1$ GeV/c are counted in the signal cone which has $\Delta R < 0.09$. Finally, centered on the jet axis tracks in an isolation cone of $\Delta R < 0.3$ are counted. Objects reconstructed in this way are considered as τ candidates if the number of tracks in both countings are the same, i.e. , there is no other track between the signal cone and the isolation cone. Candidates where all tracks have the same electric charge or which have only two tracks are removed as in these cases it is not possible to determine the charge of the reconstructed τ correctly. The hadronic

Cut	Efficiency × cross sections (pb)			
	tt (signal)	tt(other dilepton)	tt (semileptonic)	tt (hadronic)
All	15.62	38.94	218.88	218.88
Trigger	8.61	25.40	85.90	2.08
2 jets	6.97	18.90	80.08	2.04
≥ 1 Iso lepton	4.27	13.11	34.93	0.11
$\not{E}_{\mathrm{T}} \geq 40$ GeV	3.58	10.89	26.41	0.05
1 lepton	3.48	6.73	25.24	0.04
τ candidate opp. Q	0.75	0.20	0.75	0.001
b-tagging	0.29	0.07	0.30	0.0005

Table 4. Cumulative effect of the different τ selection criteria applied to simulated $t\bar{t}$ sample. Numbers correspond to accepted **LO** cross-sections.

Cut	Efficiency × cross sections (pb)				
	WW (incl)	Z+jets (lept)	ZW	QCD(80-120)	QCD(120-170)
All	69.69	1533	26.69	$2.66 \cdot 10^6$	$470.2 \cdot 10^3$
Trigger	39.52	559.24	10.99	7980.00	1410.60
2 jets	24.65	125.18	4.77	5506.20	1116.74
≥ 1 Iso lepton	4.89	62.89	0.57	38.90	17.72
$\not{E}_{\mathrm{T}} \geq 40$ GeV	3.54	17.60	0.32	11.57	6.12
1 lepton	3.31	11.08	0.28	10.97	5.61
τ candidate opp. Q	0.14	0.91	0.011	0.20	0.11
b-tagging	0.006	0.03	0.0002	0.00	0.00

Table 5. Cumulative effect of the different τ selection criteria applied to simulated backgrounds. Numbers correspond to accepted **LO** cross-sections.

tau identification efficiency extracted from the di-lepton samples is about 30% using this method as can be seen in figure 9. The variation with p_{T}, and η of the fraction of correct assignments of reconstructed τ candidates with respect to generated τ within the di-lepton sample is shown in figure 10

The τ candidates reconstructed as described above are used to select $t\bar{t}$ events decaying into dileptons in which one of the leptons is a τ decaying hadronically and the other lepton in the final state is an electron or a μ. The selection proceeds in a similar way as in the dilepton case. The events are selected by requiring the presence of at least two uncalibrated jets with $p_{\mathrm{T}} > 20$ GeV/c and $|\eta| < 2.5$. , at least one isolated lepton (electron or μ), selected as described in 2.2, sufficient missing transverse energy, and only one isolated lepton. One isolated tau candidate separated from the isolated lepton has to be present, and the isolated lepton and the tau candidate must have opposite charges. The effect of these selection criteria are described in detail for the $t\bar{t}$ sample

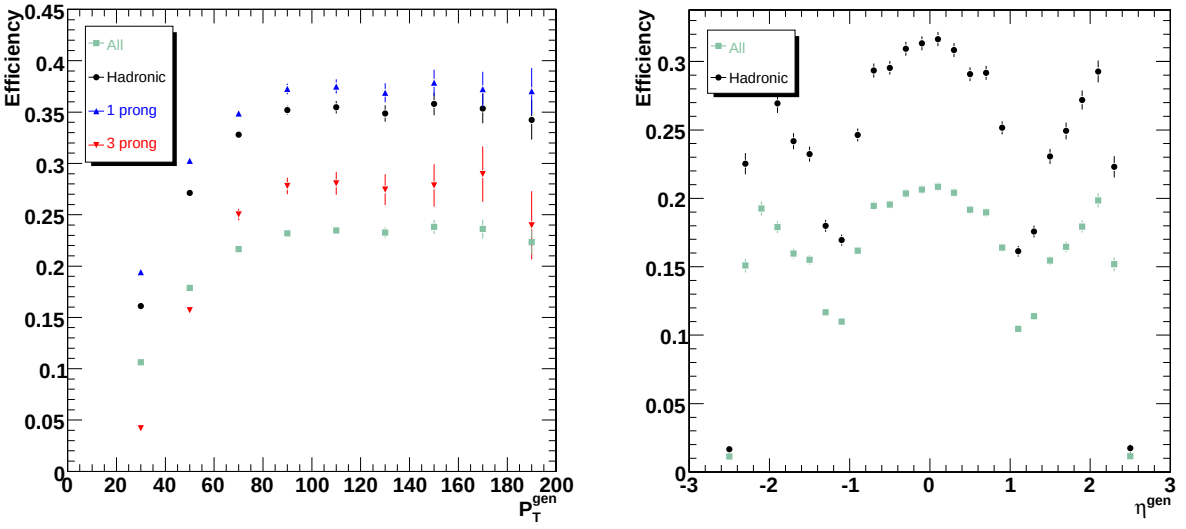

Figure 9. Reconstruction efficiency of τ candidates as a function of p_T, and η.

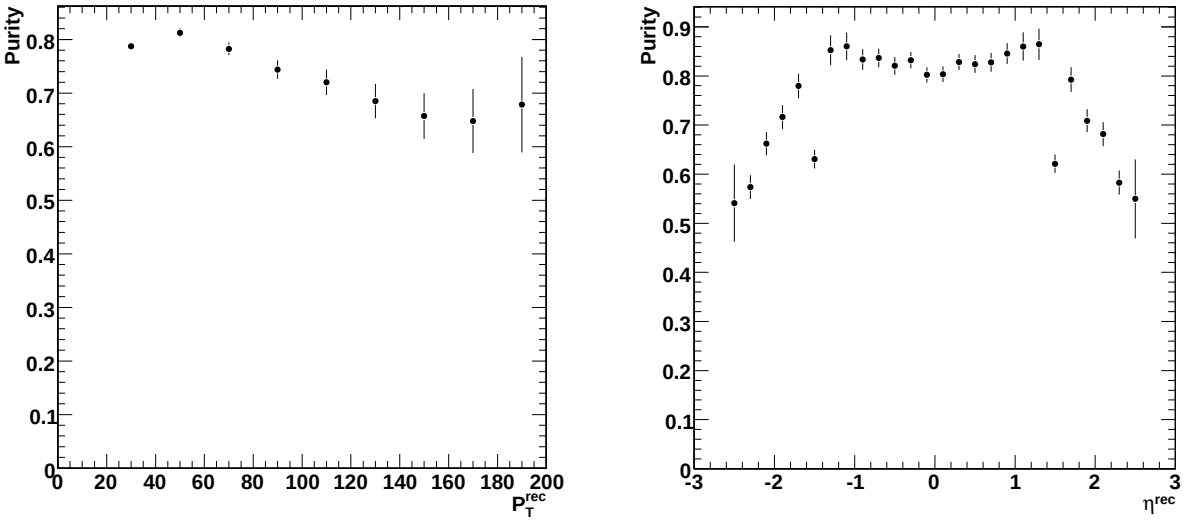

Figure 10. Fraction of correct assignments in the reconstruction of τ candidates within the di-lepton channel as a function of p_T, and η.

in table 4, and for the main backgrounds in 5. The last step in the selection of signal events is the use of the jet combined b-tag variable. Candidate events must have at least a value of 1 in each of the two jets selected. An overall efficiency close to 2% is obtained, with a high rejection power against all backgrounds considered as shown in table 4. A S/B value close to 1 is obtained, the main background being the one arising from the $t\bar{t}$ semileptonic channel.

2.6.1. Systematic uncertainties The majority of the systematic uncertainties are described in 2.2.4. There is another systematic uncertainty intrinsic to this analysis

due to the τ reconstruction and identification. The τ detection is affected by the requirements imposed on the tracks and π^0 in the isolation cone. Also the uncertainty in the energy scale uncertainty affects the τ cluster energy definition. The multiple interaction and pile up events affect the number of tracks in the signal and isolation cone. Based on preliminary studies, we assigned a 12% uncertainty to the τ reconstruction and identification. The statistical uncertainty in the cross-section determination is about 1.3% for an integrated luminosity of 10 fb^{-1}. Then combining these values with those estimated in the previous section, the relative uncertainty in the estimation of the cross-section can be written as:

$$\Delta\sigma_{t\bar{t}\ dil\ \tau,e\mu}/\sigma_{t\bar{t}\ dil\ \tau,e\mu} = 16\%\ \text{(syst.)} \pm 1.3\%\ \text{(stat.)} \pm 3\%\ \text{(luminosity)}$$

3. Semi-leptonic Top-Pair Events

This part of the paper starts with a section describing the simulation samples used for the analysis, Section 3.1. Section 3.2 elaborates on the details of the event reconstruction including the event selection. A measurement of the cross section on semi-leptonic decaying top quark pairs is described and studied in Section 3.3, including a thorough estimation of possible systematic uncertainties. Topological observables are constructed in Section 3.3.2 to differentiate between signal top quark events and background events.

For the top quark mass measurement in Section 3.4, the procedures for choosing the single-lepton final state and the jet combination in this final state are discussed in Sections 3.4.2 and 3.4.3. The top quark mass estimator is constructed from the result of a kinematic fit transformed into an ideogram of the event. The construction of this ideogram or likelihood ratio function is defined in Section 3.4.4, while in Section 3.4.5 the convolution method is formulated to determine the event likelihood as a function of the top quark mass. The result of an extensive study of systematic uncertainties is described in Section 3.4.6, where the total expected uncertainty on the inferred top quark mass is mentioned. Among the possible strategies for optimization or minimization of this total uncertainty, one related to the definition of jets is studied. The results are summarized in Section 3.4.7.

The analysis was performed on $pp \to t\bar{t} \to bW\bar{b}W \to bq\bar{q}\bar{b}\mu\nu_\mu$ events, but similar results are assumed for the electron decay channel.

3.1. Monte Carlo simulation samples

The Monte Carlo simulated events used in this note are generated with `CMKIN` using the `PYTHIA` 6.2 event generator [8]. A full `GEANT` $-$ `4` detector simulation [9] was used within `OSCAR` [10] to simulate the detector response to the $t\bar{t}$ final state. To simulate the low-luminosity machine settings a Poissonian average of 3.5 pile-up collisions (with an instantaneous luminosity of $2 \cdot 10^{33}$ cm^{-2}s^{-1}) from minimum bias events were added and simulated with `OSCAR` [11]. The `OSCAR` output was digitized with the reconstruction software of CMS. General Data Summary Tapes or DST's were produced with `ORCA`. Finally for all event reconstruction variables which were not written on the CMS standard DST's the `ORCA` was used. Table 6 summarizes the absolute quantities of single-lepton $t\bar{t}$ events which were produced for the studies presented in this note. Only $t\bar{t} \to bW\bar{b}W \to bq\bar{q}\bar{b}\mu\nu_\mu$ events were considered as signal in this study.

In order to study the systematic influence of pile-up collisions, event samples are generated with and without the addition of low-luminosity pile-up collisions. This was done only for the $t\bar{t} \to bW\bar{b}W \to bq\bar{q}\bar{b}\mu\nu_\mu$ signal events. In total more than 150k signal events are generated both with and without pile-up. The slope of the developed top quark mass estimator was estimated with event samples at three different input top quark masses: 170, 175 and 180 GeV/c^2 including low-luminosity pile-up collisions. All other event samples, for the study of systematic uncertainties, are constructed using the `FAMOS` framework [12]. The W + jets background event samples mentioned

	Number of events	Int.Luminosity fb^{-1}	Cross-section pb
$t\bar{t} \to bW\bar{b}W \to bq\bar{q}\bar{b}\mu\nu_\mu$	365k	4.39	83.0
other $t\bar{t}$	1962k	4.11	477.0
W+4jets	82.5k	0.47	174
Wbb+2jets	109.5k	6.44	17
Wbb+3jets	22.5k	3.21	7

Table 6. Overview of the number of analyzed simulated single-lepton $t\bar{t}$ and background events with their corresponding integrated luminosity calculated with the indicated Leading-Order cross-sections.

in Table 6 are generated with `AlpGen` and simulated within the `FAMOS` framework. Due to the construction of the event selection criterium, all other background processes are negligible. It will be illustrated that the expected amount of fully hadronic $t\bar{t}$ events passing the event selection is negligible. With this observation together with the Tevatron experience [7] it is assumed that the influence of QCD events is also negligible.

3.2. Reconstruction and pre-selection of the semi-leptonic $t\bar{t}$ *events*

The top quark ‡ has a branching ratio of about 100% to decay as $t \to Wb$, while the W boson decays has a leptonic branching ratio of $BR(W \to l\nu_l)=\frac{1}{3}$ and a hadronic branching ratio of $BR(W \to q\bar{q})=\frac{2}{3}$ (in the absence of QCD corrections). The generated final state topology of the semi-leptonic decay channel $pp \to t\bar{t} \to bq\bar{q}b\mu\nu_\mu$ consists of four coloured partons of which two are heavy, a muon and a neutrino. The detector final state therefore can be characterized by four hadronic jets of which two originate from a heavy quark, an isolated muon and missing transverse energy. In this part we consider the measurement of the cross section of semi-leptonic $t\bar{t}$ processes and the mass of the top quark in the semi-leptonic channel where the lepton is a muon.

Both the Level-1 and the High-Level Trigger criteria are applied on the simulated events, resulting in efficiencies shown in Table 7. The single-muon stream was used.

A muon candidate is formed when a muon track is reconstructed in the muon chambers and a matching track is found in the main tracker. Among the list of lepton candidates with their identified flavour, the lepton originating directly from the W boson decay is selected following the procedure described in [13]. This results in a unique lepton with a combined likelihood variable to be used in the event selection. In Figure 11 this likelihood variable is shown for the semi-leptonic $t\bar{t}$ signal and W+jets background processes, together with the transverse momentum, p_T, of the selected lepton candidate. The peak at zero for the likelihood variable is induced by events without a reconstructed lepton candidate in the final state. The observation of lepton candidates below the

‡ Throughout the note the charge conjugation and the inclusion of anti-matter is implicit.

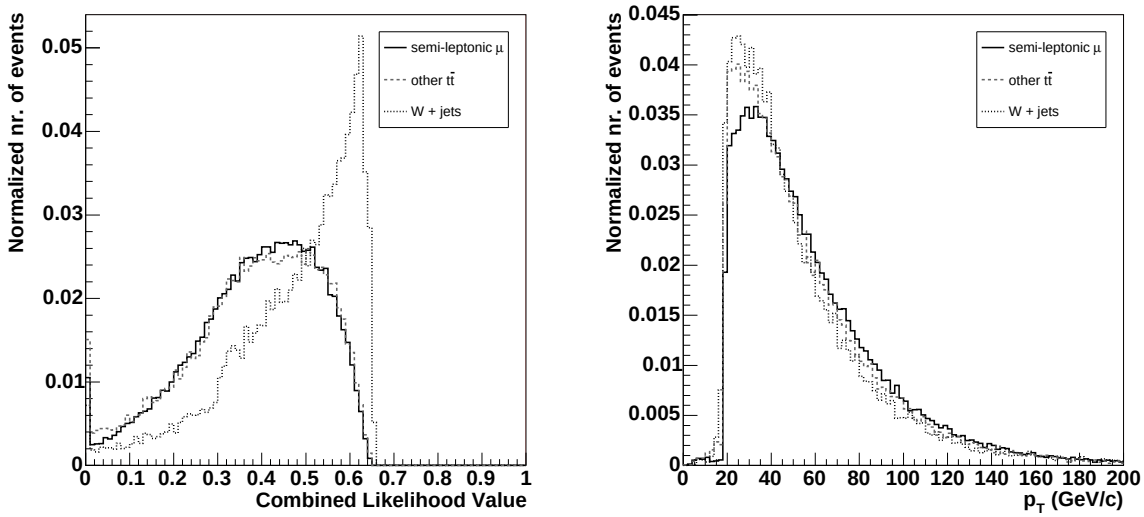

Figure 11. For the selected lepton candidate in the final state the normalized distribution of the combined likelihood variable for both semi-leptonic $t\bar{t}$ signal and W+jets background events (left) and the distribution of its transverse momentum, p_T (right).

trigger threshold on the transverse momentum comes from events which are triggered on a lepton different than the correct one coming from the $t \to bW \to bl\nu_l$ decay.

The jets are reconstructed from the combined electromagnetic and hadronic calorimeter deposites and clustered with the Iterative Cone algorithm using an opening angle of $\Delta R = 0.5$ rad. A transverse energy threshold of 0.5 GeV is applied on the input object before clustering. This results in a number of jets per event, as shown for the signal semi-leptonic $t\bar{t}$ events in Figure 12 and for the background $W + \text{jets}$ events in Figure 13. Only those jets in the vicinity of the primary vertex are considered in the analyses. Jets emerging from the pile up are vetoed using a track–based method. For a jet to be associated with the primary vertex, it is demanded that $\beta = \sum_{\text{track,PV,jet}} p_T / \sum_{\text{track,jet}} p_T > 0.04$, where the sum in the denominator is over the p_T of all tracks in the jet, while the sum in the nominator runs only over those tracks in the jet associated with the primary vertex. The low value of the β-cut reflects the aim that the tracks with the highest transverse momentum should dominate.

In Figures 12 and 13 the reduction in number of jets per event is illustrated. The energy scale of the reconstructed jets is calibrated using the methods described in [30]. The resulting transverse momentum, p_T, after applying this calibration technique is shown in both Figures. The primary vertex requirement on the reconstructed jets reject those jets with a small transverse momentum. The bump at about 35 GeV in the transverse momentum distribution is induced by the pre-selection cuts described below.

The transverse momentum components of the unobserved neutrino are estimated

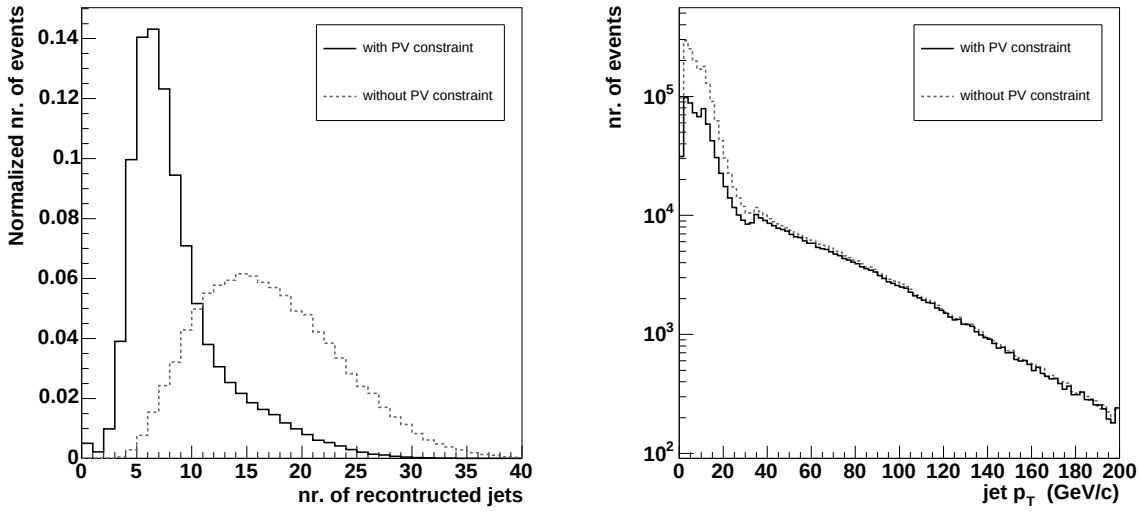

Figure 12. For semi-leptonic $t\bar{t}$ events passing the trigger requirements: the normalized distribution of the amount of reconstructed jets per event before and after applying the primary vertex constraint (left) and the distribution of the transverse momentum, p_T, of the calibrated jets before and after applying the primary vertex constraint (right).

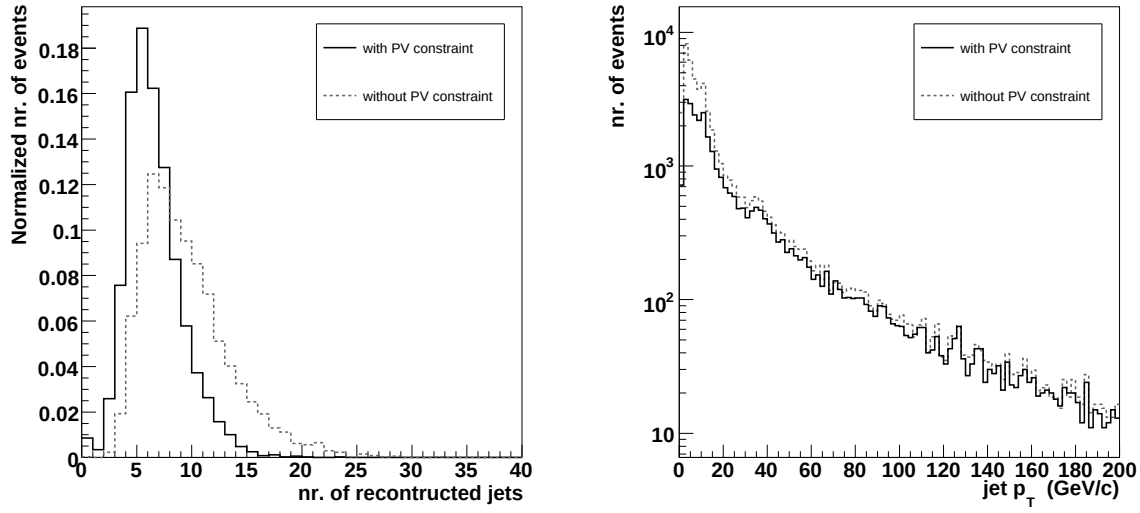

Figure 13. For W + jets events passing the trigger requirements: the normalized distribution of the amount of reconstructed jets per event before and after applying the primary vertex constraint (left) and the distribution of the transverse momentum, p_T, of the reconstructed and calibrated jets before and after applying the primary vertex constraint (right).

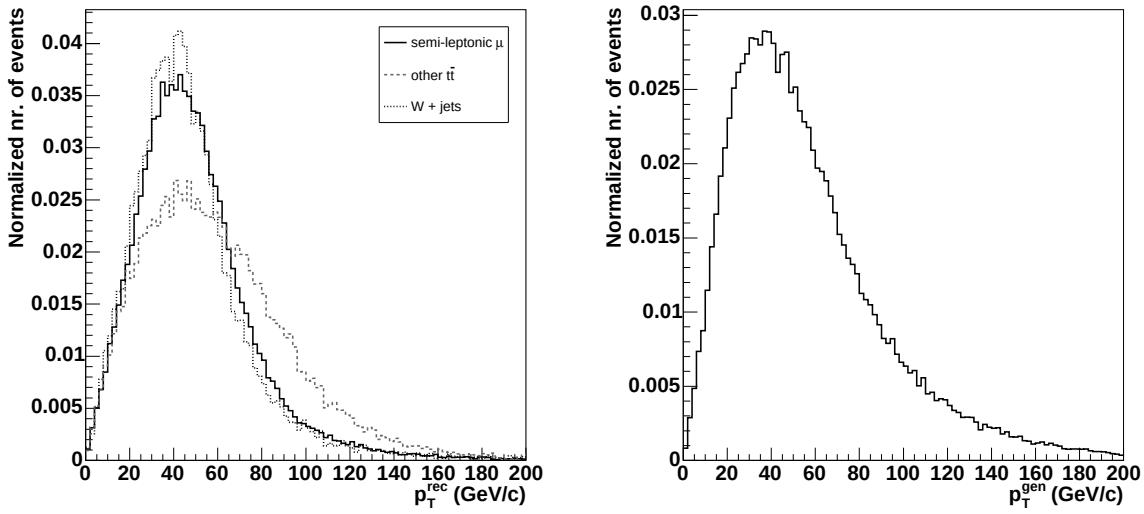

Figure 14. For events passing the trigger requirements: the normalized distribution of the reconstructed missing transverse momentum for both signal and background events (left) and the distribution of the transverse momentum of the generated neutrino for signal events (right).

via the missing transverse momentum which balances the vectorial sum of the energy deposites in the calorimeter above the transverse energy threshold mentioned. The distribution for the magnitude of the reconstructed missing transverse momentum and the transverse momentum of the generated neutrino is shown in Figure 14 both for signal and background events. No direct event selection requirement is made on the missing transverse momentum, as the resolution on the missing transverse momentum is of the same order as the expected magnitude of the missing transverse momentum in QCD (or fully hadronic $t\bar{t}$) events.

The event selection consists of a series of sequential cuts on kinematic or topological variables. A first pre-selection criterion reduces the amount of events to a manageable number by requiring at least four reconstructed jets with a transverse energy, E_T, larger than 10 GeV and with a pseudo-rapidity in the range of the tracker, $|\eta| < 2.4$. The jets must have a flight direction through the tracker to allows for a proper performance of the b-tagging algorithm. At least one lepton is required within the tracker acceptance of $|\eta| < 2.4$ and with a combined likelihood ratio value larger than 0.01.

For the remainder of the event selection several variables are examined, resulting in a definition of some simple criteria. The event is required to have at least 4 jets after applying the primary vertex constraint with a calibrated transverse energy, E_T, exceeding 30 GeV. If more than four jets match this criterion, the four leading jets needed to reconstruct the partonic $t\bar{t}$ event topology, are selected as those with the highest E_T. Of these four jets, two have to be b-tagged according to the method

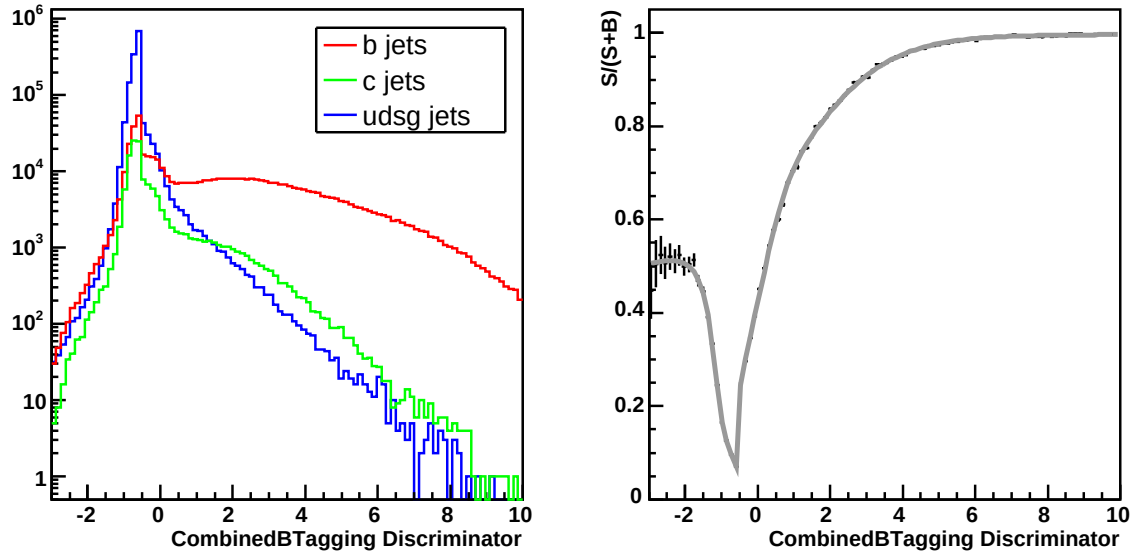

Figure 15. Distribution of the combined b-tag discriminant for jets in semi-leptonic $t\bar{t}$ events originating from different flavoured quarks, this becomes $P_i(x)$ after normalization (left). On the right the b-tag probability $L^b(x)$ (or likelihood ratio S/(S+B)) as a function of the combined b-tag discriminant.

applying a combined b-tag variable [31]. The distribution of the b-tag discriminant variable is shown in Figure 15 for several quark flavours. To transform the value of the combined b-tagging discriminant into a probability only jets are considered which are clearly connected to the simulated parton direction in order to define unambiguously their flavour. A likelihood ratio is constructed as

$$L^b(x) = \frac{P_b(x)}{P_b(x) + P_c(x) + P_{others}(x)} \tag{8}$$

where $P_i(x)$ is the probability density function of quark flavour i in the dimension of the b-tag discriminant x. The variable $L^b(x)$ of a jet is related to the b-tag discriminant of the jet and takes by definition values between 0 and 1. It is interpreted as the probability for the jet to originate from a b-flavoured parton. Hence the complement $(1 - L^b(x))$ is interpreted as the probability of the jet not to originate from a b-flavoured parton.

For the event to be selected, exactly two out of the four leading jets need to have a b-tag likelihood L^b exceeding 0.6 and the other two need to be anti-b-tagged, hence having a b-tag likelihood L^b below 0.4.

The selected lepton candidate must have a transverse momentum, p_T, larger than 20 GeV/c, while no selection cut is applied on the reconstructed missing transverse momentum. This is well above the trigger turn on curve in the single-muon trigger stream. An extra sequential cut on the reconstructed missing transverse momentum

would not increase the signal-to-noise ratio significantly, but it would introduce possibly large systematic uncertainties.

At this stage in the event selection most of the relevant background processes are reduced, as is illustrated in Table 7. For both the cross section and the mass measurement extra specific selection cuts are applied.

3.3. Cross section of semi-leptonic $t\bar{t}$ *processes*

3.3.1. Event Selection After classifying two of the four reconstructed jets as light quark and two as b-quark jets, only two jet combinations remain. A kinematic fit [14] was applied on the reconstructed event for both jet combinations forcing the reconstructed W boson mass to its precisely measured value. The event is selected if the fit converged for at least one of the combinations. The efficiency of this extra sequential cut is shown in Table 7.

The efficiencies after each sequential selection cut are shown in Table 7. From the simulated W + jets events few are selected. The selection efficiency for the signal events $pp \to t\bar{t} \to bq\bar{q}b\mu\nu_\mu$, denoted as ϵ_{sim}, is estimated to be 6.28 ± 0.04 %. The fraction between $t\bar{t}$ signal and other decay channels, denoted as F_{sim}, is estimated to be 82.8 ± 0.2 %. These numbers and uncertainties will be used when studying the properties of the cross section estimator.

The signal-to-noise ratio after the event selection is equal to 26.7, where all $t\bar{t}$ decay channels are considered as signal. In the determination of the signal-to-noise ratio only the background processes mentioned are considered. Due to the event selection all other processes should be negligible. Related to QCD-like jet production this statement can be motivated as for example a negligible amount of fully hadronic $t\bar{t}$ events pass the event selection. Applying the same event selection on signal $t\bar{t}$ event samples simulated within the FAMOS framework results in a selection efficiency of 9.23% rather than 6.28%. The disagreement is due to the difference in b-tagging performance between the OSCAR and the FAMOS framework. As the W + jets background event samples are simulated within FAMOS the obtained signal-to-noise ratio of 26.7 can therefore be considered as an underestimate, hence conservative.

3.3.2. Construction of topological observables The first strategy for estimating the cross section of the process is based on the study of topological shape observables. The statistical power of topological observables to separate $t\bar{t}$ and W + jets events is illustrated on the basis of [7]. The D0 Collaboration has exploited 6 observables which contain information to separate the signal from the background [7]. Based on these observations, the following observables are defined:

- Sphericity S and aplanarity A: extracted from the eigenvalues of the quadratic momentum tensor determined using the four-momenta of the four jets and the lepton

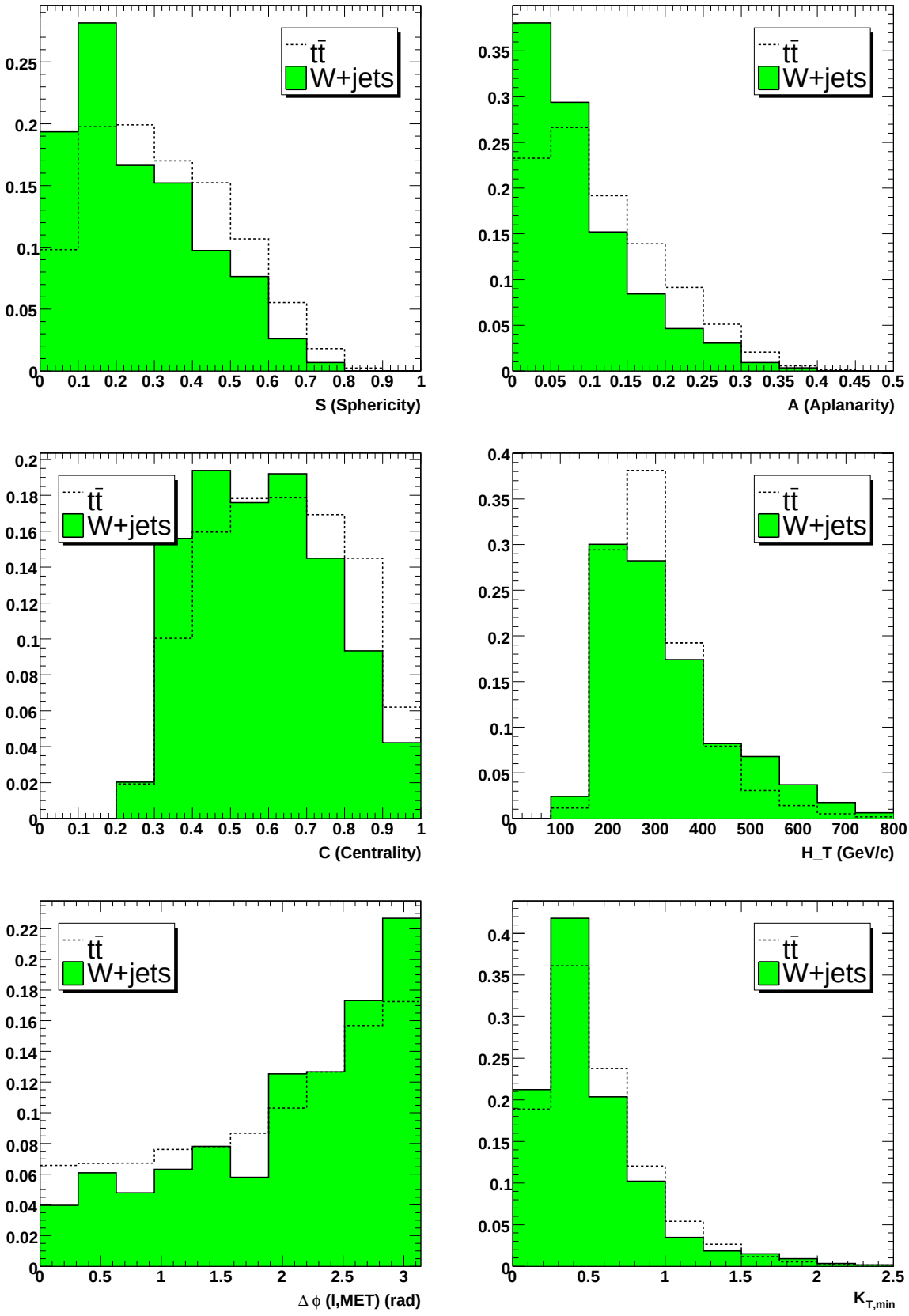

Figure 16. Normalized distributions of the observables mentioned in the text.

	Signal	Other $t\bar{t}$	W+4j	Wbb+2j	Wbb+3j	S/N
Before selection	365k	1962k	82.5k	109.5k	22.5k	5.9
L1+HLT Trigger	62.2%	5.30%	24.1%	8.35%	8.29%	7.8
Pre-selection	45.8%	2.68%	11.7%	3.94%	5.91%	9.1
Four jets E_T >30 GeV	25.4%	1.01%	4.1%	1.48%	3.37%	9.9
p_T^{lepton} >20 GeV/c	24.8%	0.97%	3.9%	1.41%	3.14%	10.3
b-tag criteria	6.5%	0.24%	0.064%	0.52%	0.79%	25.4
Kinematic fit	6.3%	0.23%	0.059%	0.48%	0.72%	26.7
Selected cross section (pb)	5.21	1.10	0.10	0.08	0.05	26.7
Scaled L=1fb^{-1}	5211	1084	104	82	50	26.7

Table 7. Overview of the selection criteria applied on the events using simulated events with pile-up collisions included. The last line indicates how many events are expected after applying the full selection criteria on a data set of 1fb^{-1}. The expected S/N values take into account the respective Leading-Order cross-sections of the processes.

$$S^{\alpha\beta} = \frac{\sum_{i=1}^{5} p_i^{\alpha} p_i^{\beta}}{\sum_{i=1}^{5} |p_i|^2} \tag{9}$$

with $\{\alpha, \beta\} = \{x, y, z\}$;

- Centrality C: scalar sum of the transverse momenta of the jets divided by the scalar sum of the energies of the jets;
- H_T: scalar sum of the transverse momentum of the four leading jets;
- $\Delta\phi(l, \mathrm{MET})$: azimuthal opening angle between the lepton and the missing transverse energy;
- $K_{T,min} = \Delta R_{ij}^{min} p_T^{min} / E_T^W$: with ΔR_{ij}^{min} the minimal separation in an (η, ϕ) metric between two jets, p_T^{min} the lowest transverse momentum in that pair and E_T^W the scalar sum of the lepton transverse momentum and the missing transverse energy.

The distributions of the above observables are shown in Figure 16. All $t\bar{t}$ decay channels are combined and from the simulation we know that this contains a fraction F_{sim} of $t\bar{t} \to bq\bar{q}b\mu\nu_\mu$ events. From each of the above observables the signal-to-noise ratio of the normalized distributions is determined as a function of the observable. These ratios, S/B, are shown in Figure 17. It is observed that the observables provide some information for the event classification into signal ($t\bar{t}$) or background (W + jets), but not as significant as in the D0 analysis.

The signal-to-noise information of each observable is combined into a combined likelihood ratio discriminant D defined as

$$D = \frac{\prod_{i=1}^{6} (S/B)_i}{\prod_{i=1}^{6} (S/B)_i + 1} \quad . \tag{10}$$

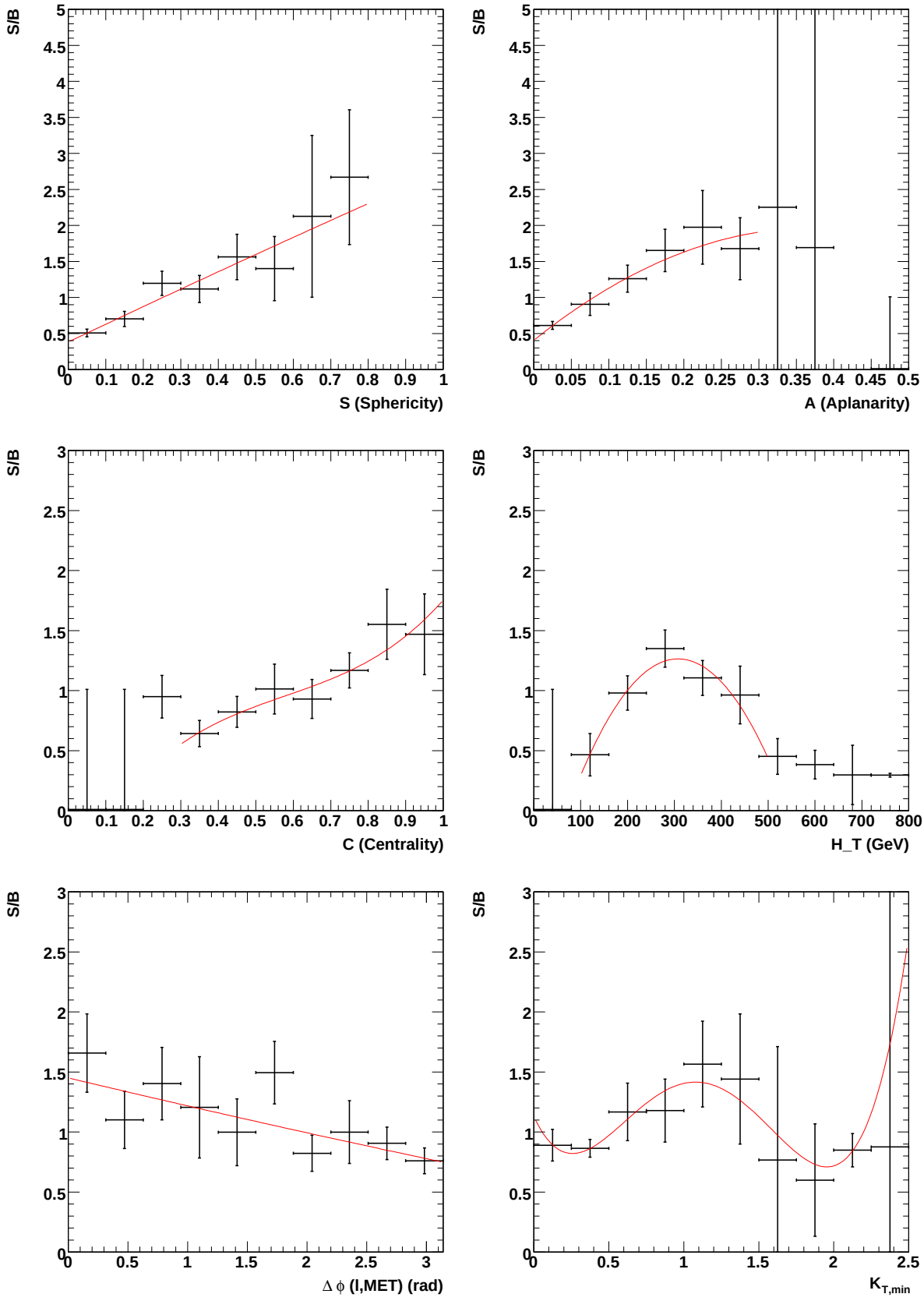

Figure 17. Distributions of the likelihood ratios of the observables mentioned in the text.

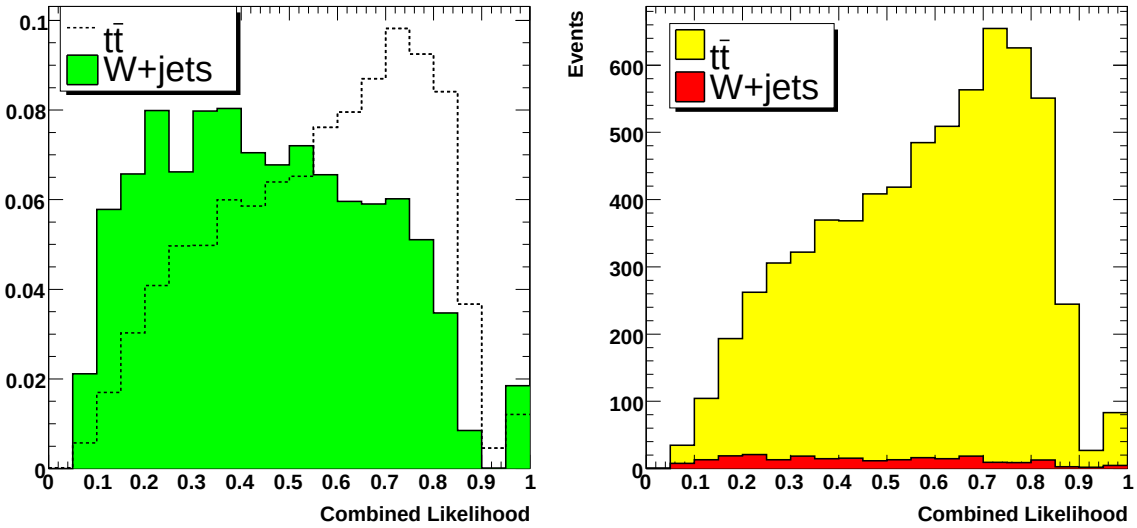

Figure 18. Distributions of the combined likelihood variable D, normalized to unity (left) and scaled to an integrated luminosity of 1fb^{-1} (right).

The distributions of D shown in Figure 18 illustrate a difference between the $t\bar{t}$ signal and the W + jets background events. This difference is however much less significant as for the $p\bar{p}$ collisions at the Tevatron [7]. Therefore it is concluded that topological observables are not very useful in separating $t\bar{t}$ from W + jets events in pp collisions at the LHC after applying a standard event selection as described in Section **??**.

3.3.3. The cross section estimator Due to the high signal-to-noise ratio after the event selection of Section **??**, the systematic effect of the background contribution is minor. Therefore a simple cross section estimator is defined which counts the events N_{sel} remaining after the event selection and determines the signal cross section via the purity (signal-to-noise ratio denoted by R) and the efficiency of the applied selection obtained from simulation studies. The cross section for the $pp \to t\bar{t} \to bq\bar{q}b\mu\nu_\mu$ process can be determined as

$$\hat{\sigma}_{t\bar{t}(\mu)} = N_{sel} \cdot (\frac{R}{R+1}) \cdot F_{sim} \cdot \frac{1}{\epsilon_{sim}} \cdot \frac{1}{\mathcal{L}} \tag{11}$$

where $\mathcal{L}$ is the integrated luminosity of the sample.

For the signal-to-noise ratio obtained by the event selection the statistical uncertainty on the estimated cross section is 1.2%, 0.6% and 0.4% for respectively 1 fb^{-1}, 5 fb^{-1} and 10 fb^{-1}.

3.3.4. Systematic uncertianties The systematic effect is introduced only on the signal events, changing the efficiency of the event selection. This effect is transformed into

	$\Delta\hat{\sigma}_{t\bar{t}(\mu)}/\hat{\sigma}_{t\bar{t}(\mu)}$
Pile-Up collisions	10.8 ± 1.4 %

Table 8. Relative effect of pile-up collisions on the estimated cross section.

a relative uncertainty on the estimated cross section according to Eq. 11. For all systematic effects the relative difference in inferred cross section is shown between the central (nominal or default) event sample and the event sample generated with the deviation from this default as indicated, hence $\hat{\sigma}^{\text{default}}_{t\bar{t}(\mu)} - \hat{\sigma}^{\text{syst.effect}}_{t\bar{t}(\mu)}$, or between the two event samples with extreme changes in the parameter settings. Similar effects on the background samples should be a second order effect on the inferred cross section.

- Limited size of simulated event samples
  Due to the limited size of the simulated event samples, an uncertainty on the event selection efficiency ϵ_{sim} has to be taken into account. For the default settings of ϵ_{sim} and the current size of the simulated event sample ($\mathcal{L} = 4.3\ \text{fb}^{-1}$), the absolute uncertainty on ϵ_{sim} is equal to 0.04%. This results in a relative uncertainty on the cross section estimator of 0.6%. The effect of the uncertainty on the fraction F_{sim} of semi-leptonic muon events in the collection of selected $t\bar{t}$ events amount 0.2% and is neglegible.
  Both uncertainties can be reduced by simulating more events, they scale as the inverse of the square root of the amount of simulated events.
- Pile-Up description
  For the signal events simulation samples of about 150k events are produced with and without the superposition of low-luminosity pile-up collisions (with an instantaneous luminosity of $2 \cdot 10^{33}\ \text{cm}^{-2}\text{s}^{-1}$). Only in-time inelastic pile-up collisions are taken into account, while the out-of-time contribution could be as large as the in-time contribution. The out-of-time pile-up contribution could however be reduced by both hard- and soft-ware applications reducing the effect on the jet energy scales used in the event selection. The systematic uncertainty is conservatively taken as 30% of the difference between the event selection efficiency obtained from the simulation sample with and without pile-up collisions, see Table 8.
- Underlying event
  Apart from the multiple proton collisions detected simultanous, the fragmented remnant of the protons of beam remnant in a single collision is also observed in the detector. The phenomenology of this so-called underlying event is modelled with QCD Monte-Carlo models like `HERWIG` or `PYTHIA` (including initial state radiation) and contains everything but the outgoing hard particles (including their final state radiation). The models contain both pertubative and non-pertubative QCD physics of which the parameters can be tuned to fit the collision data. The particles arising

	$\Delta\hat{\sigma}_{t\bar{t}(\mu)}/\hat{\sigma}_{t\bar{t}(\mu)}$
[PARP(82) = 2.4] – [PARP(82) = 3.4] (GeV)	1.5 ± 0.9 %

Table 9. Relative effect of the underlying event description on the estimated cross section.

	$\Delta\hat{\sigma}_{t\bar{t}(\mu)}/\hat{\sigma}_{t\bar{t}(\mu)}$
Light-quark jet energy scale (2%)	1.6 ± 1.6 %
Heavy-quark jet energy scale (2%)	1.0 ± 1.6 %

Table 10. Relative effect of the jet energy scale uncertainty on the estimated cross section.

from the beam remnant in the proton collisions are produced at the same primary vertex as the hard scattering event, and can therefore not be rejected by the primary vertex criterium applied in the selection of final state jets.
In the `PYTHIA` model for the underlying event the main parameter is the color screening p_T cut-off value (`PARP(82)`). When tuned to CDF and UA5 data, its value is equal to 2.9 GeV, with a symmetric 3σ confidence interval of $[2.4, 3.4]$ GeV. With `FAMOS` in total 200k signal event are produced with both color screening p_T cut-off values 2.4 GeV and 3.4 GeV. The results are shown in Table 9.
This estimation is conservative as the 3σ confidence interval for the color screening p_T cut-off value is used to obtain a 1σ systematic uncertainty of the cross section estimator. As we take both the negative and the positive sides into account, half of this shift is taken as a systematic uncertainty.

- Jet energy scale
  The top quark events are reconstructed with jets in the final state and the event selection includes cuts on the transverse momentum of the leading jets. The reconstructed angles of the jets have a much better resolution compared to the energy scale of these jets. To study the effect of systematic shifts on the inclusive jet energy scale, the 4-momenta of the jets are scaled by a factor α with the procedure

$$p^{\mu,jet}_{scaled,\pm\alpha} = ((1 \pm \alpha)E, (1 \pm \alpha)p_x, (1 \pm \alpha)p_y, (1 \pm \alpha)p_z) \tag{12}$$

  where a difference is made between jets origination from light (u,d,s,c) or heavy (b) quarks. A non-zero value of α was applied before the event selection and before the kinematic fit, resulting in a systematic shift in the value of the inferred cross section. The systematic effects of a 2% uncertainty on the jet energy scale of light quark jets [15] and a 2% uncertainty on the jet energy scale of the b-quark jets are added linearly. The individual shifts are shown in Table 10 while the combined result is shown in Table 14. The significance of the effect is however low.

	$\Delta\hat{\sigma}_{t\bar{t}}(\mu)/\hat{\sigma}_{t\bar{t}}(\mu)$
[Λ_{QCD}=0.35 GeV] - [Λ_{QCD}=0.15 GeV]	-6.1 $\pm$ 0.9 %
[Q^2_{max}=4 Q^2_{hard}] - [Q^2_{max}=0.25 Q^2_{hard}]	10.6 $\pm$ 0.9 %

Table 11. Systematic uncertainties due to QCD radiation effects as described in the text. The values of Q^2_{max} are those for the initial state radiation, while those for the final state radiation are changed simultaneously according to the description in the text.

- Pertubative QCD Radiation
  Both initial and final state radiation (ISR and FSR) are produced according to the Dokshitzer-Gribov-Lipatov-Altarelli-Parisi (DGLAP) evolution equations [16] in the `PYTHIA` showering algorithm where color coherence in the parton shower is accounted for. The main parameters in this model are the general QCD sale parameter Λ_{QCD} used in the DGLAP evolution (`PARP(61)`, `PARP(72)`, `PARJ(81)`) and the virtuality cut-off scale Q^2_{max} which defines the allowed phase-space for initial state radiation (`PARP(67)`) and indicates where the final state radiation takes over (`PARP(71)`). The central values of these parameters are taken according to the tuning of the model to the CDF data as mentioned in [17] and used to simulate a `FAMOS` event sample for the signal. The value of Λ_{QCD} is changed from 0.25 GeV to respectively 0.15 and 0.35 GeV, while the value of Q^2_{max} is shifted by changing `PARP(67)` to get $Q^2_{max} = 0.25Q^2_{hard}$ and $Q^2_{max} = 4Q^2_{hard}$ for the initial state and simultaneous changing `PARP(71)` to get $Q^2_{max} = 1Q^2_{hard}$ and $Q^2_{max} = 16Q^2_{hard}$ for the final state perturbative radiation. The resulting shifts in the cross section estimator is shown in Table 11. It is found that the cross section estimator is very sensitive to the quality of the tuning or the choice of these pertubative QCD parameters. The values of the parameters are however changed to extreme values which are several standard deviations from central tuned values ([18] for example for Lambda$_{QCD}$). The maximum of the absolute value of the two extreme shifts is taken as a systematic uncertainty. To scale back to a realistic interval, this average has to be divided by a factor of 4 (including a factor of two to account for the fact that both the positive and the negative sides are considered). This factor is still very conservative and does not take into account the correlation between both parameters.
- Hadronization
  When the pertubative DGLAP evolution equation breaks down, the non-pertubative fragmentation or hadronization takes over providing the observed hadrons. The phenomenology of this process happens in the confined phase-space of low-momentum transfer and as the process is not yet understood from first principles it is modelled. At this stage no new jets are formed with a high transverse momentum with respect to their parent parton. The local parton-hadron duality

	$\Delta\hat{\sigma}_{t\bar{t}(\mu)}/\hat{\sigma}_{t\bar{t}(\mu)}$
[*Lund b*=0.60] - [*Lund b*=0.44]	0.6 ± 1.0 %
[σ_q=0.46 GeV] - [σ_q=0.34 GeV]	0.3 ± 1.0 %

Table 12. Systematic uncertainties due to our knowledge of the fragmentation as described by the Lund string model implemented in PYTHIA.

supposes that the flow of momentum and quantum numbers at the hadron level tends to follow that flow established at the parton level. All of the present models are formulated in a probabilistic language to allow them to be simulated by Monte Carlo techniques. In PYTHIA the so-called string hadronization is performed [19]. The parameters of the fragmentation models are tuned to for example LEP and SLD data introducing a large correlation between the parameter values. Two main parameters can be identified, the others being strongly correlated to these. The first is *Lund b* (PARJ(42)), strongly anti-correlated to *Lund a* (PARJ(41)), as both arise in the same Lund fragmentation functions for light quarks. These functions express the probability that a hadron consumes a given fraction of the available longitudinal energy-momentum. For the heavy quark fragmentation the Peterson function is used instead. The transverse momenta p_T of the hadrons are generated according to a flavour independent Gaussian probability density function of width σ_q (PARJ(21)), the second of two main parameters. It is predicted to be of the order of 0.3 GeV.
The values of both *Lund b* and σ_q tuned to the OPAL data are respectively equal to 0.52 ± 0.04 and 0.40 ± 0.03 GeV. These uncertainties are however only indications of the resolution of these parameters within the Lund string model in PYTHIA. The fit of the model parameters is performed on several data distributions, but even the best fit results in a χ^2/NDF which is significantly deviating from unity, as the phenomenology and/or implementation of the model does not reflect the true physics.
When changing the parameters *Lund b* and σ_q from their central values to 2σ deviations, a shift is obtained on the inferred cross section. Simulating with FAMOS event samples in these different configurations results in shifts shown in Table 12. The maximum of the absolute values of the two extreme shifts is taken as a systematic uncertainty. This value is divided by two to account for the fact that both the negative and the positive side of the interval are considered.

- Algorithms for b-tagging
  In [20] a method is described to measure the b-tagging efficiency of the combined b-tag algorithm from real data. A potential relative uncertainty on this efficiency is demonstrated of about 4% (in the barrel region) and 5% (in the endcap region) applying the method on 10 fb^{-1} of data. This would result in a change of the efficiency ϵ_{sim} determined from simulation.

	$\Delta\hat{\sigma}_{t\bar{t}(\mu)}/\hat{\sigma}_{t\bar{t}(\mu)}$
L^B=70%	15.3 ± 1.6 %
L^B=65%	6.8 ± 1.6 %
L^B=55%	-7.1 ± 1.6 %
L^B=50%	-15.6 ± 1.6 %

Table 13. Systematic uncertainties due b-tagging algorithms.

To illustrate the effect on the estimated cross section, the b-tag criterium in the event selection was changed. Nominally exactly two jets are required to have a b-tag probability L^B above 60%. This limit is changed and the effect on the cross section estimator is shown in Table 13. In the estimation of the statistical uncertainty on the systematic shift the correlation between the central and the deviated event selection is not taken into account.
For an uncertainty of 5% on the b-tag efficiency a corresponding shift in the applied b-tagging cuts in the dimension of the combined b-tag discriminant is determined. The inclusive distributions of the b-tagging discriminant are shown for the simulated $t\bar{t}$ events in Figure 15 for different quark flavours. In the event selection the criteria L^B=70% corresponds to a combined b-tag discriminant value of about 1.0. In order to select 5% more b-quarks in a jet sample, this cut-value of the discriminant should shift from 1.0 to 0.74, corresponding according to Figure 15 (right) to a value of L^B equal to 65%. Assuming a linear dependency between L^B and the b-tagging discriminant in the relevant region around the value L^B=60%, it is therefore concluded that the 5% uncertainty in the estimate of the b-tagging efficiency transforms into a 5% change in the value of L^B. The systematic uncertainty due to the b-tagging algorithms is defined as the average of the relative shifts on the cross section estimator when changing L^B from 60% to both 55% and 65%.

- Parton density function
  The parton density functions or PDF's of protons are an essential ingredient in the simulation of the proton-proton scattering process. The parton distribution are the probability density functions for finding a particle with a certain longitudinal momentum fraction x and a momentum transfer Q^2 in the proton. As they cannot be obtained from pertubative QCD, they are determined from global analyses using deep inelastic and other hard scattering data for example from the HERA ep collisions probing the proton. Several functional forms can be used to fit different parts of the data. The reference method is taken to be `CTEQ6M` which includes Next-to-Leading Order QCD corrections. The central PDF's can be reweighted according to the estimated uncertainties (both to the positive ($j+$) and negative ($j-$) side of the central fitted value (c)) on the 20 parameters used in the `CTEQ` fit method. The event weight depends on the value of x, the flavour of the partons

in the hard process and the Q^2 value of the event taken to be equal to m_t^2. This procedure results in 40 shifted selection efficiencies (or $\Delta\hat{\sigma}_{t\bar{t}(\mu)}$ according to Eq. 11) from the central efficiency (or $\hat{\sigma}_{t\bar{t}(\mu)}$ according to Eq. 11). The actual effect due to the uncertainties arising from the CTEQ fits is determined via the following procedure :

$$(\Delta^{+}_{PDF}\hat{\sigma}_{t\bar{t}(\mu)})^2 = \sum_{j=1}^{20} \left(max \left[\hat{\sigma}^{j+}_{t\bar{t}(\mu)} - \hat{\sigma}^{c}_{t\bar{t}(\mu)} \ , \ \hat{\sigma}^{j-}_{t\bar{t}(\mu)} - \hat{\sigma}^{c}_{t\bar{t}(\mu)} \ , \ 0 \right] \right)^2 \tag{13}$$

and

$$(\Delta^{-}_{PDF}\hat{\sigma}_{t\bar{t}(\mu)})^2 = \sum_{j=1}^{20} \left(max \left[\hat{\sigma}^{c}_{t\bar{t}(\mu)} - \hat{\sigma}^{j+}_{t\bar{t}(\mu)} \ , \ \hat{\sigma}^{c}_{t\bar{t}(\mu)} - \hat{\sigma}^{j-}_{t\bar{t}(\mu)} \ , \ 0 \right] \right)^2 \tag{14}$$

where $\hat{\sigma}^{c}_{t\bar{t}(\mu)}$ is the central cross section inferred from the FAMOS simulated event sample applying the central CTEQ6M fit. This procedure takes into account the sign of the correlation between the PDF parameters and the inferred observable of interest, in this case the cross section. The resulting systematic uncertainties are $\Delta^{+}_{\mathrm{PDF}}\hat{\sigma}_{t\bar{t}(\mu)} = 3.4\%$ and $\Delta^{-}_{\mathrm{PDF}}\hat{\sigma}_{t\bar{t}(\mu)} = 3.3\%$. The largest of the two is taken as a systematic uncertainty.

- Integrated luminosity
  Measuring the luminosity at hadron colliders is challenging and results in relative large uncertainties. The goal is to estimate the integrated luminosity with a relative uncertainty of about 10%, 5% and 3% for integrated luminosities of respectively 1 fb^{-1}, 5 fb^{-1} and 10 fb^{-1}.
- Background processes
  An uncertainty of about 25% on the W + jets background cross section results in a relative uncertainty of 0.9% on the estimated cross section of the $pp \to t\bar{t} \to bq\bar{q}b\mu\nu_\mu$ process. This estimate is conservative as the background event samples are simulated within FAMOS for which the selection efficiency is larger compared to the efficiency determined within the OSCAR framework.
- Combining systematic uncertainties
  In Table 14 all systematic uncertainties determined are quoted. For some of the effects the influence on the cross section estimator is significant, while for other effects the statistical uncertainty on the systematic shift dominates. For the effects where the statistical uncertainty of the effect dominates, the statistical uncertainty is quoted rather than the systematic shift.
  In the combination of the individual components of the systematic uncertainty the correlation between the effects was not accounted for. Hence the squared sum of the individual components was taken. It is observed that the systematic uncertainty dominates the statistical uncertainty already in LHC start-up scenarios. The measurement of the cross section is dominated by the uncertainty on the b-tagging efficiency. The proposed data-based method to estimate this b-tagging

	$\Delta\hat{\sigma}_{t\bar{t}(\mu)}/\hat{\sigma}_{t\bar{t}(\mu)}$
Statistical Uncertainty ($1fb^{-1}$)	1.2%
Statistical Uncertainty ($5fb^{-1}$)	0.6%
Statistical Uncertainty ($10fb^{-1}$)	0.4%
Simulation samples (ϵ_{sim})	0.6%
Simulation samples (F_{sim})	0.2%
Pile-Up	3.2%
Underlying Event	0.8%
Jet Energy Scale (light quarks)	1.6%
Jet Energy Scale (heavy quarks)	1.6%
Radiation	2.6%
Fragmentation	1.0%
b-tagging	7.0%
Parton Density Functions	3.4%
Background level	0.9%
Total Systematic Uncertainty	9.2%
Integrated luminosity ($1fb^{-1}$)	10%
Integrated luminosity ($5fb^{-1}$)	5%
Integrated luminosity ($10fb^{-1}$)	3%
Total Uncertainty ($1fb^{-1}$)	13.7%
Total Uncertainty ($5fb^{-1}$)	10.5%
Total Uncertainty ($10fb^{-1}$)	9.7%

Table 14. Overview of the systematic uncertainties on the inferred cross section.

efficiency is however dominated by systematic uncertainties due to radiation effects. It can therefore be assumed that this uncertainty is reducable with a factor of 2 when a better understanding of the radiation phenomenology in proton collisions become available.

3.3.5. Conclusion The total relative systematic uncertainty on the developed cross section estimator $\hat{\sigma}_{t\bar{t}(\mu)}$ is 9.2% (syst) $\pm$ 5.0% (lumi) which can be compared to a relative statistical uncertainty of 0.6% at 5 fb^{-1}. The total uncertainty of 10.5% scales with the integrated luminosity as shown in Figure 19. In this plot it is assumed that the uncertainty on the determination of the integrated luminosity scale as the square root of the integrated luminosity. At an integrated luminosity of about $5fb^{-1}$ the total uncertainty is dominated by the uncertainty on the b-tagging performance. Similar results are expected for the measurement of the cross section of the process $pp \to t\bar{t} \to bq\bar{q}be\nu_e$.

The top quark mass can be inferred from the knowledge of the cross section of the

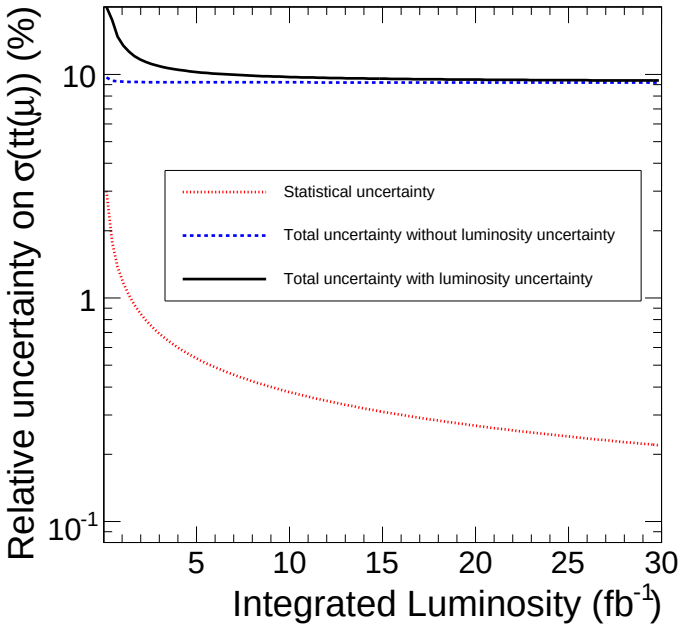

Figure 19. Statistical and systematical uncertainty on the inferred cross section of the process $pp \to t\bar{t} \to bq\bar{q}b\mu\nu_\mu$ as a function of the integrated luminosity.

process $pp \to t\bar{t}$, as shown in [21]. A total uncertainty of 9.7% on the determination of the cross section would give an indirect measurement of the top quark mass with an uncertainty of about 3 GeV/c^2.

Although it is believed that QCD events have a minor impact on the measurement of the cross section of semi-leptonic $t\bar{t}$ events (certainly for the muonic decays), their influence should be studied when simulation tools become available to produce a large amount of realistic QCD jet-like events.

3.4. Top Quark Mass measurement

3.4.1. Event Selection In addition to the event selection described in Section 3.2, the four leading jets should not overlap in an (η, ϕ)-metric to reduce ambiguities in the jet energy scale calibration procedure. This results in the efficiencies quoted in Table 15.

In the selected $t\bar{t}$ sample about $\frac{1}{6}$ is generated in a different decay channel. The selected background catalogued as other $t\bar{t}$ decay channels, breaks down according to the generated information in

- 27.6% of $t\bar{t} \to \tau\nu_\tau + X$;
- 0.10% of $t\bar{t} \to e\nu_e + X$;
- 1.75% of $t\bar{t} \to \tau\nu_\tau + \tau\nu_\tau + X$;
- 0.00% of $t\bar{t} \to e\nu_e + e\nu_e + X$;

	Signal	Other $t\bar{t}$	W+4j	Wbb+2j	Wbb+3j	S/N
Before selection	365k	1962k	82.5k	109.5k	22.5k	0.032
L1+HLT Trigger	62.2%	5.30%	24.1%	8.35%	8.29%	0.74
Pre-selection	45.8%	2.68%	11.7%	3.94%	5.91%	1.10
Four jets E_T >30 GeV	25.4%	1.01%	4.1%	1.48%	3.37%	1.69
p_T^{lepton} >20 GeV/c	24.8%	0.97%	3.9%	1.41%	3.14%	1.72
b-tag criteria	5.5%	0.21%	0.052%	0.47%	0.70%	3.73
No jet overlap	3.0%	0.11%	0.027%	0.25%	0.44%	3.87
P_{χ^2}-cut 20%	1.4%	0.039%	0.0097	0.061	0.07	5.3
P_{sign}-cut 80%	1.2%	0.025%	0.0085	0.052	0.05	6.8
P_{comb}-cut 50%	0.7%	0.013%	0.0036	0.013	0.	8.2
Scaled L=1fb^{-1}	588	64	6	2	0	8.2

Table 15. Overview of the selection criteria applied on the events using simulated events with pile-up collisions included. The last line indicates how many events are expected after applying the full selection criteria on a data set of 1fb^{-1}. The expected S/N values take into account the respective Leading-Order cross-sections of the processes.

- 8.80% of $t\bar{t} \to \mu\nu_\mu + \mu\nu_\mu + X$;
- 33.0% of $t\bar{t} \to \mu\nu_\mu + e\nu_e + X$;
- 25.7% of $t\bar{t} \to \mu\nu_\mu + \tau\nu_\tau + X$;
- 2.19% of $t\bar{t} \to e\nu_e + \tau\nu_\tau + X$;
- 0.92% of $t\bar{t} \to X$ or the fully hadronic decay channel;

where X denotes colored partons. The first two decay channels contain on the hadronic side a fully hadronic decay of a top quark, and hence contain the same information about its mass as the signal $t\bar{t} \to bq\bar{q}\bar{b}\mu\nu_\mu$ channel. All others give by construction a biased top quark mass information. About $\frac{2}{3}$ of the selected events in the other $t\bar{t}$ channels reflect a di-leptonic topology with one of the leptons being a muon, while only about $\frac{1}{3}$ reflect a semi-leptonic decay with a τ lepton wrongly identified as a muon candidate. The fraction of fully hadronic $t\bar{t}$ events selected is negligible, illustrating that the influence of QCD produced jet events is minor. This fraction is further reduced by the topological cuts described in the next Sections.

3.4.2. Selection of the correct $t\bar{t}$ *decay channel* To reduce the amount of events produced via a different $t\bar{t}$ decay channel in the selected event sample, three observables are constructed:

- the transverse momentum of the selected muon candidate;

- the transverse momentum of the lepton candidate with the second largest likelihood ratio variable in the list of reconstructed lepton candidates in the event;
- the smallest transverse energy among the four leading jets.

The distribution of these observables are shown in Figure 20 together with the likelihood ratio defined as $S/(S+B)$ where S are the $t\bar{t}$ semi-leptonic muon decays and B all other $t\bar{t}$ decay channels. The dependency of $S/(S+B)$ is fitted as a function of the three observables defined above. The information of the three likelihood ratios is combined into a combined likelihood by multiplication. The distribution of the combined likelihood L_{sign} is shown in Figure 21. From these distributions a probability is determined for the selected event to be a semi-leptonic muon $t\bar{t}$ event. In the event selection an extra sequential cut is applied by requiring this probability P_{sign} to exceed 0.8. The efficiency of this extra cut is shown in Table 15. In the selected event sample 14% of the semi-leptonic muon events are rejected, while 36% of the other $t\bar{t}$ events are removed.

3.4.3. Jet combinations When the event has been selected as described above, it will have 4 reconstructed jets with a transverse energy exceeding 30 GeV and a muon with a transverse momentum exceeding 20 GeV/c.

Among the four reconstructed jets, three have to be choosen to form the hadronic decaying top quark. The efficiency or purity of this selection was largely enhanced by applying a likelihood ratio method combining the information from several sensitive variables. The event selection requires exactly two jets with a b-tag probability above 0.6 and two below 0.4. This classification is used to define the two light quark jets from the hadronic W boson decay, and reduces the possible combinations to two.

For each jet combination a constraint kinematic fit was applied as described in [14] forcing the correct W boson mass, M_W, for the hadronic decaying W boson in the event. Before applying the kinematic fit the energy scale of the light quark jets are corrected for an overall bias in the reconstructed W boson mass. Following the method described in [15] after the event selection mentioned above, an inclusive jet energy scale correction of -9.7% was obtained and applied to light quark jet candidates. The reconstructed hadronic W boson mass spectrum before and after applying this correction in shown in Figure 24. The energy scale of the jets defined with a b-quark flavour is unchanged.

The jet objects are parametrized as (E_T, η, ϕ) objects with a fixed mass equal to zero. The resolution of the jet kinematic variables are differentiated as a function of their transverse energy. In Figure 25 the dependency is shown. In general the angular resolution and the relative resolution on the tranverse energy improves when the jet has a larger transverse energy.

Within an event only jet combinations are considered with a probability of the kinematic fit calculated from its χ^2/ndf exceeding 0.2. For some events non of the jet combinations fulfill this criterium, therefore reducing the total event selection efficiency.

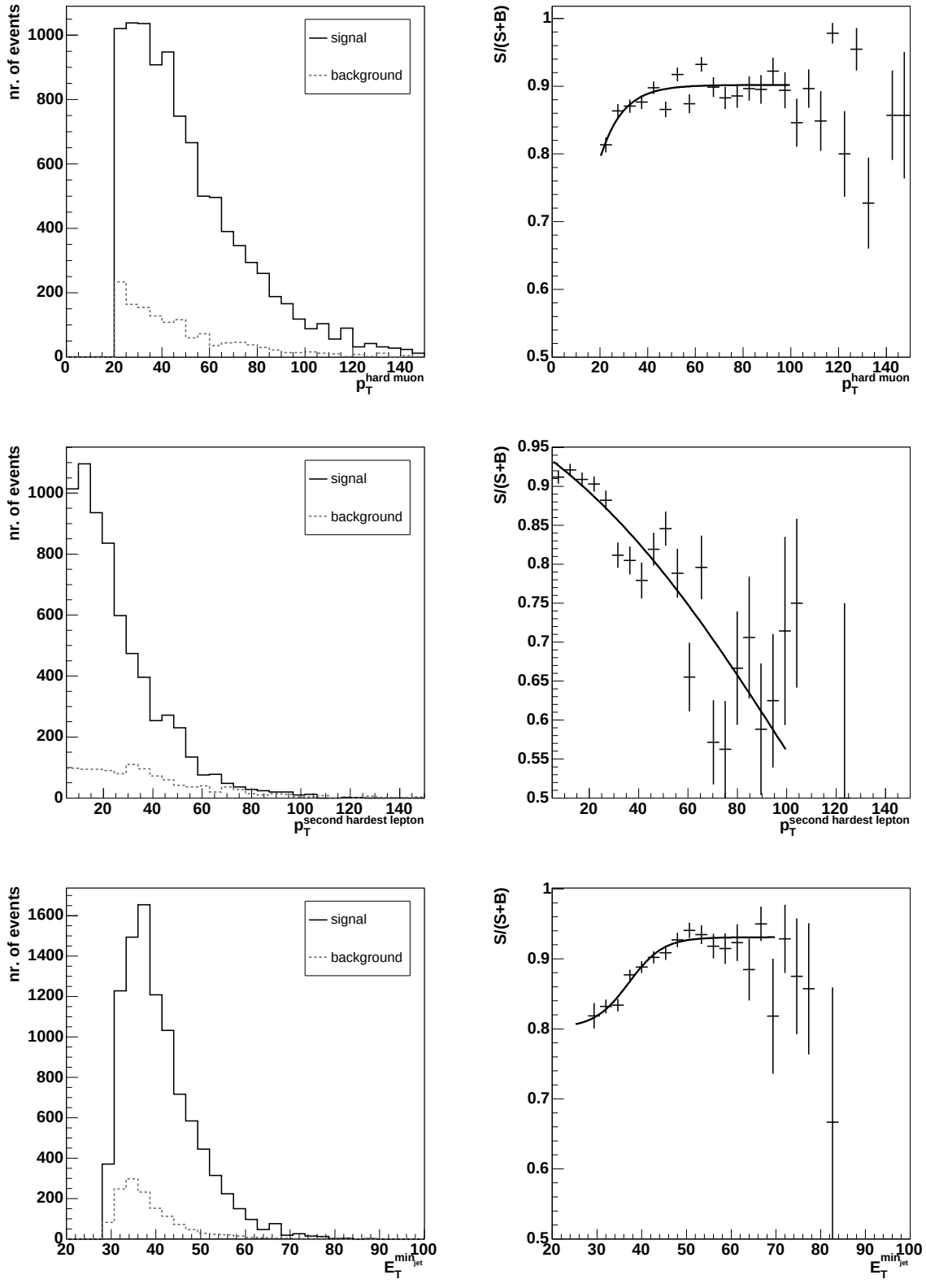

Figure 20. Distributions of the observables used to select the correct $t\bar{t}$ decay channel (left) and the corresponding likelihood ratios (right).

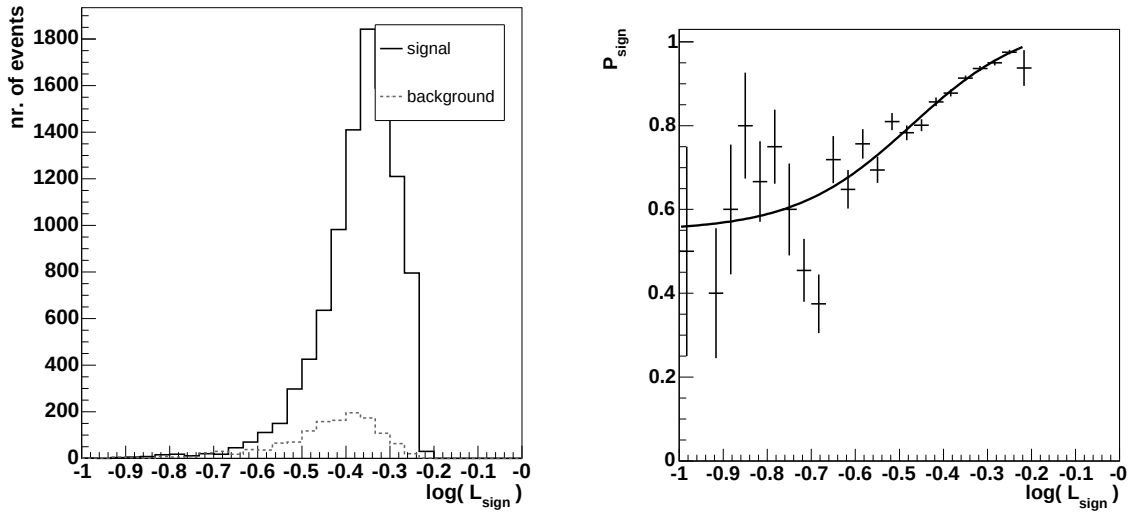

Figure 21. Distribution of the combined likelihood value for signal semi-leptonic $t\bar{t}$ decays and background other $t\bar{t}$ decays , and for the same events the relation between the combined likelihood variable L_{sign} and the probability P_{sign} (= S/(S+B)) for the choosen combination to be signal (right).

Additional the information of several observables is used to select which of the two b-quark jets combines with the hadronic W boson to a top quark

- $\Delta R(b_{lep}, l)$: angle in an (η, ϕ)-metric between the b-quark jet from the leptonic top quark decay and the lepton;
- ΔQ : combined electric charge observable defined as the charge of the lepton multiplied by the difference in jet; charge of the b-quark jets from respectively the hadronic and leptonic top quark decay;
- $p_T^{top} / < p_T^{top} >$: magnitude of the reconstructed transverse momentum of the hadronic top quark in this jet combination relative to the average of the transverse momentum of the top quarks over all possible jet combinations in the event;
- $\Delta R(b_{had}, W_{had})$: angle in an (η, ϕ)-metric between the b-quark jet and the reconstructed W boson direction both from the hadronic top quark decay.

For the signal $t\bar{t}$ events the distributions of these variables are shown in Figures 22 and 23. The information of the observables is combined via a likelihood ratio method similar to the one described in [20].

The distribution of the combined likelihood ratio L_{comb} is shown in Figure 26 for both the correct and wrong jet combinations in agreement with the above criteria for events containing a correct combination. In Figure 27 this is plotted for all jet combinations. If no jet combination in the event matches the generated true

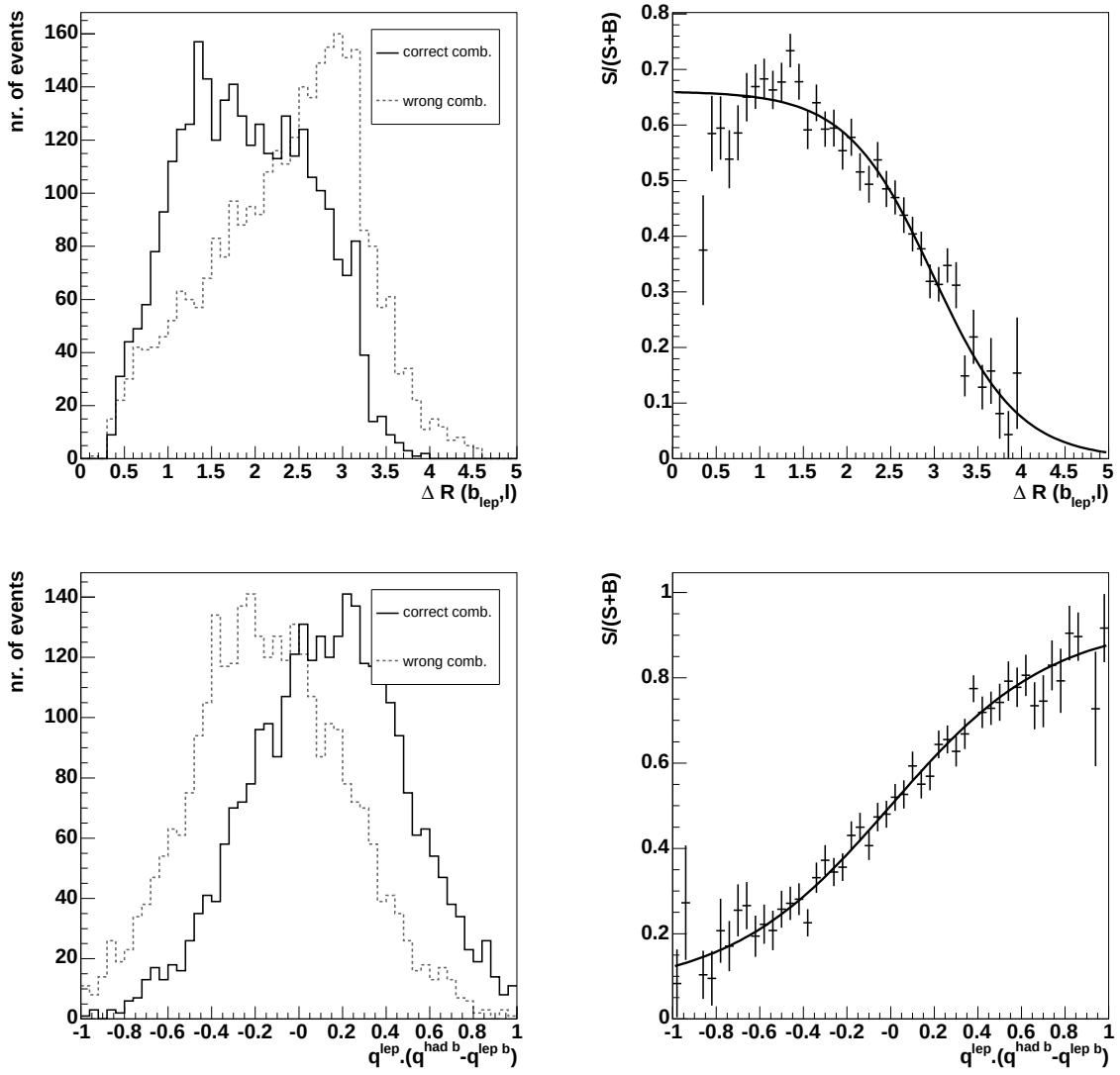

Figure 22. Distributions of the observables used to select the correct jet combination from the signal $t\bar{t}$ events (left) and the corresponding likelihood ratios (right).

combination, all possible jet combinations of the event were treated as combinatorial background. The jet combination with the largest L_{comb} value was taken as the best pairing. The L_{comb} value is transformed into a probability P_{comb} for the choosen combination to be the correct one, as shown in Figure 26. In a window of 25 GeV/c^2 around the expected top quark mass of about 175 GeV/c^2, the purity was above 76.6%. The event probability P_{comb} is used in the event selection where events are selected if their value for P_{comb} exceeds P^{cut}_{comb}. Relative to the events remaining after the event selection the efficiency and purity of this sequential cut is shown in Figure 27, where a scan is made over the full range of P^{cut}_{comb}. When considering only events for which the

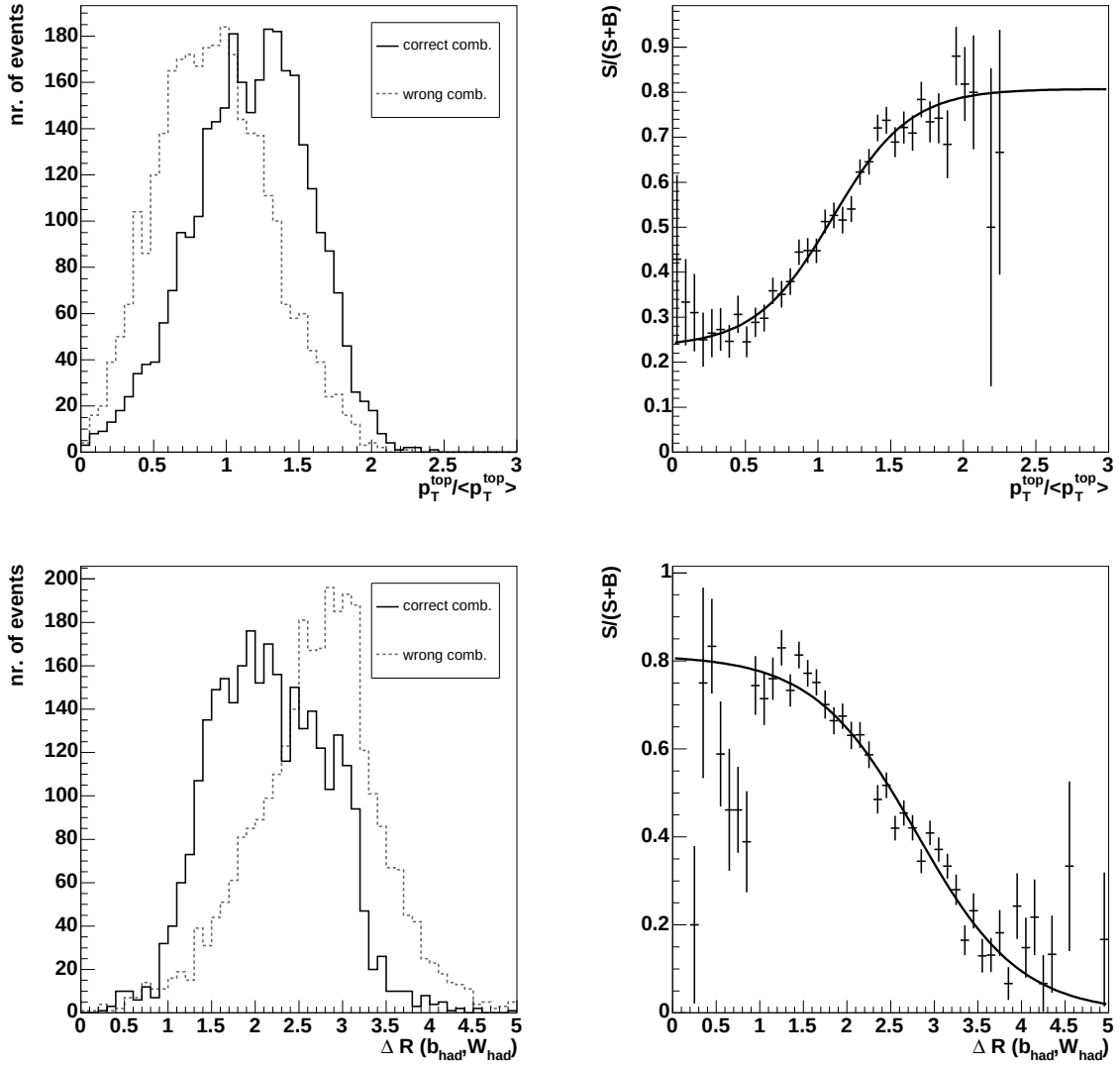

Figure 23. Distributions of the observables used to select the correct jet combination from the signal $t\bar{t}$ events (left) and the corresponding likelihood ratios (right).

best pairing has a probability P_{comb} larger than P_{comb}^{cut}=60%, the purity of the selected jet pairings is increased to 81.6%. The impact of this selection cut is illustrated in Figure 28 and mentioned in Table 15.

The jet combination procedure described results in a unique value for the hadronic top quark mass for each selected event. This is shown for true jet combinations in Figure 29 both before and after applying the kinematic fit. When estimating the top quark mass, M_t, from the selected event sample via the estimator $\hat{m}_t$ of a simple Gaussian fit, $G(m_t|\hat{m}_t)$, in a range of 20 GeV/c^2 in both directions around the modal bin, a value of $\hat{m}_t^{before} = 176.5 \pm 0.65$ GeV/c^2 is obtained before applying the kinematic fit and $\hat{m}_t^{after}$

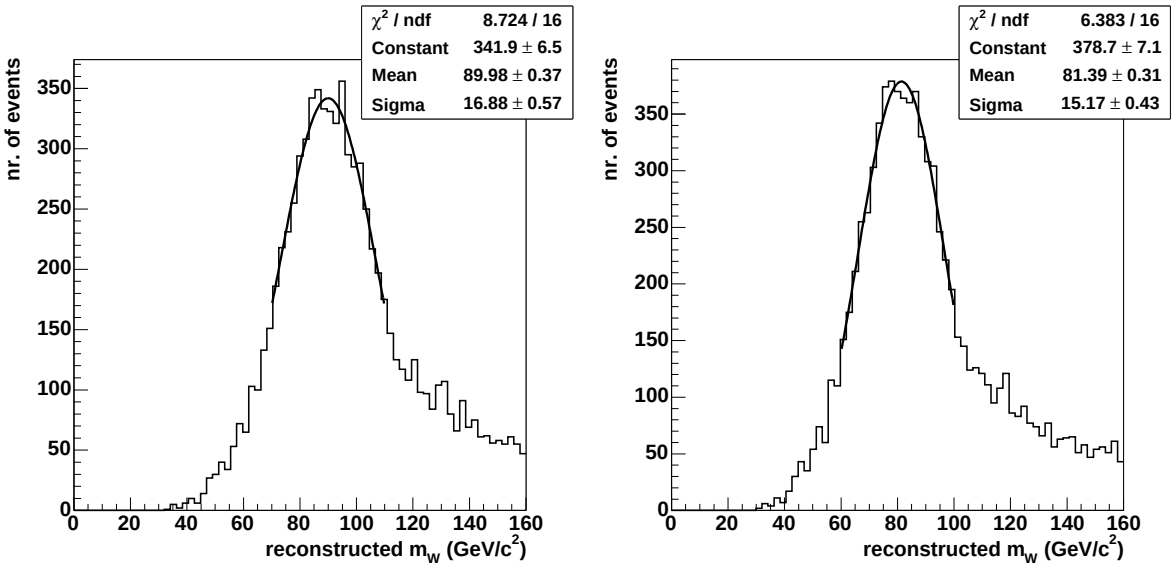

Figure 24. For the selected events the distribution of the reconstructed hadronic W boson mass before (left) and after (right) applying the post-calibration corrections on the energy scale of the light quark jets.

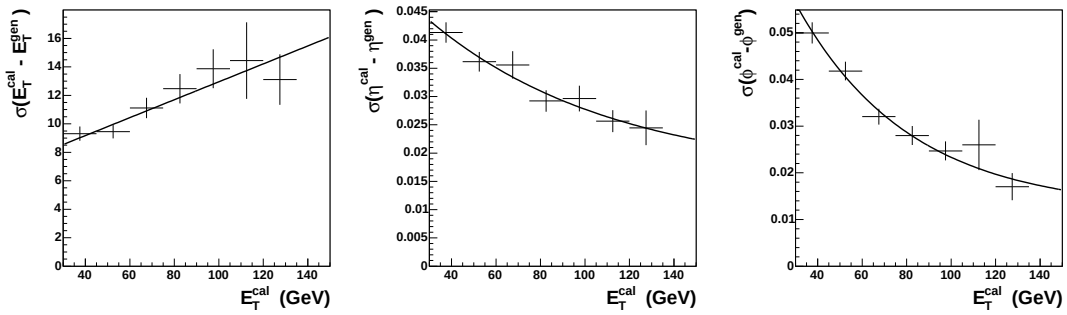

Figure 25. As a function of the transverse momentum, the applied Gaussian resolution on the variables (E_T, η, ϕ) of the parametrized jet objects.

$= 172.2 \pm 0.48$ GeV/c^2 after applying the kinematic fit. The estimator $\hat{m}_t^{\text{before}}$ would obtain the same statistical precision as $\hat{m}_t^{\text{after}}$ when it is applied on a data sample with an increased number of events by a factor 2, hence collecting twice as much data. The width of the top quark mass distribution is reduced from 15.0 GeV/c^2 to 13.0 GeV/c^2 when applying the kinematic fit. The top quark mass after the kinematic fit is shown in Figure 30 for all relevant processes contributing to the selected event topology.

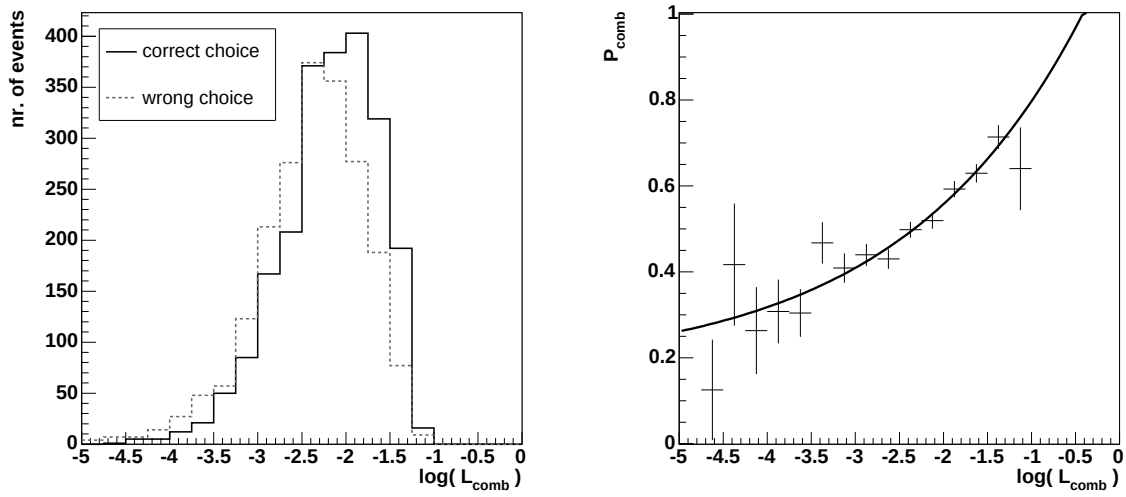

Figure 26. Distribution of the combined likelihood value for the chosen correct and wrong jet combinations of the signal $t\bar{t}$ events containing a correct combination (left), and for the same events the relation between the combined likelihood variable L_{comb} and the probability P_{comb} (= S/(S+B)) for the choosen combination to be the correct one (right).

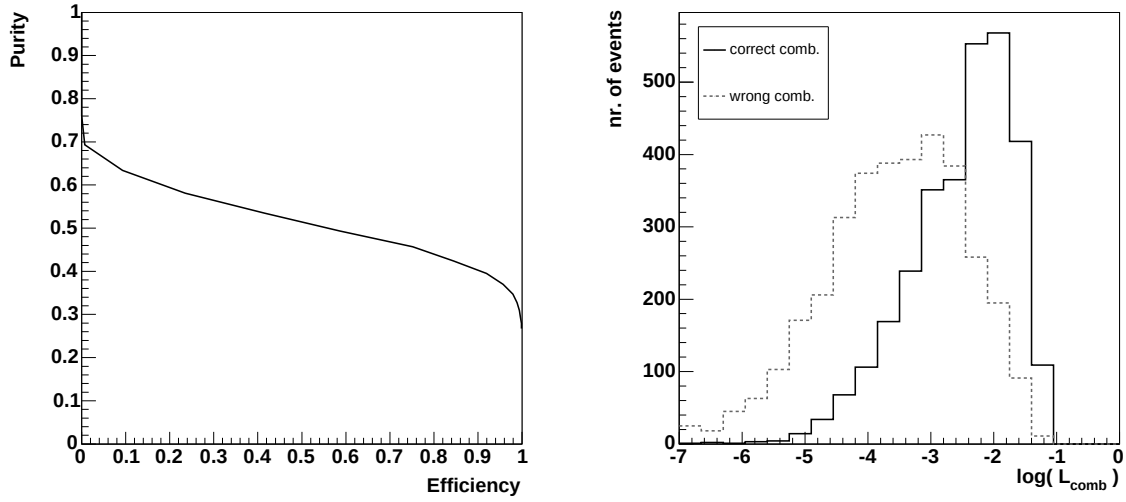

Figure 27. Efficiency for selecting the correct jet pairing and purity with respect to wrong jet pairings relative to the events remaining after the event selection (right), after applying the sequential cut on P_{comb}. A full scan is made over the cut value P^{cut}_{comb} as described in the text. Distribution of the combined likelihood value for all correct and wrong jet combinations of the signal $t\bar{t}$ events (left).

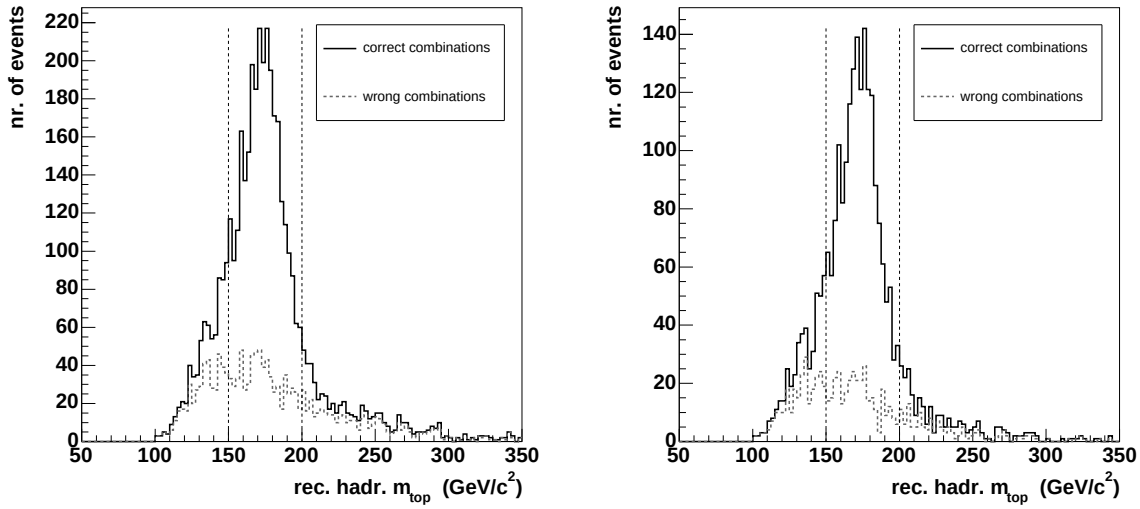

Figure 28. For signal $t\bar{t}$ events only, the distribution of the mass of the hadronic decaying top quark before (left) and after (right) applying the 60% cut on the best pairing probability P_{comb}.

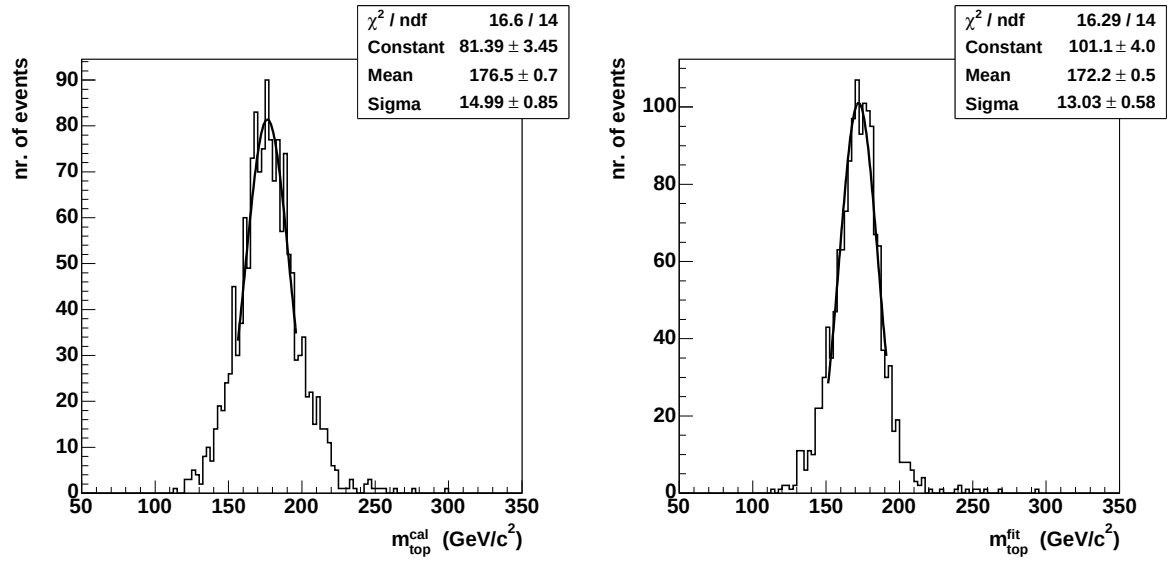

Figure 29. Distribution of the mass of the hadronic decaying top quark before (left) and after (right) applying the kinematic fit forcing the W boson mass to its precise measured value.

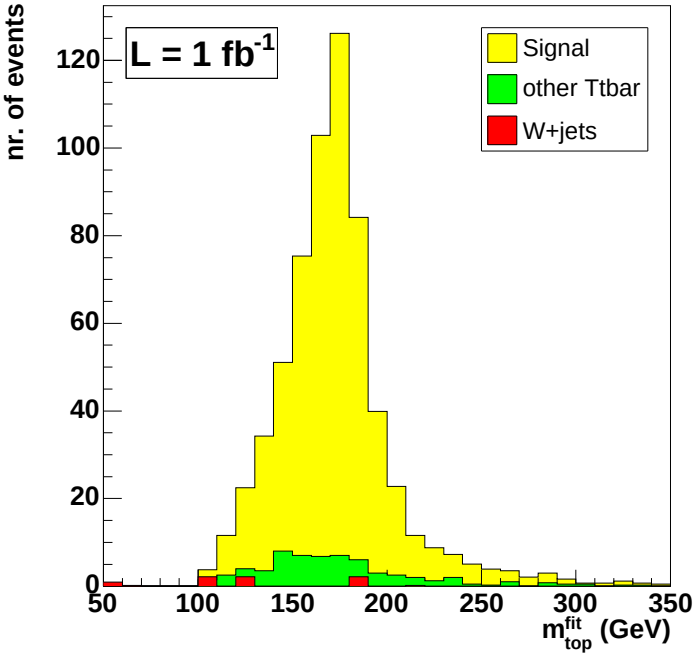

Figure 30. Distribution of the mass of the hadronic decaying top quark for the selected events after applying the kinematic fit. The contribution of all relevant background processes is shown.

.

3.4.4. Construction of the events ideogram Rather than developing top quark mass estimators on samples of events, an event-by-event likelihood approach is pursued. The fitted kinematics of the three jets connected to the hadronic decaying top quark are used to determine the top quark mass. From the covariance matrices of the kinematics of these three fitted jets the uncertainty on the top quark mass can be determined for each event via error propagation. The result can be written as

$$\chi^2(\{\overline{p}_j\}|m_t) = \left(\frac{m_t - m_t^{fit}}{\sigma_{m_t}^{fit}}\right)^2 \tag{15}$$

for the measured event kinematics $\{\overline{\mathrm{p}}_\mathrm{j}\}$ of the reconstructed event to agree with a reconstructed top quark mass $\mathrm{m_t}$ given the result from the kinematic fit as $\mathrm{m_t^{fit}}$ and the uncertainty $\sigma_{\mathrm{m_t}}^{\mathrm{fit}}$. This χ^2 variable can be transformed into a probability as

$$P(\{\overline{p}_j\}|m_t)\ dm_t \ \sim\ exp\left(-\frac{1}{2}\cdot\chi^2(\{\overline{p}_j\}|m_t)\right) \tag{16}$$

where $\mathrm{P}(\{\overline{\mathrm{p}}_\mathrm{j}\}|\mathrm{m_t})$ represents the resolution function or likelihood ratio mapping of the event in the space of the reconstructed top quark mass $\mathrm{m_t}$. It is often called an ideogram

of the event [32]. It reflects the relative compatibility of the reconstructed kinematics of the event with the hypothesis that one heavy object with mass m_t decays into three jets of which two originate from the W boson.

This probability scan $P(\{\overline{p}_j\}|m_t)$ can also be determined explicitly by forcing a reconstructed top quark mass to the event in the kinematic fit. The hypothesis of a Gaussian resolution function on the fitted top quark mass is not needed in this approach, but the computing time is increase by a large factor. In Figure 31 the one-dimensional ideogram is shown for several selected events, and as an illustration a comparison is made between both approaches. For the results below both the parametrized and the full probability scan are used. In the discussion of the systematic uncertainties the advantage of each is illustrated.

When applying the full probability scan for the ideogram $P(\{\overline{p}_j\}|m_t)$, the event is only selected if the largest probability provided by the kinematic fit exceeds 0.2 in the relevant mass range $125 < m_t < 225$ GeV/c^2.

Only for the comparison of the parametrized and the full ideogram, the maximum of the function $P(\{\overline{p}_j\}|m_t)$ is fixed at unity. The width of the full ideogram is narrower compared to the parametrized ideogram. The covariance matrix of the fitted b-quark jet was used to determine the full ideogram, while its covariance matrix at the reconstruction level was used for the parametrized ideogram. This could induce the observed difference between the parametrized and full ideograms.

3.4.5. Top quark mass estimator As the amount of W + jets events in the selected event sample is neglegible, the are not considered in the estimation of the top quark mass.

To obtain information about the true value of the top quark mass M_t we convolute the reconstructed ideogram with the theoretical expected probability density function $P(m_t|M_t)$ in the reconstruction space

$$\mathcal{L}_i(M_t) = \int P(\{\overline{p}_j\}|m_t) \cdot P(m_t|M_t)\ dm_t \tag{17}$$

where one integrates over the kinematic relevant range of m_t to obtain a likelihood function $\mathcal{L}_i(M_t)$ for each event i in the true top quark mass dimension. Several contributions should be added in the expected density $P(m_t|M_t)$: a Breit-Wigner shape for the correct jet combinations $S(m_t|M_t)$, a parametrized combinatorial background contribution $B_{comb}(m_t)$ and a parametrized process background contribution $B_{proc}(m_t)$. This results in a function

$$P(m_t|M_t) = P_{sign} \cdot [P_{comb} \cdot S(m_t|M_t) + (1 - P_{comb}) \cdot B_{comb}(m_t)] + (1 - P_{sign}) \cdot B_{proc}(m_t) \tag{18}$$

where each contribution is weighted according to the probabilities extracted from the observed event. The probability P_{comb} is determined for each selected event as the likelihood ratio value provided by L_{comb}, see Figure 26. The probability P_{sign} is

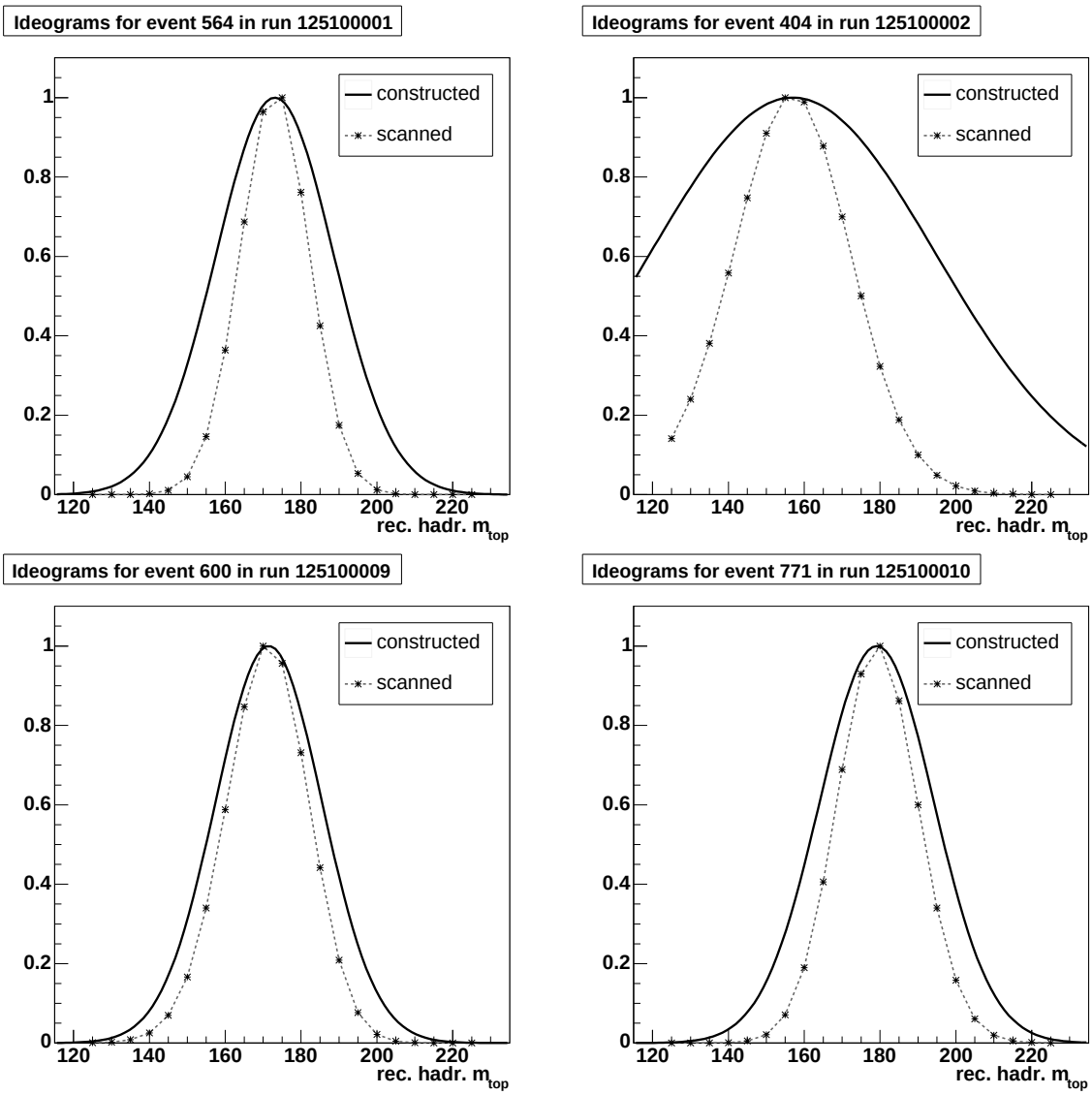

Figure 31. For some typical selected signal $t\bar{t}$ events the reconstructed ideogram from both a kinematic fit where M_t is free (full line) and a complete scan over several top quark mass hypotheses (dashed line).

determined according to the combined likelihood ratio shown in Figure 21. The two background contributions do not depend (in first order) on the value of M_t. The possible effect of an M_t dependency of $B_{proc}(m_t)$ for process background from other $t\bar{t}$ final states is included as a systematic uncertainty.

After combining the likelihoods $\mathcal{L}_i(M_t)$ from all selected events, a maximum likelihood method is applied to obtain the best value for the estimator $\hat{M}_t$. The linearity of the estimator has been checked and illustrated in Figure 32. The slope of the curve of the measured versus the generator top quark mass is found to be 0.86 ± 0.18 for the

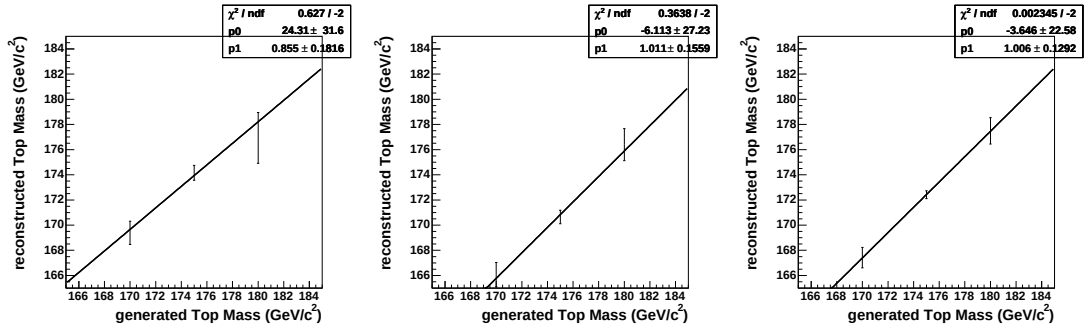

Figure 32. Estimated top quark mass versus the generated top quark mass used in the event generator. Left: simple Gaussian fit, middle: parametrized ideogram, right: full ideogram.

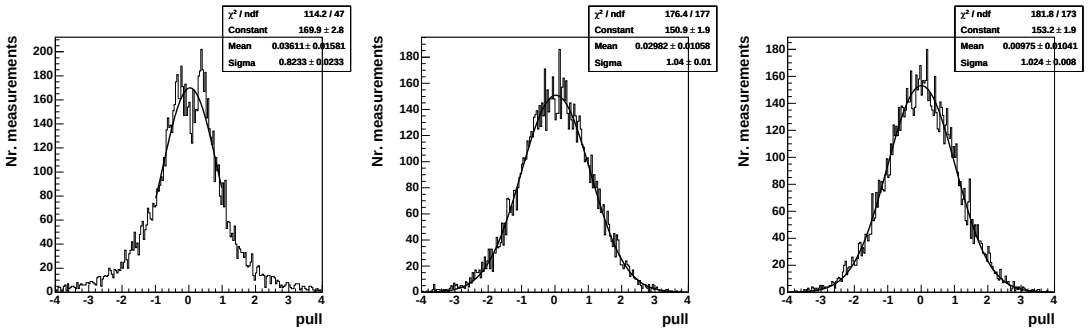

Figure 33. Pull distribution of the different top quark mass estimators $\hat{m}_t$. Similar order as in Figure 32.

simple $\hat{M}_t^{fit}$ estimator fitting a Gaussian function on the reconstructed m_t distribution in the range of 30 GeV/c^2 around the modal bin. This becomes 1.01 $\pm$ 0.16 for the $\hat{M}_t^{ParIdeo}$ estimator using the parametrized ideogram and 1.01 $\pm$ 0.13 for the $\hat{M}_t^{FullIdeo}$ estimator using the full ideogram. It is observed that these slopes are compatible with unity.

The width of the pull distribution of the top quark mass estimators $\hat{M}_t$, shown in Figure 33, are found to be 0.82 for $\hat{M}_t^{fit}$, 1.04 for $\hat{M}_t^{ParIdeo}$ and 1.02 for $\hat{M}_t^{FullIdeo}$. The resulting statistical uncertainty on the estimators $\hat{M}_t$ is rescaled with this number. The resulting top quark mass for the estimator $\hat{M}_t^{fit}$ applied on the simulated events samples with a generated top quark mass of 175 GeV/c^2 is 174.16 $\pm$ 0.59 GeV/c^2, hence reflecting a bias of -0.84 GeV/c^2. For the convolution method this is 170.65 $\pm$ 0.54 GeV/c^2 and 172.42 $\pm$ 0.31 GeV/c^2 for respectively the $\hat{M}_t^{ParIdeo}$ and the $\hat{M}_t^{FullIdeo}$ estimator, reflecting respectively biases of -4.35 GeV/c^2 and -2.58 GeV/c^2. The statistical uncertainties mentioned are corrected to obtain a pull distribution with a width equal to unity.

	Gaussian Fit	Gaussian Ideo	Full Scan Ideo
Bias (GeV/c^2)	-0.84±0.59	-4.35±0.54	-2.58±0.31
Pull	0.82	1.01	1.01
Exp. uncertainty for 1fb^{-1} (GeV/c^2)	1.01	1.14	0.66
Exp. uncertainty for 10fb^{-1} (GeV/c^2)	0.32	0.36	0.21

Table 16. Overview of the statistical properties of the three top quark mass estimators defined in the text. The expected uncertainty quoted is rescaled for a non-unity pull.

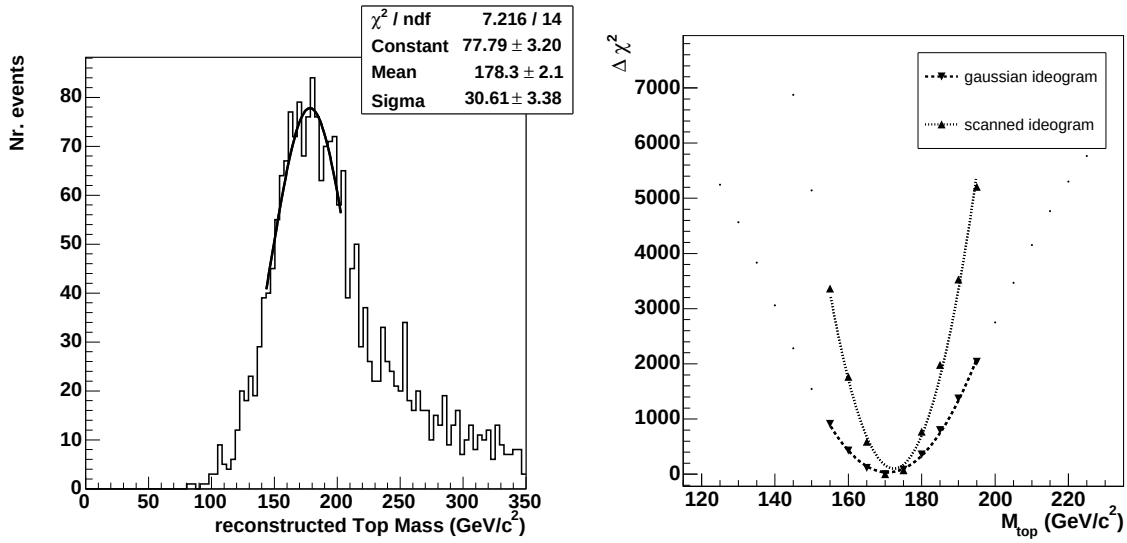

Figure 34. Distribution of the mass of the hadronic decaying top quark before the kinematic fit used for the $\hat{M}_t^{fit}$ estimator (left) and the combined $\Delta\chi^2(M_t)$ function over all events for both ideogram based estimators $\hat{M}_t^{ParIdeo}$ and $\hat{M}_t^{FullIdeo}$ (right).

These numbers together with the expected statistical uncertainty on the top quark mass estimators with semi-leptonic $t\bar{t}$ (the lepton being a muon) for both 1 and 10 fb^{-1} of integrated luminosity are shown in Table 16. Figure 34 shown the distribution for the simple Gaussian fit top quark mass estimator together with the combined likelihood curves for the ideogram based estimators. The $\Delta\chi^2(M_t)$ curves are fitted with a parabol in the region of ±20 GeV/c^2 around the minimum.

In the convolution method described only one event reconstruction hypothesis is taken into account. For example only one definition is taken into account of the jets, the lepton and the missing transverse energy, and the information of only one jet combination is used. As an extension of the convolution method several event reconstruction hypotheses h_k can be included. The ideogram $P(\{\overline{p}_j\}|m_t, h_k)$ can be constructed for several jet combinations, or for several jet clustering algorithms. The

combined event ideogram $P(\{\overline{p}_j\}|m_t, \{h_k\})$ would be a sum or weighted sum of the individual ideograms of each element k in the set of event reconstruction hypotheses $\{h_k\}$. This strategy is to be followed in the future when optimizing the analysis results for systematic uncertainties.

3.4.6. Systematic uncertainties Several systematic effects could induce an uncertainty on the top quark mass estimator. They originate from our understanding of the detector performance, the robustness of the reconstructed objects, for example jets, and the general description of the proton collisions in the simulation. For the theoretical or phenomenological uncertainties the prescription of [17] was used.

As mentioned below the effect of the background processes on the top quark mass estimator is small. Therefore the systematic effects described are only introduced in the signal events as the same effect in the background processes would only be a second order effect.

To enhance the correlation between the sample with and the sample without the systematic effect, the same generated events are used in the simulation of both samples. The Jackknife method is applied to take this correlation into account when estimating the uncertainty on the difference in top quark masses from both samples being Δm_t. Starting from a sample of N measurements $\tilde{x}$, the Jackknife begins by throwing out the first measurement x_1, leaving a Jackknived data set of $N-1$ values. The statistical analysis in performed on the reduced sample, giving a measured value of a parameter $\Delta m_t^{Jack,1}$. The process is repeated for each measurement i in the sample, resulting in a set of parameter values $\{\Delta m_t^{Jack,i} \mid i \in \{1, ..., n\}\}$. The standard uncertainty on the parameter, being $\sqrt{Var[\Delta m_t]}$, estimated on the full sample of N measurements is given by the formula:

$$Var[\Delta m_t] = \frac{N-1}{N} \cdot \sum_{i=1}^{n} \left(\Delta m_t^{Jack,i} - \Delta m_t\right)^2 \tag{19}$$

where Δm_t is the result of inferring the parameter on the full sample. The advantage of using this method compared to other bootstrap techniques is that no knowledge is assumed about the underlying probability density function.

The systematic effects are determined on the three estimators described above: a simple Gaussian fit on the reconstructed top quark mass spectrum, a convolution technique with a Gaussian parametrization of the ideogram and a convolution technique with a full probability scan. The advantages of the choice for the latter are demonstrated.

If the systematic effect on the top quark mass is compatible with zero within its statistical uncertainty, then for this systematic effect as summarized in Table 25 a number is quoted which corresponds to the statistical presicion of the test. The components which are dominated by their precision are denoted by $*$ in Table 25.

- Pile-Up description

	Gaussian Fit Δm_t (GeV/c^2)	Gaussian Ideo Δm_t (GeV/c^2)	Full Scan Ideo Δm_t (GeV/c^2)
30% Δm_t(no pile up − with pile up)	-1.9±0.4	-1.4±0.4	-1.2±0.3

Table 17. Effect of the primary vertex constrain on the systematic uncertainty due to pile-up collisions.

	Gaussian Fit Δm_t (GeV/c^2)	Gaussian Ideo Δm_t (GeV/c^2)	Full Scan Ideo Δm_t (GeV/c^2)
$\frac{1}{2}$ Δm_t(PARP(82) = 2.4 − PARP(82) = 3.4)	-1.0±0.2	-0.7±0.2	-0.5±0.1

Table 18. Systematic uncertainty due to the underlying event.

On the same simulated event samples as used for the systematic uncertainty on the cross section estimator, the effect of pile-up collisions on the top quark mass estimators is evaluated. The difference in the estimated top quark mass is determined and the values obtained for the three estimators are shown in Table 25. It is shown that the convolution methods with the parametrized or the full ideogram are less sensitive to the present of pile-up collisions. The effect is reduced with a factor 2 compared with the simple to quark mass estimator $\hat{M}_t^{fit}$. The systematic uncertainty is defined as 30% of the observed shift when neglecting pile-up collisions completely.

- Underlying event
  Similar to the underlying event effect on the cross section estimator, the effect is determined for the top quark mass estimators. Half of the difference on the top quark mass between both samples is taken as a systematic uncertainty. This estimation is conservative as the 3σ confidence interval for the color screening p_T cut-off value is used to obtain a 1σ systematic uncertainty of the top quark mass estimator.
- Jet energy scale
  Following the procedure of Section 3.3.4 the effect of the uncertainty on the jet energy scale is evaluated for the top quark mass estimators. A non-zero value of α was applied before the event selection and before the kinematic fit, resulting in a systematic shift on the value of the inferred top quark mass shown in Figure 35 and Figure 36, respectively for a light and heavy quark jet energy scale shift. The effect is shown for the three top quark mass estimators described above.
  In the reconstruction of the top quark both light and heavy quark jets are included, hence the effect of including both systematic shifts most be combined. The effect

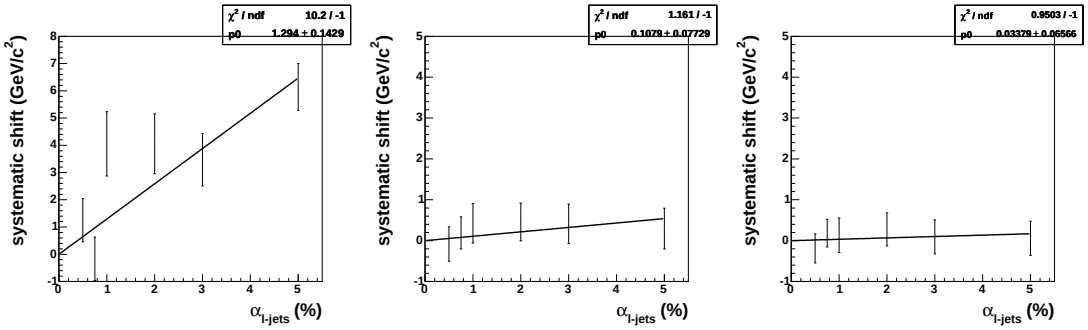

Figure 35. Estimated shift in the top quark mass versus a shift α applied on the inclusive light quark jet energy scale. This is shown for the three different top quark mass estimators: gausian fit (left), gaussian ideogram (middle) and full scan ideogram (right).

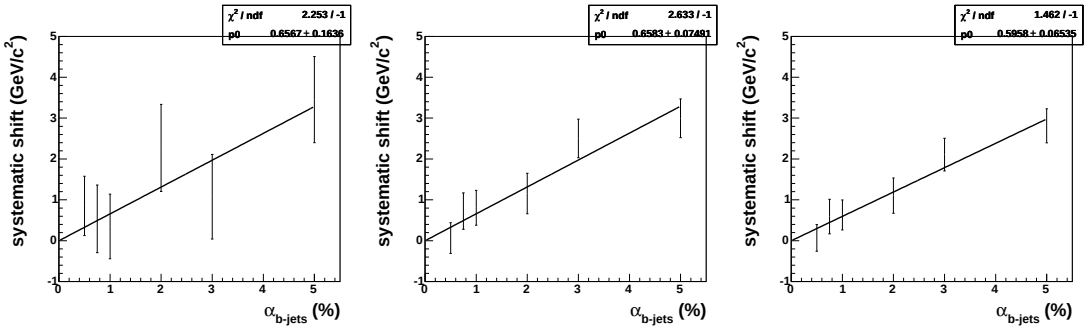

Figure 36. Estimated shift in the top quark mass versus a shift α applied on the inclusive heavy quark jet energy scale. This is shown for the three different top quark mass estimators: gausian fit (left), gaussian ideogram (middle) and full scan ideogram (right).

of applying the same value of α for both light and heavy quark jets is shown in Table 19. The effect due to the light quark jet energy scale is only present in the case of the simple Gaussian fit estimator as the m_W inclusive calibration was not applied for this estimator. As the m_W inclusive calibration only influences the light quark jet energy scale, this large differentiation between the estimators is not present for the heavy quark jet energy scale systematics.

The potential uncertainty on the inclusive jet energy scale for light quark jets is estimated to be around 3% with 1 fb^{-1} of accumulated data and could reach 2% with 10 fb^{-1} [15]. As the analysis described in this paper focusses on data sets with a larger integrated luminosity a value of 2% systematic uncertainty on the inclusive jet energy scale was taken as a benchmark. The estimated systematic uncertainties

	Gaussian Fit Δm_t (GeV/c^2)	Gaussian Ideo Δm_t (GeV/c^2)	Full Scan Ideo Δm_t (GeV/c^2)
3% light quarks JES shift (1fb^{-1})	3.6±0.6	0.32±0.23	0.10±0.20
2% light quarks JES shift (10fb^{-1})	2.4±0.2	0.22±0.08	0 08±0.07
3% heavy quarks JES shift (1fb^{-1})	2.0±0.5	2.0±0.2	1.8±0.2
2% heavy quarks JES shift (10fb^{-1})	1.4±0.2	1.3±0.07	1.2±0.07

Table 19. Systematic uncertainties due to a 3% and 2% systematic uncertainty on the inclusive jet energy scale of both light and heavy quark jets.

	Gaussian Fit Δm_t (GeV/c^2)	Gaussian Ideo Δm_t (GeV/c^2)	Full Scan Ideo Δm_t (GeV/c^2)
$\frac{1}{4}\ \Delta m_t(\Lambda_{QCD} = 0.35\text{GeV} - \Lambda_{QCD} = 0.15\text{GeV})$	-0.8±0.1	-0.27±0.08	-0.22±0.07
$\frac{1}{4}\ \Delta m_t(Q^2_{max} = 4Q^2_{hard} - Q^2_{max} = 0.25Q^2_{hard})$	0.6±0.1	0.06±0.09	-0.03±0.08

Table 20. Systematic uncertainties due to QCD radiation effects as described in the text. The values of Q^2_{max} are those for the initial state radiation, while those for the final state radiation are changed simultaneously according to the description in the text.

on the top quark mass for both the 1 and 10 fb^{-1} jet energy scale benchmarks are shown in Table 19. The systematic uncertainties of 2% on both the light and the heavy quark jet energy scale are combined linearly.

- Pertubative QCD Radiation
  Identical to the studies of pertubative QCD radiation effects for the cross section estimator, the resulting shifts in the three top quark mass estimators is shown in Table 20.
  For both parameters in the pertubative radiation the extreme shift in the top quark mass is determined, hence $\Delta m_t(\Lambda_{QCD} = 0.35\text{GeV} - \Lambda_{QCD} = 0.15\text{GeV})$ and $\Delta m_t(Q^2_{max} = 0.25Q^2_{hard} - Q^2_{max} = 4Q^2_{hard})$ where the Q^2_{max} value for the initial state radiation is changed (with corresponding changes in the Q^2_{max} value for the final state radiation). The systematic uncertainty is defined as the maximum of both shifts divided by four (a factor of two as both the negative and positive side around the central value are accounted for, and another factor of two to reduce this extreme shift to a more realistic interval).
- Hadronization
  When changing the parameters *Lund b* and σ_q as described in Section 3.3.4 from their central values to 2σ deviations, a shift is obtained on the inferred top quark

	Gaussian Fit Δm_t (GeV/c^2)	Gaussian Ideo Δm_t (GeV/c^2)	Full Scan Ideo Δm_t (GeV/c^2)
$\frac{1}{2}\ \Delta m_t(Lundb = 0.60 - Lundb = 0.44)$	0.2±0.2	0.1±0.2	0.0±0.2
$\frac{1}{2}\ \Delta m_t(\sigma_q = 0.46\text{GeV} - \sigma_q = 0.34\text{GeV})$	0.4±0.2	0.4±0.2	0.3±0.1

Table 21. Systematic uncertainties due to our knowledge of the fragmentation as described by the Lund string model implemented in PYTHIA.

	Gaussian Fit Δm_t (GeV/c^2)	Gaussian Ideo Δm_t (GeV/c^2)	Full Scan Ideo Δm_t (GeV/c^2)
L^B_{up}=70% and L^B_{lower}=40%	-0.1±0.5	0.1±0.4	0.2±0.3
L^B_{up}=65% and L^B_{lower}=40%	-0.1±0.3	0.5±0.3	0.3±0.2
L^B_{up}=55% and L^B_{lower}=40%	0.0±0.3	-0.4±0.2	-0.2±0.2
L^B_{up}=50% and L^B_{lower}=40%	-0.1±0.5	-0.9±0.4	-0.4±0.3
L^B_{up}=60% and L^B_{lower}=50%	0.8±0.5	0.4±0.3	0.4±0.3
L^B_{up}=60% and L^B_{lower}=45%	0.8±0.4	0.1±0.3	0.1±0.2
L^B_{up}=60% and L^B_{lower}=35%	0.0±0.4	0.2±0.3	0.0±0.2
L^B_{up}=60% and L^B_{lower}=30%	1.4±0.8	0.2±0.4	-0.2±0.4
L^B_{up}=70% and L^B_{lower}=50%	0.8±0.7	0.5±0.5	0.5±0.4
L^B_{up}=50% and L^B_{lower}=30%	1.3±0.9	-0.2±0.5	-0.3±0.5
L^B_{up}=70% and L^B_{lower}=30%	1.2±1.0	0.5±0.6	0.3±0.5
L^B_{up}=50% and L^B_{lower}=50%	1.0±0.7	-0.2±0.5	0.0±0.4

Table 22. Systematic uncertainties due to b-tagging algorithms.

mass. Simulating with FAMOS event samples in these different configurations results in shifts shown in Table 21. For both parameters the average shift from both directions is calculated. The systematic uncertainty is defined as the maximum of the averages of both parameters.

- Algorithms for b-tagging
  To illustrate the effect of the b-tagging algorithm on the estimated top quark mass, the b-tag criterium in the event selection was changed. Nominally exactly two jets are required to have a b-tag probability L^b above L^b_{up}=60% and two below L^b_{lower}=40%. These limits are changed relative the the nominal ones and the effect on the top quark mass estimators is shown in Table 22.
  For an uncertainty of 5% on the b-tag efficiency a corresponding shift in the applied b-tagging cuts in the dimension of the combined b-tag discriminant is determined. The inclusive distributions of the b-tagging discriminant are shown for the simulated

	Gaussian Fit Δm_t (GeV/c^2)	Gaussian Ideo Δm_t (GeV/c^2)	Full Scan Ideo Δm_t (GeV/c^2)
Other $t\bar{t}$ decays -20%	0.1±0.5	-0.1±0.4	-0.2±0.4
Other $t\bar{t}$ decays +20%	0.2±0.4	-0.4±0.4	-0.4±0.4

Table 23. Systematic uncertainties due to the scale of the background processes.

$t\bar{t}$ events in Figure 15 for different quark flavours. In the event selection the criteria L^B_{up}=70% corresponds to a combined b-tag discriminant value of about 1.0. In order to select 5% more b-quarks in a jet sample, this cut-value of the discriminant should shift from 1.0 to 0.74, corresponding according to Figure 15 (right) to a value of L^B_{up} equal to 65%. Assuming a linear dependency between L^B_{up} and the b-tagging discriminant in the relevant region around the value L^B_{up}=60%, it is therefore concluded that the 5% uncertainty in the estimate of the b-tagging efficiency transforms into a 5% change in the value of L^B_{up}. The systematic uncertainty due to the b-tagging algorithms is defined as the average of the relative shifts on the top quark mass estimators when changing L^B_{up} from 60% to both 55% and 65%.

- Background processes
  To estimate the effect of the other $t\bar{t}$ background processes, the individual event weight for these background events is rescaled from unity to 1.2 or 0.8 reflecting a change of ± 20% in the cross-section of the process involved. The effect on the top quark mass estimators is shown in Table 23. It is found to be neglegible for each of the three top quark mass estimators. As it is expected that W + jets and QCD processes have a negligible contribution after the event selection, it is assumed that their influence on the top quark mass estimators is negligible.
- Parton density function
  The procedure described in Section 3.3.4 results in 40 shifts Δm_t^j from the central value of m_t^c, as shown in Figure 37. The typical uncertainty on the difference between the top quark mass inferred from the central set and the reweighted set is 0.02 GeV/c^2, hence significantly smaller than the shift on the mass itself. The actual effect due to the uncertainties arising from the `CTEQ` fits is determined via the following procedure :

$$(\Delta^+_{PDF} m_t)^2 = \sum_{j=1}^{20} \left(max\left[{m_t}^{j+} - {m_t}^c \ , \ {m_t}^{j-} - {m_t}^c \ , \ 0\right]\right)^2 \qquad (20)$$

and

$$(\Delta^-_{PDF} m_t)^2 = \sum_{j=1}^{20} \left(max\left[{m_t}^c - {m_t}^{j+} \ , \ {m_t}^c - {m_t}^{j-} \ , \ 0\right]\right)^2 \qquad (21)$$

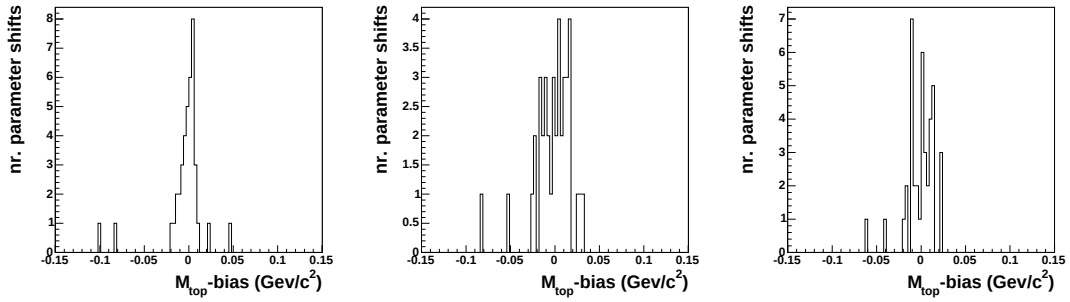

Figure 37. The 40 values of Δm_t obtained by applying the three top quark mass estimators on the reweighted samples rather than the central sample as described in the text: simple Gaussian fit (left), Gaussian parametrized ideogram (middle) and full scanned ideogram (right).

	Gaussian Fit	Gaussian Ideo	Full Scan Ideo
$\Delta_{\rm PDF} m_t^+$ (GeV/c^2)	0.09 $\pm$ 0.02	0.08 $\pm$ 0.01	0.06 $\pm$ 0.01
$\Delta_{\rm PDF} m_t^-$ (GeV/c^2)	0.12 $\pm$ 0.02	0.10 $\pm$ 0.02	0.08 $\pm$ 0.02

Table 24. Systematic uncertainties due to the estimated uncertainties on the fitted parameters of the `CTEQ6M` parton distribution fits as described in the text.

where $m_t{}^c$ is the central top quark mass inferred from the `FAMOS` simulated event sample applying the central `CTEQ6M` fit. This procedure takes into account the sign of the correlation between the PDF parameters and the inferred observable of interest, in this case the top quark mass. The resulting systematic uncertainty, $\Delta^+_{\rm PDF} m_t$ and $\Delta^-_{\rm PDF} m_t$ are quoted in Table 24 . The largest of the two is taken as a systematic uncertainty.

- Reducing systematic uncertainties
  The largest systematic uncertainty originates from the definition of the 4-momenta of hadronical jets. In the analysis described only the Iterative Cone (IC) algorithm was applied, although several alternative clustering algorithms exist. The top quark mass estimator could be made more robust against systematic uncertainties when a set of different clustering algorithms result in the same direction of the four leading jets in the final state. The Midpoint Cone (MC) and the k_T (KT) algorithms are applied to the events, and angular deviations between the four selected leading jets are studied. These four jets are selected from those connected to the primary vertex and with the highest transverse momentum. All possible jet-to-jet pairings are made between the three different clustering algorithms, and the sum of the angular difference in an (η, ϕ)-metric is determined and denoted as $\alpha_{a,b}$ for the differences between jet clustering algorithm a and b. Among all jet-to-jet pairings

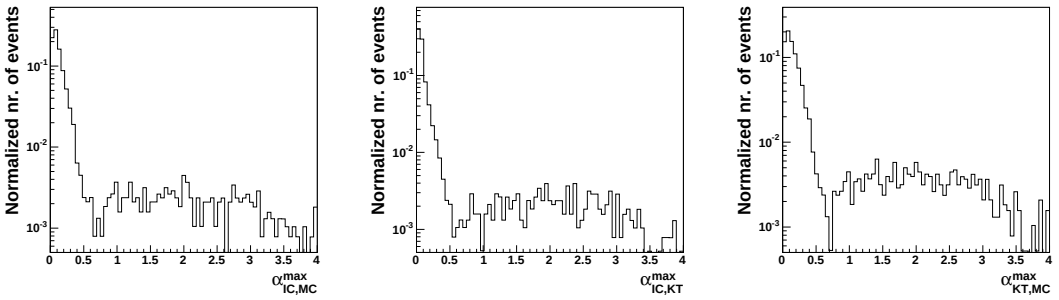

Figure 38. Values of $\alpha^{\max}_{\mathrm{IC,MC}}$ (left), $\alpha^{\max}_{\mathrm{IC,KT}}$ (middle) and $\alpha^{\max}_{\mathrm{MC,KT}}$ (right) as described in the text for the selected signal events.

within an event, the one resulting in the smallest value of $\alpha_{\mathrm{a,b}}$ is choosen. For that jet-to-jet pairing between events clustered with different algorithms, a single jet pair results in the largest distance in an (η, ϕ)-metric among the four pairs in the event, this distance is denotes as $\alpha^{\max}_{\mathrm{a,b}}$. In Figure 38 the values for $\alpha^{\max}_{\mathrm{IC,MC}}$, $\alpha^{\max}_{\mathrm{IC,KT}}$ and $\alpha^{\max}_{\mathrm{MC,KT}}$ are shown for the selected signal events. The four leading jets rather than the three from the hadronic top quark decay are considered to be independent of the jet combination method within an event.

For 85.7%, 87.5% and 78.1% of the selected signal events, the value of respectively $\alpha^{\max}_{\mathrm{IC,MC}}$, $\alpha^{\max}_{\mathrm{IC,KT}}$ and $\alpha^{\max}_{\mathrm{MC,KT}}$ is larger than 0.3. On the basis of this observation an alternative selection is proposed including an extra event selection cut which rejects those events where one of the values $\alpha^{\max}_{\mathrm{IC,MC}}$, $\alpha^{\max}_{\mathrm{IC,KT}}$ or $\alpha^{\max}_{\mathrm{MC,KT}}$ exceeds 0.3. The efficiency of this cut for the selected signal events is 76.1%. Applying the full scanned ideogram based top quark mass estimator on this sample of events, results in systematic uncertainties shown in Table 25.

The total systematic uncertainty on the top quark mass estimator is not significantly reduced from 1.9 GeV/c^2 for the standard event selection. When including the extra event selection cut on $\alpha^{max}_{a,b}$ where a and b are the Iterative Cone, Midpoint Cone or $\mathrm{k_T}$ clustering algorithm only a small improvement is observed on the systematic uncertainty from the knowledge of the jet energy scale. This improvement in not significant, but should be checked with larger simulated event samples.

- Combining systematic uncertainties

  The systematic uncertainties as described above are summarized in Table 25. Conservatively a total precision on the top quark mass of 1.9 GeV/c^2 can be reached. The uncertainty is dominated by systematic effects like pile-up collisions and the knowledge of the jet energy scale of b-quark jets. Upon a better understanding of the accelerator settings and the detector performance however this total uncertainty will reduce. When both in-time and out-of-time pile-up collisions will be monitored the residual uncertainty is provided by the uncertainties in the description of the

	Standard Selection			Altern. Selection
	Gaussian Fit Δm_t (GeV/c^2)	Gaussian Ideo Δm_t (GeV/c^2)	Full Scan Ideo Δm_t (GeV/c^2)	Full Scan Ideo Δm_t (GeV/c^2)
Pile-Up	1.9	1.4	1.2	1.2
Underlying Event	1.0	0.7	0.5	0.5
Jet Energy Scale (light)	2.4	0.1	0.1	0.1
Jet Energy Scale (heavy)	1.4	1.3	1.2	1.2
Radiation (pQCD)	0.8	0.3	0.2	0.2
Fragmentation	0.4	0.4	0.3	0.3
b-tagging	2.0	0.5	0.3	0.3
Background (∗)	0.4	0.4	0.4	0.4
Parton Density Functions	0.1	0.1	0.1	0.1
Total Syst. uncertainty	4.9	2.3	1.9	1.9
Stat. Uncertainty (10fb^{-1})	0.32	0.36	0.21	0.31
Total Uncertainty	4.9	2.3	1.9	1.9

Table 25. Overview of all uncertainty components for the top quark mass estimators described in the text. When the component is marked with (∗) the statistical uncertainty dominated the systematic shift of the effect.

underlying event and to a smaller extend due to systematic fluctuations in the pile-up. The main effect of the pile-up collisions is on the energy scale of the reconstructed jets, which will be measured with dedicated analyses performed on data. Therefore the largest part of this systematic uncertainty on the top quark mass overlaps with the uncertainty quoted from the jet energy scale. The effect of the description of the underlying event on each of the top quark estimators is mentioned in Table 25 and is small but not negligible. In Table 25 a 3σ effect on the most important parameter in the tuning of the underlying event description is accounted for, hence conservative. Our understanding of the underlying event model can be considered (and certainly in the future when new tuning data becomes available) as being better with a factor of two. In Table 26 the systematic uncertainty on the top quark mass due to the underlying event description is therefore reduced with a factor of two.

It is believed that the magnitude of pile-up collisions can be monitored to the level of 10%. This reduces the uncertainties quoted in Table 25 with a factor of 3. For example for the $\hat{M}_t^{\mathrm{FullIdeo}}$ estimator the pile-up effect can be extrapolated to 0.42 GeV/c^2 which overlaps with the uncertainty due to the jet energy scale knowledge. To take into account this overlap, the systematic shift in the top quark mass estimators due to a 10% variation in the pile-up collisions is divided by two, hence 0.21 GeV/c^2 for the $\hat{M}_t^{\mathrm{FullIdeo}}$ estimator.

The uncertainty on the energy scale of b-quark jets is taken to be 2% in Table 25. This energy scale can be calculated either from independent event samples like $Zb\bar{b}$ or can be determined as a ratio with respect to the energy scale of light quark jets. This number can be extrapolated to about 1.5% upon a better understanding of the detector performance and with the application of advanced tools like energy flow algorithms. Also the worse understood regions in the detector could rejected for the measurement of the top quark mass. For example for the $\hat{M}_t^{\mathrm{FullIdeo}}$ estimator the effect of a 1.5% uncertainty on the jet energy scale is 0.96 GeV/c^2 which is a linear combination of the effect on light and heavy quark jets.
In Table 25 for the b-tagging performance a 5% uncertainty is taken on the b-tag efficiency dominated by systematic uncertainties of radiation effects. The experience at the Tevatron collider [33] illustrates that an uncertainty of 2% could be reached. Therefore the uncertainties on the top quark mass estimators can be rescaled to match this precision. For example for the $\hat{M}_t^{\mathrm{FullIdeo}}$ estimator the effect of the b-tagging uncertainty becomes 0.18 GeV/c^2.
The systematic effect determined on the top quark mass estimators due to the remaining background (20% variation) is dominated by its statistical precision. All of the 6 shifts in Table 23 deviate from zero by no more than 1 standard deviation. It is therefore assumed that the real effect, extrapolated to larger simulated event samples, is half of this statistical precision. For example for the $\hat{M}_t^{\mathrm{FullIdeo}}$ estimator the effect of the background becomes 0.25 GeV/c^2.
Table 26 summarizes and combines the extrapolated systematic uncertainties on each of the top quark mass estimators. The uncertainty on the inferred top quark mass of about 1 GeV/c^2 is dominated by the uncertainty on the energy scale of the b-quark jets. This relative uncertainty is taken to be 1.5% which is feasible by selecting only events which have their leading jets in a detector region which is better understood, usually the central or barrel region of the detector. Also in this central region the contributions from underlying event and pile-up are smaller compared to the more forward regions. The inclusive jet energy scale and its resolution can be improved by applying more advanced reconstruction tools as for example energy or particle flow algorithms connecting the calorimeter information with the information provided by the central tracker device. An uncertainty of 1.5% on the b-quark jet energy scale can therefore be set as a goal for the performance of jet calibration methods.

3.4.7. Conclusion The reconstruction and selection of semi-leptonic $t\bar{t}$ events is described for the decay channel where the lepton is a muon. The event selection reaches a high signal-to-noise ratio and the background from non-$t\bar{t}$ processes is neglegible. A kinematic fit is applied to force the reconstructed W boson mass into the event to its precise measured value, resulting in improved resolutions of the four-momentum of the jets. Remaining $t\bar{t}$ events from other decay channels are reduced by a likelihood ratio method combining the information of three sensitive observables. The correct

	Standard Selection			Altern. Selection
	Gaussian Fit Δm_t (GeV/c^2)	Gaussian Ideo Δm_t (GeV/c^2)	Full Scan Ideo Δm_t (GeV/c^2)	Full Scan Ideo Δm_t (GeV/c^2)
Pile-Up	0.32	0.23	0.21	0.21
Underlying Event	0.50	0.35	0.25	0.25
Jet Energy Scale (light)	1.80	0.15	0.06	0.06
Jet Energy Scale (heavy)	1.05	0.98	0.90	0.90
Radiation (pQCD)	0.80	0.27	0.22	0.20
Fragmentation	0.40	0.40	0.30	0.30
b-tagging	0.80	0.20	0.18	0.18
Background	0.30	0.25	0.25	0.25
Parton Density Functions	0.12	0.10	0.08	0.10
Total Syst. uncertainty	3.21	1.27	1.13	1.07
Stat. Uncertainty (10fb^{-1})	0.32	0.36	0.21	0.31
Total Uncertainty	3.23	1.32	1.15	1.11

Table 26. Overview of all uncertainty components for the top quark mass estimators, extrapolated to a better understanding of both the proton collisions at the LHC and the detector performance.

jet combination is choosen according to another likelihood ratio method combining the information of several topological observables which can differentiate the correct from the wrong combinations. Three different top quark mass estimators are constructed: a simple fit on the reconstructed top quark mass spectrum and two event-by-event likelihood methods which convolute the resolution function of the event or so-called ideogram with the expected theoretical template. In the theoretical template used in the convolution several event weights are applied according to the likelihood of having the correct $t\bar{t}$ decay channel and the correct jet combination. The properties of each of the three estimators are studied. The results indicate a slope of unity between the generated and estimated top quark mass, a unit width of the pull distribution and a small bias. The improvement of the convolution techniques with respect to the fit on the reconstructed top quark mass spectrum is shown to be significant.

The effect on the estimated top quark mass from all relevant systematic uncertainties is estimated for each of the three estimators. Again a clear improvement is demonstrated by applying the event-by-event convolution methods including a kinematic fit with respect to the simple approach of fitting the reconstructed top quark mass spectrum. Measuring the top quark mass at the LHC with an uncertainty below 2 GeV/c^2 is feasible. Aiming for an uncertainty below 1 GeV/c^2 remains challenging, but after a better understanding of mostly the jet energy scale of b-quark jets and the invent of more advanced analysis tools still feasible. Benchmarks or goals for the performance

of jet calibration tools are set. An uncertainty of 1.5% on the jet energy scale of b-quark jets should be obtained in part of the detector range to measure the top quark mass with a precision of about 1 GeV/c^2.

Apart from the theoretical uncertainties which are conservatively estimated in this note, the most important systematical uncertainties are the uncertainty on the b-jet energy scale and the influence of pile-up collisions. With the reconstructed tools and statistical inference methods applied in this note a significant reduction of the uncertainty on the top quark mass is obtained compared to simple top quark mass estimators.

Constraining the analysis to events for which the three main jet clustering algorithms give comparable results for the direction of the four leading jets, a small but not significant improvement is observed on the total uncertainty on the inferred top quark mass.

4. Fully Hadronic Channel

The fully hadronic decay channel denotes the case where the two W bosons from the decaying top quarks, decay both in a quark and anti-quark pair. This branching ratio is about equal to the branching ratio of the semi-leptonic decay channel. The final state is characterized by the nominal six-jets topology $t\bar{t} \to WW\mathrm{b\bar{b}} \to qqqq\mathrm{b\bar{b}}$ and has the largest branching fraction (46%), and kinematics that can be fully reconstructed. However, this channel is affected by a large background from QCD multi-jet production, which makes the isolation of the signal rather challenging. Improvements in the signal-to-background ratio are possible by requiring the presence of b-quark jets and by selecting central and very high-energy kinematic configurations which are expected for jets arising from the decay of a massive object like the top quark. A specific multi-jet trigger that uses b-tagging information has been devised for this analysis and an optimized selection has been applied.

4.1. Simulation

For the analysis described, event samples generated with PYTHIA 6.2 have been used. The signal consists of 500k inclusive $t\bar{t}$ events, from which a subsample of 230k million fully hadronic $t\bar{t}$ events is extracted. The background consists of 1500k QCD multi-jet events generated with $50 < \hat{p_{\mathrm{T}}} < 470$ GeV/c, where the $\hat{p_{\mathrm{T}}}$ symbol indicates the transverse momentum of the most energetic parton of the hard scattering before the final-state radiation processes. The full $\texttt{GEANT} - 4$ detector simulation is equal to the one described in Section 3.1 and contains pile-up collisions from minimum bias events according to the low-luminosity settings of the LHC.

4.2. Reconstruction and selection

The trigger preselection uses the inclusive jet trigger envisaged in [22], which considers multi-jets with different E_{T} thresholds depending on the number of jets, up to 4 jets, and a special inclusive b-jet trigger [24], implemented according to the following criteria:

- Level-2: jet reconstruction with the following minimal E_{T} thresholds:
  1-jet or 2-jet events: 350 GeV E_{T} for highest-E_{T} jet
  3-jet events: all 3 jest with at least 150 GeV E_{T}
  4-jet events: all 4 jets with at least 55 GeV E_{T}
- Level-2.5: b-tagging based on fast pixel track and vertex reconstruction as ingredients, on the two most energetic jets requiring 2 tracks with impact parameter significance exceeding 2σ;
- Level-3: b-tagging based on regional full track reconstruction and same vertex reconstruction as ingredients, on the two most energetic jets requiring 3 tracks with impact parameter significance exceeding 2.5σ.

The jets are reconstructed with an iterative cone algorithm with a fixed cone size of 0.5 and are calibrated using γ+jet events. The b-tagging algorithm is based on the impact parameters of charged particle tracks and exploits the lifetime properties of weakly-decaying b-hadrons.

The trigger requires either multiple jets in the event (n-jet) or a b-tagged jet among the two highest-E_{T} jets (b-jet). The rates and the effective cross sections, respectively for the QCD and $t\bar{t}$ fully hadronic events, at the production and at the different levels of the trigger preselection, are given in Tab. 27. The signal efficiencies are also reported. The b-jet stream significantly improves the efficiency of the inclusive jets stream for fully hadronic final states (15%).

After the trigger preselection the QCD rate is reduced to 23 Hz, the signal efficiency is 16.8% and the signal to background ratio, S/B, amounts to 1/300.

The $t\bar{t}$ fully hadronic efficiency (factorizing out the trigger efficiency) and the QCD rate are shown in Fig. 39 as a function of the jet transverse energy cut for different values of the minimum number of jets considered. A discriminant selection is needed in order to improve the signal to background ratio. Different choices on the minimum number of jets and jet transverse energy are possible as shown in the figures.

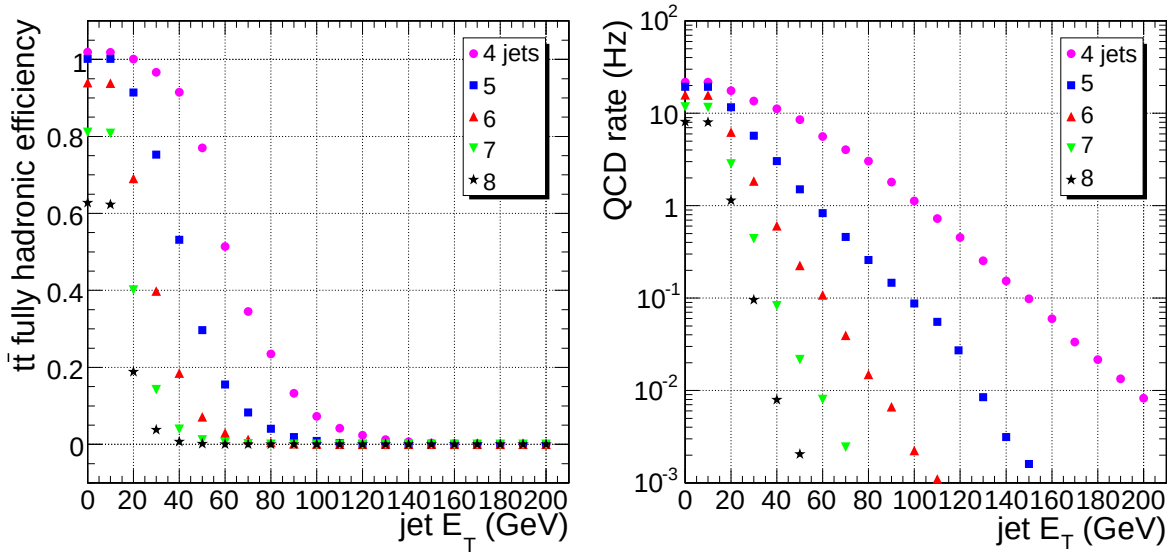

Figure 39. $t\bar{t}$ fully hadronic efficiency (left) and QCD rate (right) as a function of jet transverse energy for different values of the minimum number of jets considered, after the trigger preselection.

The optimal selection is based on the best statistical significance of the signal achievable, defined as $S/\sqrt{S+B}$, for an integrated luminosity of $\mathcal{L} = 1$ fb^{-1}.

The first step of the selection requires a topology of $6 \leq N_{jet} \leq 8$, consistent with the basic physical process considered and taking into account possible additional jets from final state radiation. For a jet to be counted, the jet pseudorapidity must satisfy $|\eta| < 2.4$ and its transverse energy must be greater than 30 GeV. The effective cross

Channel	QCD $50 < \hat{p_{\mathrm{T}}} < 470$ GeV/c				
	Production	Level-1	HLT		
			b-jet	n-jet	n-jet + b-jet
Rate [Hz]	49k	3.3k	19.4	6.3	**23.2**
$\sigma\epsilon$ [pb]	25M	1.7M	9.7k	3.2k	**11600**

(a)

Channel	$t\bar{t} \to qqqq\mathrm{b\bar{b}}$				
	Production	Level-1	HLT		
			b-jet	n-jet	n-jet + b-jet
Rate [Hz]	0.45	0.26	0.07	0.02	**0.08**
$\sigma\epsilon$ [pb]	225	130	34	10	**38**
Efficiency (%)	100	57.2	14.9	4.4	**16.8**

(b)

Channel	Rate [Hz]				
QCD $\hat{p_T}$	Production	Level-1	HLT		
			b-jet	n-jet	n-jet + b-jet
50 ÷ 80	42 k	2 k	0	0	0
80 ÷ 120	5.9 k	752	1.6	0.2	1.8
120 ÷ 170	1 k	372	4.0	0.7	4.5
170 ÷ 230	202	141	4.3	1.6	5.4
230 ÷ 300	47.7	44.3	3.5	1.8	4.6
300 ÷ 380	12.8	12.7	3.8	1.3	4.4
380 ÷ 470	3.8	3.8	2.2	0.7	2.5

(c)

Table 27. QCD rates and effective cross-sections (a) and $t\bar{t}$ fully hadronic rates, effective cross-sections and efficiencies (b), at production level and at different levels of trigger preselection (Level-1, HLT b-jet stream, n-jet stream and n-jet-or-b-jet). Details on single QCD $\hat{p_T}$ rates are also given in (c).

section of $t\bar{t}$ and QCD events for minimum jet transverse energy of $E_{\mathrm{T}} > 30$ GeV is represented in Fig. 40 as a function of the number of jets.

Different variables of shape in the phase space, potentially able to separate the signal from the background are then taken into account. The useful variables with the corresponding cuts applied in sequence are:

- centrality, $\mathcal{C} \geq 0.68$, where $\mathcal{C}$ is the fraction of the hard scatter energy going in the transverse plane $\sum E_{\mathrm{T}}/\sqrt{\hat{s}}$. Here, $\hat{s} = (\sum E)^2 - (\sum Pz)^2$, and all sums here and in the following run over the reconstructed jets
- aplanarity, $\mathcal{A} \geq 0.024$, where $\mathcal{A} = \frac{3}{2}Q_1$, Q_1 being the smallest of the three

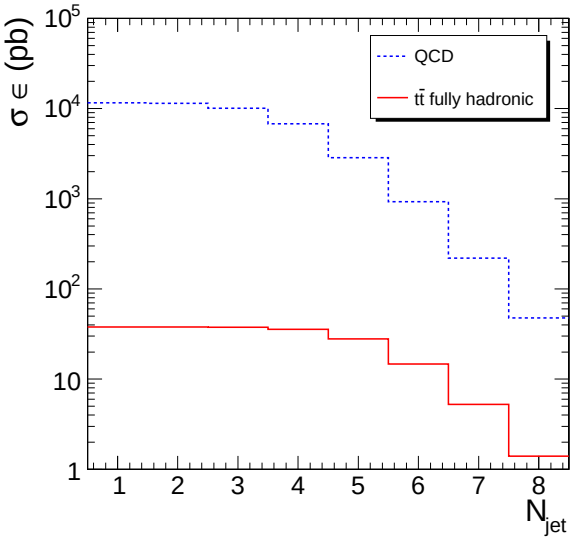

Figure 40. Effective cross section of $t\bar{t}$ and QCD events as a function of the number of jets for a request of minimum jet transverse energy $E_{\mathrm{T}} > 30$ GeV.

normalized eigenvalues of the sphericity tensor $M_{ab} = \sum_j P_{ja} P_{jb}$

- non-leading jet total transverse energy obtained removing the two most energetic jets $\sum E_{\mathrm{T}} - E_{\mathrm{T}}(1) - E_{\mathrm{T}}(2) = \sum_3 E_{\mathrm{T}} \geq 148$ GeV

The distributions of these variables for $t\bar{t}$ and QCD events are shown in Fig. 41.

After the selection a b-tagging is applied to the surviving samples of $t\bar{t}$ all-hadronic and QCD events. Selection criteria of at least one b-jet and of two b-jets are considered.

Table 28 lists the $t\bar{t}$ fully hadronic and QCD effective cross sections, the signal to background ratio, the statistical significance (referred to $\mathcal{L} = 1\ \mathrm{fb}^{-1}$) and the $t\bar{t}$ fully hadronic efficiency at each step of the selection (applied in cascade) starting from values obtained after the trigger preselection. After the selection and b-jet requirement, the signal to background ratio amounts to 1/17 (1/9) respectively for 1 (2) b-tag samples, for a signal efficiency of 3.8% (2.7%) relative to the fully-hadronic $t\bar{t}$ sample.

4.3. Cross section measurement

The signal efficiency relative to the total inclusive $t\bar{t}$ sample, to be used in the calculation of the total $t\bar{t}$ production cross section, becomes 2.3% (1.6%), respectively for the 1 (2) b-tag requirement.

The estimated statistical uncertainty on the cross section is reported in Tab. 29, with the expected number of signal and background events, for an integrated luminosity $\mathcal{L} = 1\ \mathrm{fb}^{-1}$.

In addition to the statistical uncertainties, significant systematic uncertainties on the signal efficiency (fragmentation model, PDF, ISR/FSR, jet energy scale, b-tagging), the expected background, and the integrated luminosity, are expected. The fine-tuning of the optimized selection will be derived considering these uncertainties.

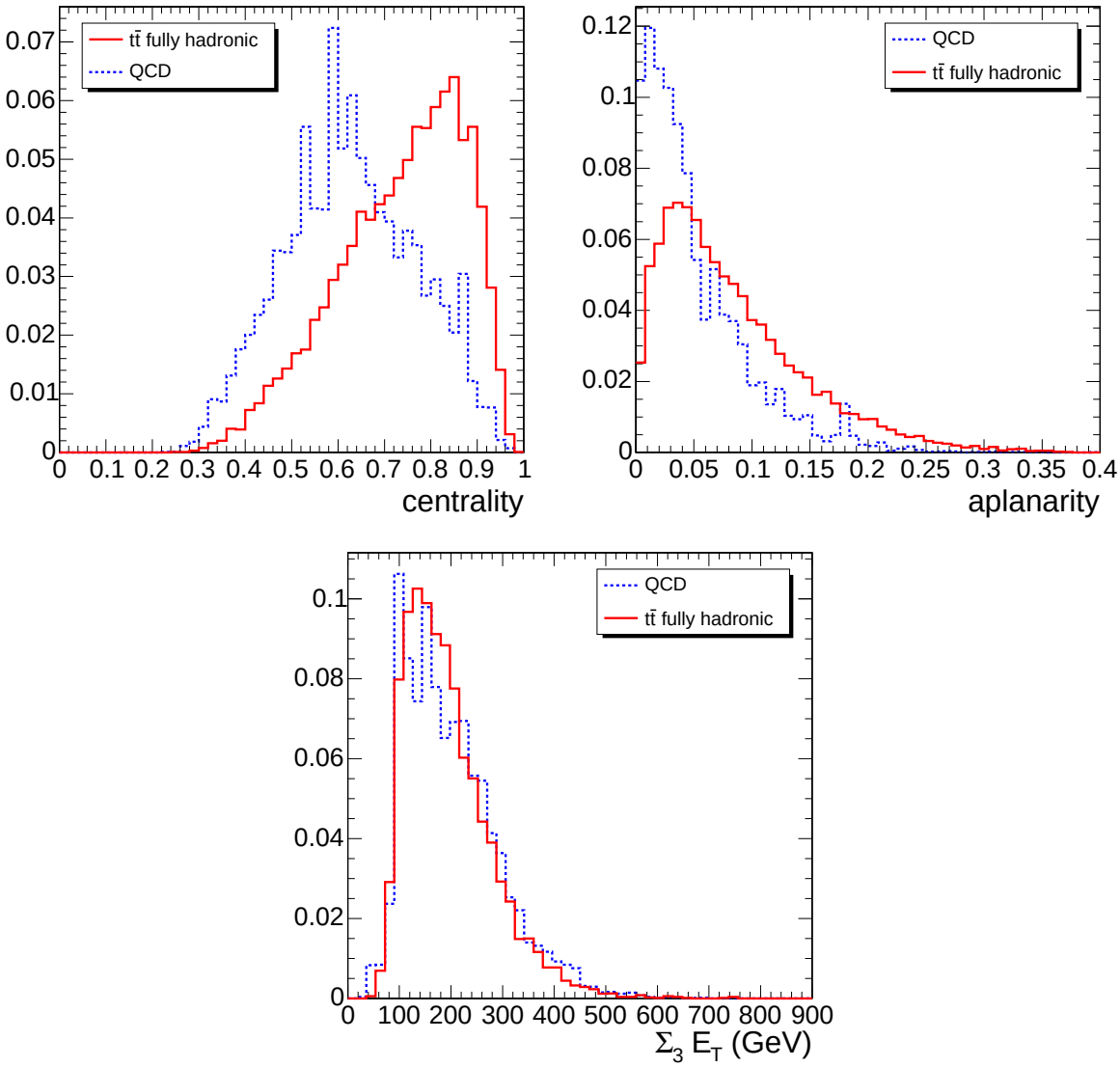

Figure 41. Distributions of centrality (left), aplanarity (right) and $\sum_3 E_T$ (bottom) for $t\bar{t}$ and QCD events (normalized to the same area).

Sources of systematic uncertainty are studied as described in detail in Section 2.2.4. ¿From the experience of CDF and DØ experiments at Tevatron [25], one of the dominating systematic uncertainties arises from the uncertainty on the jet energy scale. This contribution, evaluated according to the functional form given in [26], amounts to about 11.2%.

The systematic uncertainty related with the trigger preselection is calculated considering contributions from b-tagging and jet energy scale. The b-tagging efficiency is measured using two independent triggers, muon and b-jet, applied to inclusive $t\bar{t}$ events, and counting events triggered by single stream and doubles/both stream. This gives a relative uncertainty below to 5%.

Table 30 summarizes the contributions due to the total uncertainty on the cross

Selection	Requirement	$\sigma\epsilon_{t\bar{t}}$ [pb]	$\sigma\epsilon_{QCD}$ [pb]	S/B	$S/\sqrt{S+B}$ ($\mathcal{L} = 1$ fb^{-1})	$\epsilon_{t\bar{t}}$ (%)
Trigger	HLT jet+b-tagging	38	11600	1/300	11.1	16.8
Event	$6 \leq N_{jet} \leq 8$	35	7900	1/225	12.4	15.5
	$E_{\mathrm{T}} \geq 30$ GeV	15	930	1/60	15.4	6.6
	centrality ≥ 0.68	9.9	324	1/33	17.1	4.4
	aplanarity ≥ 0.024	9.0	251	1/28	17.7	4.0
	$\sum_3 E_{\mathrm{T}} \geq 148$ GeV	9.0	229	1/25	18.4	4.0
b-tagging	1 b-tag	8.6	148	**1/17**	21.7	**3.8**
	2 b-tag	6.0	54	**1/9**	24.1	**2.7**

Table 28. Selection steps with the corresponding $t\bar{t}$ and QCD effective cross sections, signal to background ratio, statistical significance achieved and $t\bar{t}$ fully hadronic efficiency.

Requirement	$\mathcal{L} = 1$ fb^{-1}				
	events $t\bar{t}$	events QCD	ϵ (%)	$(\Delta\sigma)_{\mathrm{stat}}$ [pb]	$(\Delta\sigma/\sigma)_{\mathrm{stat}}$ (%)
1 b-tag	11500	148000	**2.3**	**17**	**3.5**
2 b-tag	8000	54000	**1.6**	**15**	**3.0**

Table 29. Number of $t\bar{t}$ and QCD events, $t\bar{t}$ efficiency, absolute and relative statistical uncertainties expected on the cross section measurement for an integrated luminosity of 1 fb^{-1}.

section, which combined lead to a relative uncertainty of:

$$\Delta\sigma/\sigma = 3\% \text{ (stat.)} + 20\% \text{ (syst.)} + 5\% \text{ (luminosity)}$$

4.3.1. Selection based on neural net A more refined selection can be based on a neural net exploiting the same variables considered so far. Such approach is attempted in order to investigate the possibility of improving the S/B ratio and/or the efficiency.

Due to systematics related with the Monte Carlo description of the background, both approaches are considered. The previous selection which will be called "early" selection could represent a more conservative approach for the first LHC analyses.

The neural net used for the analysis is the Multilayer perceptron (MLP) implemented inside ROOT[27] through the class *TMultiLayerPerceptron*. This is a simple feed-forward network with an input layer, some hidden layer and an output layer. In this implementation one single hidden layer with $2n$ nodes, being n the number of input variables, is used. One single output node, which provides a convenient selection variable to cut on, is chosen.

	$\Delta\sigma/\sigma$ (%)
HLT	5.9
Pile Up	10.0
Underlying Event	4.1
Fragmentation	1.9
PDF	4.2
IS/FS Radiation	7.9
Jet Energy Scale	11.2
b-tagging	2.0
Background	5.0
Integrated Luminosity	5.0
Statistical Uncertainty (1 fb^{-1})	3.0

Table 30. Systematic uncertainty contributions to the cross section measurement.

The training is made on subsets of the $t\bar{t}$ and QCD samples containing the same number of events. For this purpose the QCD datasets are weighted using the correspondent effective cross section and merged. The learning method used is the Broyden, Fletcher, Goldfarb, Shanno (BFGS) method. The neural net is then applied on the whole sample of signal ($t\bar{t}$) and background (QCD) events.

Different neural network configurations have been applied and studied starting from events satisfying the topology request of $6 \leq N_{jet} \leq 8$ (jet pseudorapidity $|\eta| < 2.4$). Different cuts on jet transverse energy are considered.

The most effective among the studied neural net configurations is the one referring to the signal and background samples after a cut on jet transverse energy of $E_{\mathrm{T}} > 25$ GeV and consists of 6 input nodes:

- E_{T} 1st jet
- E_{T} 6th jet
- Centrality
- Aplanarity
- $\sum_3 E_{\mathrm{T}}$
- Sphericity

which are the same variables used for the "early" selection, plus the sphericity and transverse energy of the first and 6th jet, where jets are ordered by E_{T}.

The output of the training is shown in Fig. 42. In Fig. 43 a layout of the network, where the thickness of the lines is proportional to the weight, and the difference between background and signal for each input variable are shown.

The output distributions when the neural net is applied to the whole sample of $t\bar{t}$ and QCD events are shown in Fig. 44.

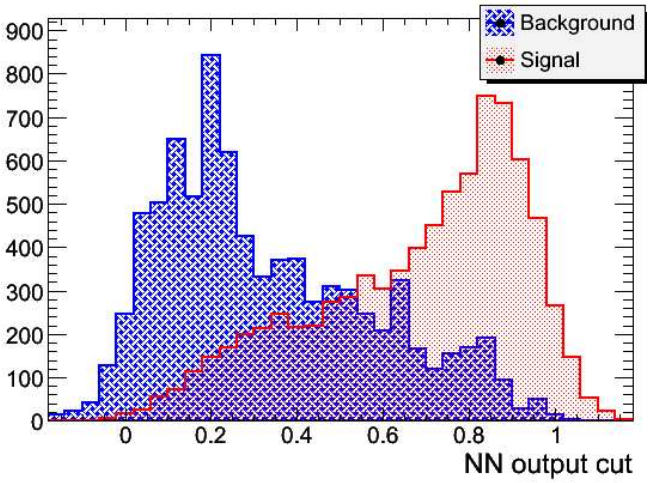

Figure 42. Output of the neural net after the training as evaluated on a "test" sample containing the same number of $t\bar{t}$ and QCD events.

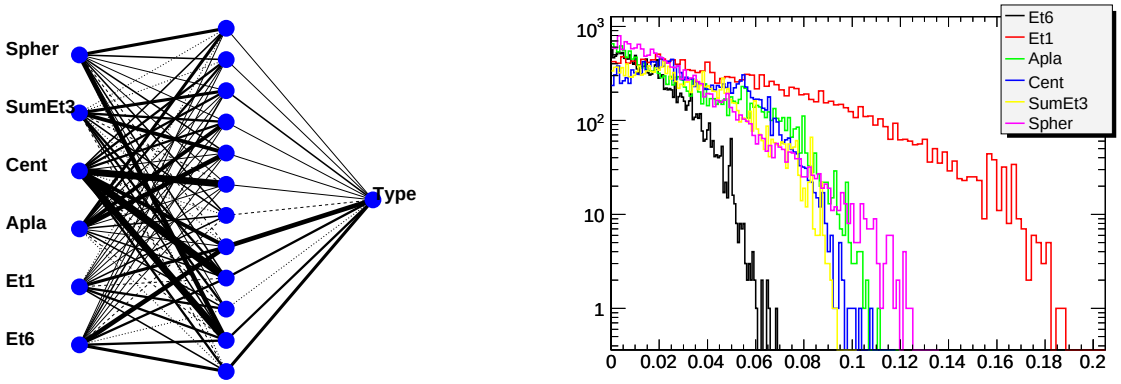

Figure 43. Neural net description (left) where the thickness of the lines is proportional to the weight, and differences between background and signal variables (right) where units on the x-axis are arbitrary.

The performance of the neural net is quantified in Fig. 45. The signal efficiency and the expected S/B ratio as a function of the cut on the neural net output are plotted. Superimposed on the plots are the values corresponding to the "early" selection.

In Fig. 46 instead the S/B ratio as a function of the $t\bar{t}$ efficiency is reported. The superimposed point is the value corresponding to the "early" selection. With respect to the "early" selection, the request for a neural net output ≥ 0.77 improves the S/B ratio from 1/25 to 1/10 with same effciency (i.e. 4%).

As done after the "early" selection, a b-tagging is applied to the surviving samples of $t\bar{t}$ all-hadronic and QCD events. Selection criteria requiring at least one b-jet or two b-jets are considered.

Table 31 lists the $t\bar{t}$ fully hadronic and QCD effective cross sections, the signal to background ratio, the statistical significance (referred to $\mathcal{L} = 1\,\mathrm{fb}^{-1}$) and the $t\bar{t}$ fully hadronic efficiency at each step of the selection (applied in cascade) starting from values

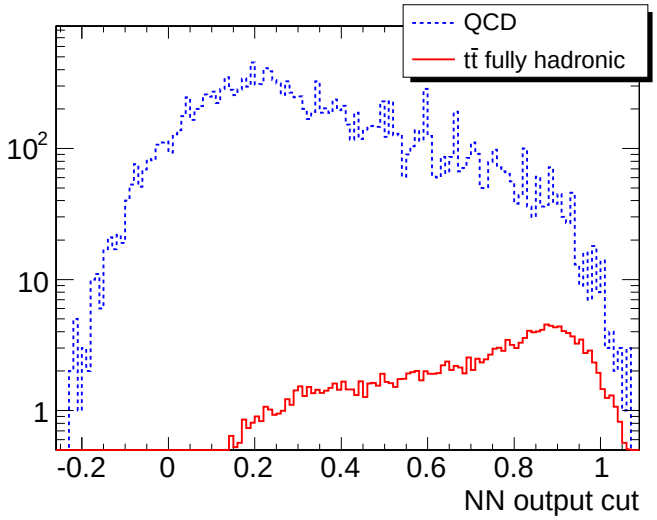

Figure 44. Output of the neural net on the whole sample of $t\bar{t}$ and QCD events. The distributions are normalized to the effective cross section.

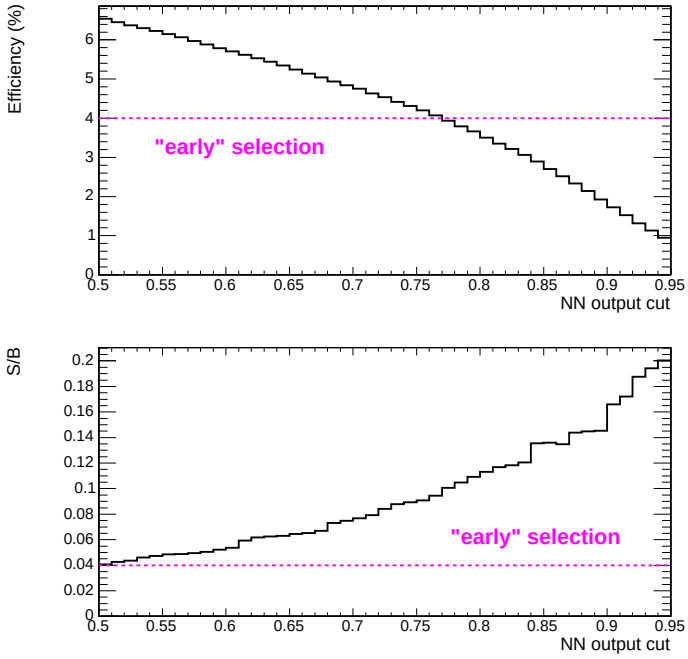

Figure 45. Signal efficiency (top) and S/B ratio (bottom) as a function of the NN output cut. Also shown (dashed lines) are the values for "early" selection.

obtained after the trigger preselection. The "early" selection cuts are replaced by the neural net. After b-jet requirement, the signal to background ratio amounts to 1/7 (1/3) respectively for 1 (2) b-tag samples, for a signal efficiency of 3.8% (2.7%) relative to the fully-hadronic $t\bar{t}$ sample.

The signal efficiency relative to the total inclusive $t\bar{t}$ sample, to be used in the calculation of the total $t\bar{t}$ production cross section, becomes 2.3% (1.6%), respectively

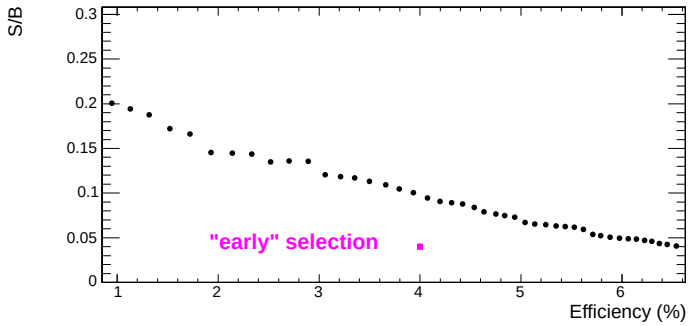

Figure 46. S/B ratio as a function of $t\bar{t}$ efficiency. Also shown (square) is the the values for "early" selection.

Selection	Requirement	$\sigma\epsilon_{t\bar{t}}$ [pb]	$\sigma\epsilon_{QCD}$ [pb]	S/B	$S/\sqrt{S+B}$ ($\mathcal{L} = 1$ fb^{-1})	$\epsilon_{t\bar{t}}$ (%)
Trigger	HLT jet+b-tagging	38	11600	1/300	11.1	16.8
Event	$6 \leq N_{jet} \leq 8$	35	7900	1/225	12.4	15.5
	$E_{\mathrm{T}} \geq 25$ GeV	20	1650	1/80	15.5	8.7
	neural net	9.0	91	1/10	28.5	4.0
b-tagging	1 b-tag	8.6	61	**1/7**	32.6	**3.8**
	2 b-tag	6.0	20	**1/3**	37.2	**2.7**

Table 31. Selection steps with the corresponding $t\bar{t}$ and QCD effective cross sections, signal to background ratio, statistical significance achieved and $t\bar{t}$ fully hadronic efficiency.

for the 1 (2) b-tag requirement.

The estimated statistical uncertainty on the cross section is reported in Tab. 32, with the expected number of signal and background events, for an integrated luminosity $\mathcal{L} = 1$ fb^{-1}.

Requirement	$\mathcal{L} = 1$ fb^{-1}				
	events $t\bar{t}$	events QCD	ϵ (%)	$(\Delta\sigma)_{\mathrm{stat}}$ [pb]	$(\Delta\sigma/\sigma)_{\mathrm{stat}}$ (%)
1 b-tag	11500	61000	**2.3**	**12**	**2.3**
2 b-tag	8000	20000	**1.6**	**10**	**2.0**

Table 32. Number of $t\bar{t}$ and QCD events, $t\bar{t}$ efficiency, absolute and relative statistical uncertainties expected on the cross section measurement for an integrated luminosity of 1 fb^{-1}.

4.4. Top quark mass measurement

The sample selected with the cuts described in Section 4.2, including the demand for two b-tags, represents the starting point for a kinematic top-mass reconstruction in fully hadronic events. Applying an additional cut of the form 100 GeV/c < p_{T} < 300 GeV/c on the two leading jets, whose distributions are shown in Fig. 47, affects the signal purity only minimally but is effective against the intrinsic backgrounds of the selected signal events. These backgrounds stem from mis-reconstructed events according to the jet-parton-matching, see Section 4.4.1, and from combinatorial background, described in Section 4.4.2.

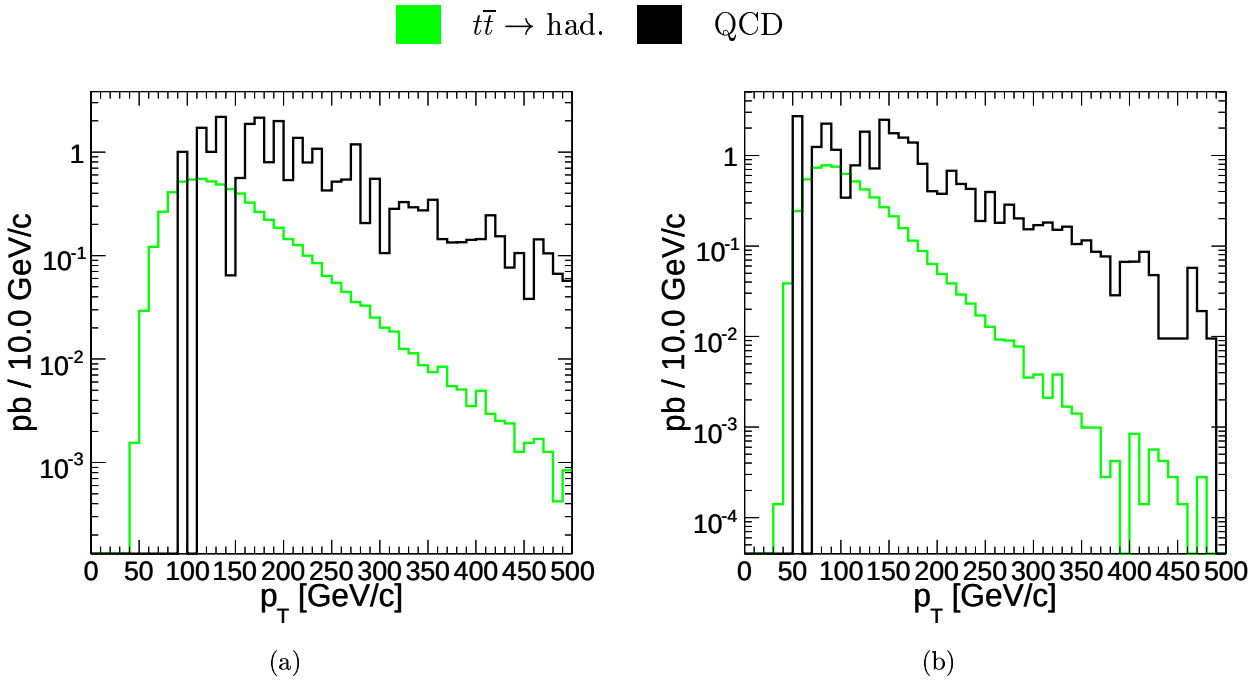

Figure 47. p_{T}-distributions for selected signal and background events (a) for leading and (b) second-leading jet.

4.4.1. Jet-parton-matching The six partons in $pp \rightarrow t\bar{t} \rightarrow bW^+\bar{b}W^- \rightarrow bq_1\bar{q}_1'\bar{b}q_2\bar{q}_2'$ are matched to six reconstructed jets by picking the matching which minimises the sum of the angular separation between reconstructed jet and matched parton. Only jets satisfying our selection requirements, $p_{\mathrm{T}} > 30$ GeV/c and $|\eta| < 2.4$, are taken into account in the matching process. The resulting angular sums are shown in Figs. 48(a) and 48(b), using already the following definition of three disjunct classes of signal events:

- good jet-parton-matching: Each of the six partons and jets differ only by 15° and the jet-reconstructed tops also differ only by 15° from their corresponding parton-level direction.
- half-good jet-parton-matching: Three of the partons and jets forming one top differ only by 15° and this jet-reconstructed top also differs only by 15° from his

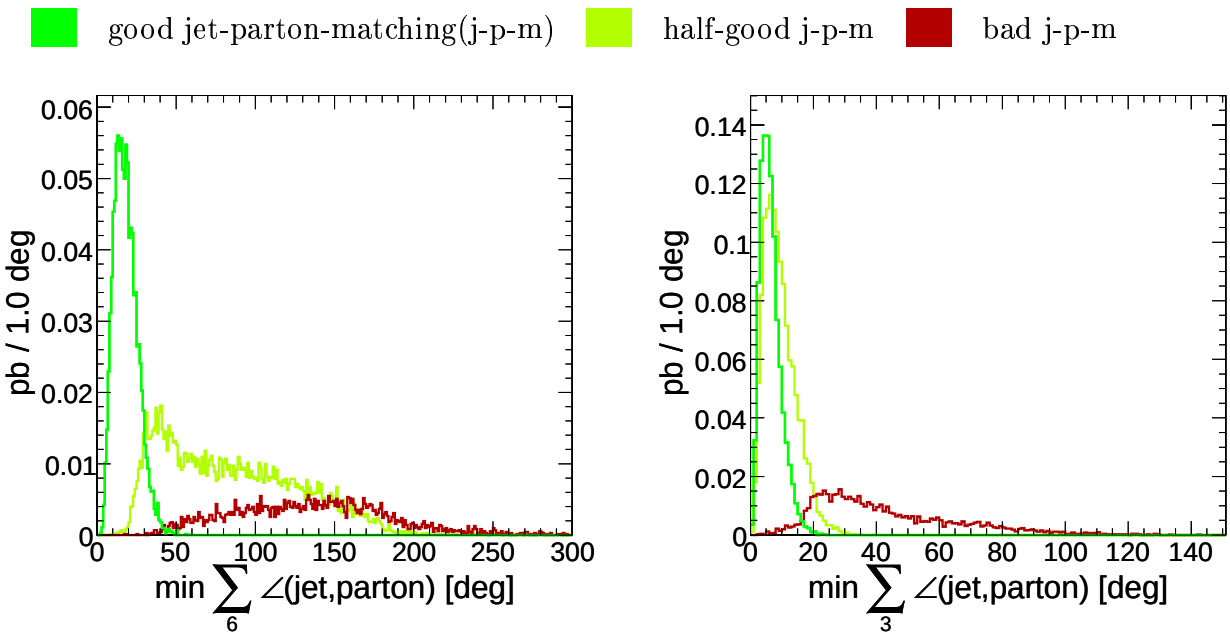

(a) (b)

Figure 48. Jet-parton-matching quality plots for the three classes of signal events discussed in the text: (a) minimal space-angle sum for both tops and (b) minimal space-angle sum for the best matched of the two tops.

corresponding parton-level direction.

- bad jet-parton-matching: Everything else.

The value of 15° is somewhat arbitrary, but Fig. 48(a) shows a distribution well below $6 \cdot 15° = 90°$ for the good jet-parton-matching, confirming a separate observation that usually at most one matched jet exhibits a high angular separation from its parton.

The origin of the mismatches can be traced to parton-level properties, shown in Fig. 49. Badly matched jet-parton events often contain high $|\eta|(> 2.4)$ and low $p_{\mathrm{T}}(< 20\ \mathrm{GeV}/c)$ partons, see Figs. 49(b) and 49(d) respectively, thus a corresponding jet falls probably outside our jet-defintion. The energy in a cone of $R = 0.2$ around a parton normalised to the energy of the parton, plotted in Fig. 49(f), indicates also hard gluon radiation, which once again the fully and partially mismatched events exhibit strongly, resulting again in a difficult jet-reconstruction.

The first class, which amounts to 36% of all selected signal events, are the most sensitive to the top-mass estimation, while the second class, those with half-good matched jet-partons, will be salvaged by trying to choose the well-reconstructed top, since it represents 45% of all selected signal events.

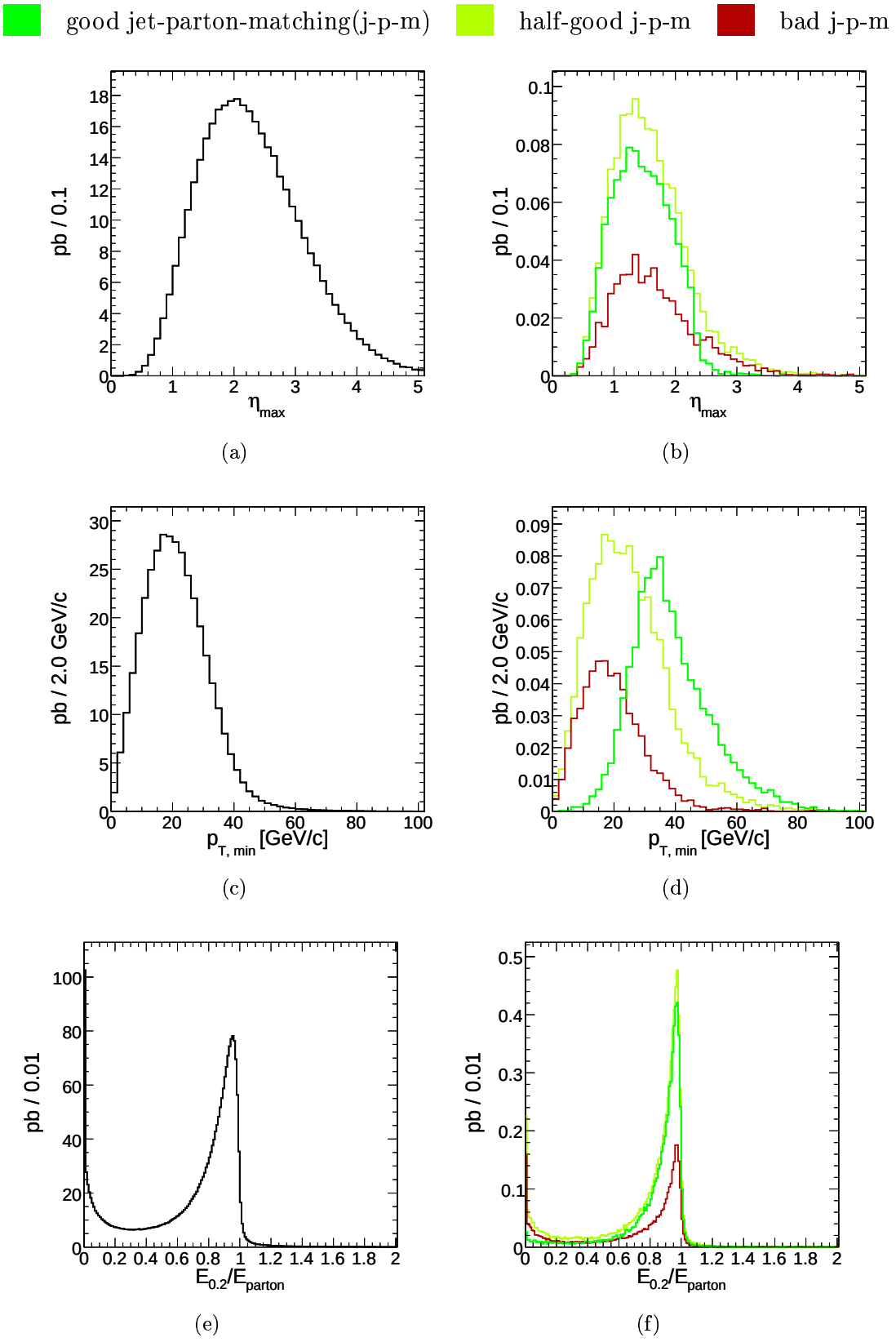

Figure 49. Parton-level properties of the six quarks in $pp \to t\bar{t} \to bW^+\bar{b}W^- \to bq_1\bar{q}_1'\bar{b}q_2\bar{q}_2'$, on the left for all hadronic $t\bar{t}$ events and on the right for the selected ones accordingly divided in the three matching classes. (a), (b): maximal $|\eta|$ of the six quarks. (c), (d): minimal p_T of the six quarks. (e), (f): energy in a cone of $R = 0.2$ around each parton normalized to the energy of the parton.

4.4.2. Jet-pairing There are 10 pairings to combine 6 jets into 2 unique top vectors, as visualised in Fig. 50. On the one hand, the number of pairings decreases to 6, if both b-jets are known and used. On the other hand, the number of pairings increases by a factor of $\binom{n}{6}$ for n reconstructed jets and based on the selection $6 \leq n \leq 8$ can occur and is taken into account.

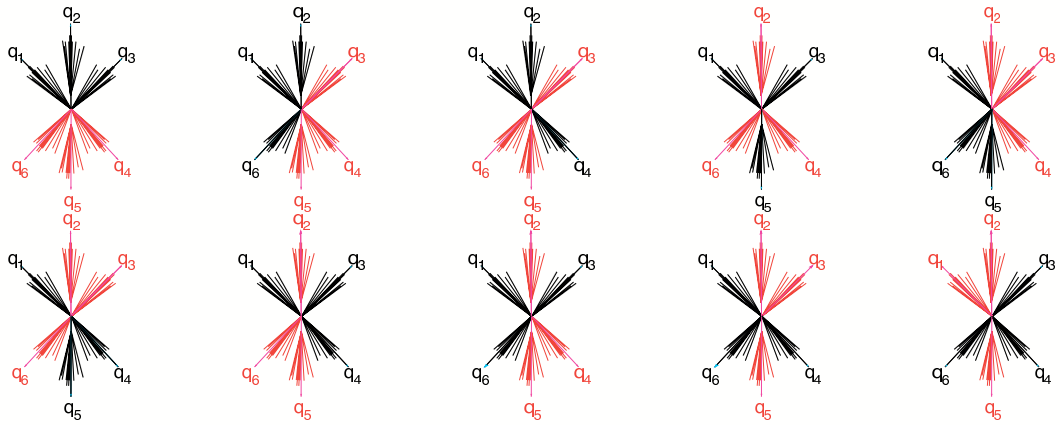

Figure 50. 10 pairings to combine 6 jets into 2 unique top vectors.

	reconstruction	pairing	[pb]
$t\bar{t} \rightarrow$ had.	good	correct	0.62 (35%)
		wrong	0.26 (14%)
	half-good	correct	0.46 (25%)
		wrong	0.26 (15%)
	bad	always wrong	0.20 (11%)

Table 33. Distribution of the different signal event classses after imposing the pairing that gives the maximal output of the likelihood pairing function and discarding events with values smaller than 0.99.

In order to perform the correct jet-pairing, a likelihood variable is constructed from the following event observables:

a) average of the W-candidates' masses
b) difference of the W-candidates' masses
c) sum of the W-candidates' jet-angles $\angle(\mathrm{q}_1\bar{\mathrm{q}}_1') + \angle(\mathrm{q}_2\bar{\mathrm{q}}_2')$
d) difference of the top-candidates' masses
e) sum of the top-candidates' jet-angles $(\angle(\mathrm{bq}_1) + \angle(\mathrm{b}\bar{\mathrm{q}}_1') + \angle(\mathrm{q}_1\bar{\mathrm{q}}_1')) + \left(\angle(\bar{\mathrm{b}}\mathrm{q}_2) + \angle(\bar{\mathrm{b}}\bar{\mathrm{q}}_2') + \angle(\mathrm{q}_2\bar{\mathrm{q}}_2')\right)$
f) angle between the top-candidates

The distributions of these inputs for the likelihood pairing function are shown in Fig. 51 and are based on the selected signal events with good jet-parton-matching. The resulting likelihood variable discriminates nicely between correct and wrong pairings, as can be seen in Fig. 52.

Taking for each event the pairing with the highest likelihood value results in the distribution shown in Fig. 53, and after cutting on this output at a value of 0.99 one gets the pairing efficiencies detailed in Tab. 33. Out of the defined three reconstruction classes, the additional differentiation between correct and wrong pairing is only applicable to the good and half-good reconstructed events, resulting in five event classes.

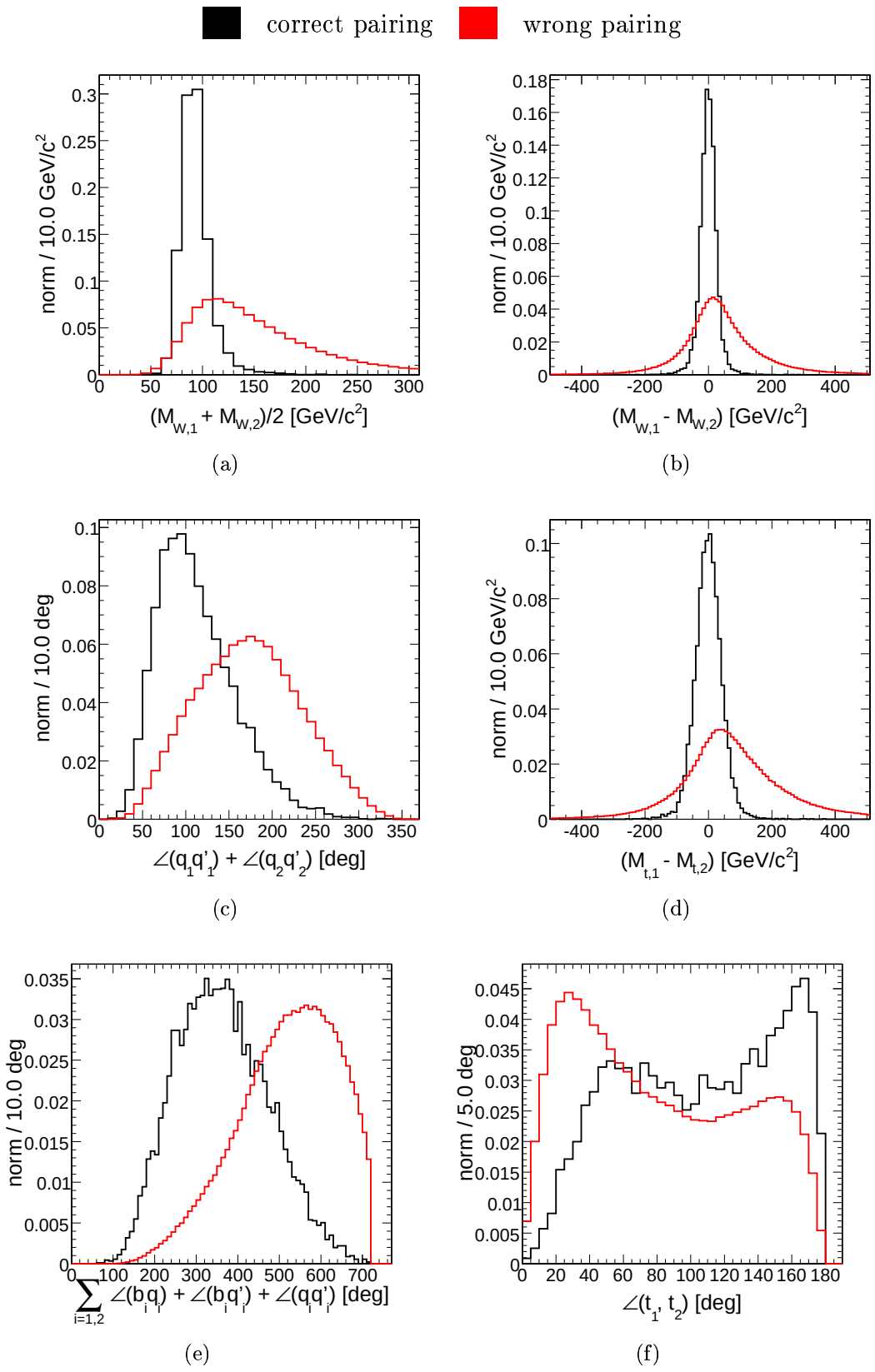

Figure 51. Inputs for the likelihood pairing function: (a) average of the W-candidates' masses, (b) difference of the W-candidates' masses, (c) sum of the W-candidates' jet-angles $\angle(q_1\bar{q}'_1) + \angle(q_2\bar{q}'_2)$, (d) differences of the top-candidates' masses, (e) sum of the top-candidates' jet-angles $(\angle(bq_1) + \angle(b\bar{q}'_1) + \angle(q_1\bar{q}'_1)) + (\angle(\bar{b}q_2) + \angle(\bar{b}\bar{q}'_2) + \angle(q_2\bar{q}'_2))$, (f) angle between the top-candidates.

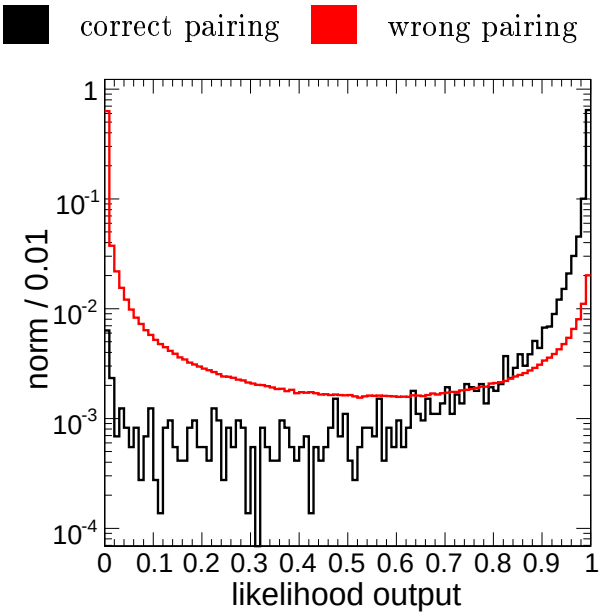

Figure 52. Output of the likelihood pairing function for all pairings.

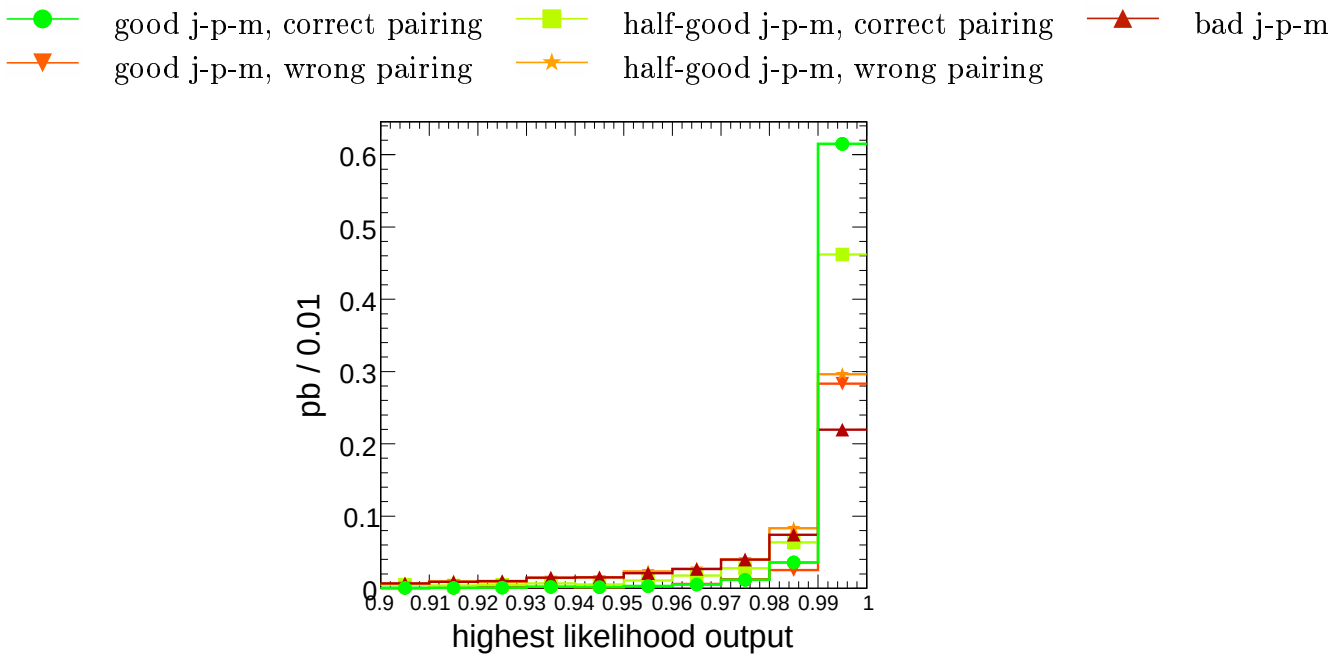

Figure 53. Maximal output value of the likelihood pairing function for all selected signal events divided into their a posteriori five event classes.

4.4.3. Top-choice In order to recover some signal from the intrinsic backgrounds of our selected hadronic $t\bar{t}$ events, only one top is chosen for the kinematic mass determination. Once again a likelihood variable is constructed, this time from the following event observables:

a) top-candidate's smallest jet-p_T from its constituents $b_i, q_i, \bar{q}'_i$

b) top-candidate's enclosed W-mass

c) top-candidate's jet-angles $(\angle(b_i q_i) + \angle(b_i \bar{q}'_i) + \angle(q_i \bar{q}'_i))$

The distributions of these inputs for the top-choice likelihood are shown in Fig. 54 and are based on the selected signal events with half-good jet-parton-matching and correct pairing. The resulting likelihood variable discriminates decently between correct and wrong choice, as can be seen in Fig. 54(d). Taking the top with the higher likelihood output yields a 72% efficiency, far greater than the 50% efficiency of a random choice.

The differentiation of the selected signal events into the now six classes is summarised in Tab. 34, where the six classes are being mapped onto two labels, indicating whether the events are considered signal- or background-like.

	reconstruction	pairing	[pb]	top-choice	[pb]	label
$t\bar{t} \to$ had.	good	correct	0.62 (35%)	always correct	0.62 (35%)	sig.
		wrong	0.26 (14%)	always wrong	0.26 (14%)	bkg.
	half-good	correct	0.46 (25%)	correct	0.33 (18%)	sig.
				wrong	0.13 (7%)	bkg.
		wrong	0.26 (15%)	always wrong	0.26 (15%)	bkg.
	bad	always wrong	0.20 (11%)	always correct	0.20 (11%)	bkg.

Table 34. Distribution of the different signal event classes after jet-pairing and top-choice. The label column indicates whether the class is considered signal- or background-like.

4.4.4. Mass determination With all the pieces in place a kinematic reconstruction of the top quarks is straightforward. The resulting invariant mass distribution of the chosen top, with the paired non-b-jets rescaled such that they yield the W-mass, is shown in Fig. 55(c).

As expected the signal-like events form a narrow peak, while the background-like events, which still contain top-mass information, have a far broader shape. As a comparison, the distribution of the average invariant mass is shown in Fig. 55(d), now with only events coloured as signal-like, where both top quarks are paired correctly. Fitting a Gaussian to the peak of the invariant mass distributions with a fit range corresponding to all bins containing more than 40% of the entries at the maximum, as

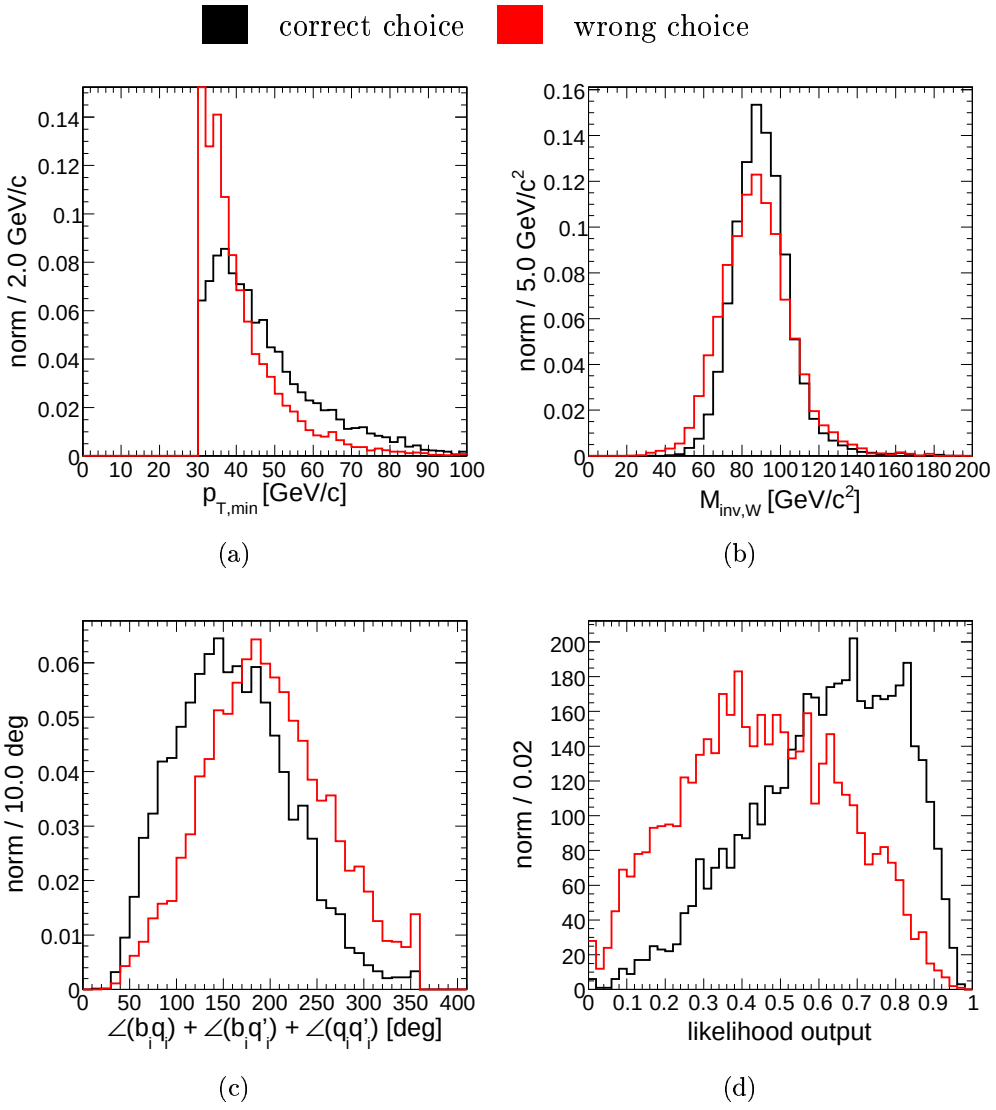

Figure 54. Input for the top-choice likelihood: (a) top-candidate's smallest jet-p_T from its constituents $b_i, q_i, \bar{q}'_i$, (b) top-candidate's enclosed W-mass, (c) top-candidate's jet-angles ($\angle(b_i q_i) + \angle(b_i \bar{q}'_i) + \angle(q_i \bar{q}'_i)$), resulting in the output (d).

shown in Figs. 55(c) and 55(d), serves as a simple mass estimator. Its linearity is shown in Figs. 55(e) and 55(f). The non-averaged mass distribution yields the best linearity, with a slope closer to unity. The deviation is still large enough to demand a correction factor depending on the value of the slope. The extracted top-mass is

$$m_t = 175.0 \pm 0.6\ (\text{stat.}) \pm 4.2\ (\text{syst.})\ \text{GeV}/c^2$$

for an input top-mass of 175 GeV/c^2 and an integrated luminosity $\mathcal{L} = 1\ \text{fb}^{-1}$, and already the statistical error becomes negligible compared to the systematic ones.

The same systematic sources described in detail in Section 2.2.4 have been considered. Their influence on the kinematic top-mass determination with fully hadronic events has been summerised in Tab. 35.

	Δm_t[GeV/c^2]
Pile Up	0.4
Underlying Event	0.6
PDF	1.4
IS/FS Radiation	2.3
Fragmentation	0.9
Jet Energy Scale	2.3
b-Tagging	0.3
Background	2.0

Table 35. Summary of the systematic uncertainties for the top-mass determination with fully hadronic events.

Most of the systematic uncertainties have been estimated according to the suggestions in reference [3]. The pile-up value is derived as the full difference between simulated samples with and without in-time pile-up for the low luminosity $\mathcal{L} = 2\times10^{33}$ cm^{-2} s^{-1} scenario. The jet energy scale is treated according to the functional form given in [26], estimated to be valid for the first $1 - 10$ fb^{-1} of data. For offline b-tagging an uncertainty of 4%(barrel)/5%(endcap) [2] has been investigated.

By far the biggest systematic uncertainty is the QCD background. The signal-to-background ratio in the displayed mass window of Figs. 55(a) and 55(b) is $\sim 2/3$, the QCD background having been further suppressed by the likelihood pairing function cut and by having invariant masses above 350 GeV/c^2. The low number of remaining QCD events, namely 28 events, selected from the full 1.5M events of the official simulated datasets, coupled with the high cross-section scaling factors, lead to the spike structure shown in the figures, and it is hard to quantify the uncertainty at this stage. Further studies with more simluated events will be required to reveal its shape more precisely. Improved selections, like the neural network based one in section 4.3.1, or even completely mass-specific selections should be able to further suppress the QCD background. Experience from CDF at the Tevatron [34, 35] indicates that this uncertainty can be understood at the ~ 2 GeV/c^2 level, when using data for background estimation.

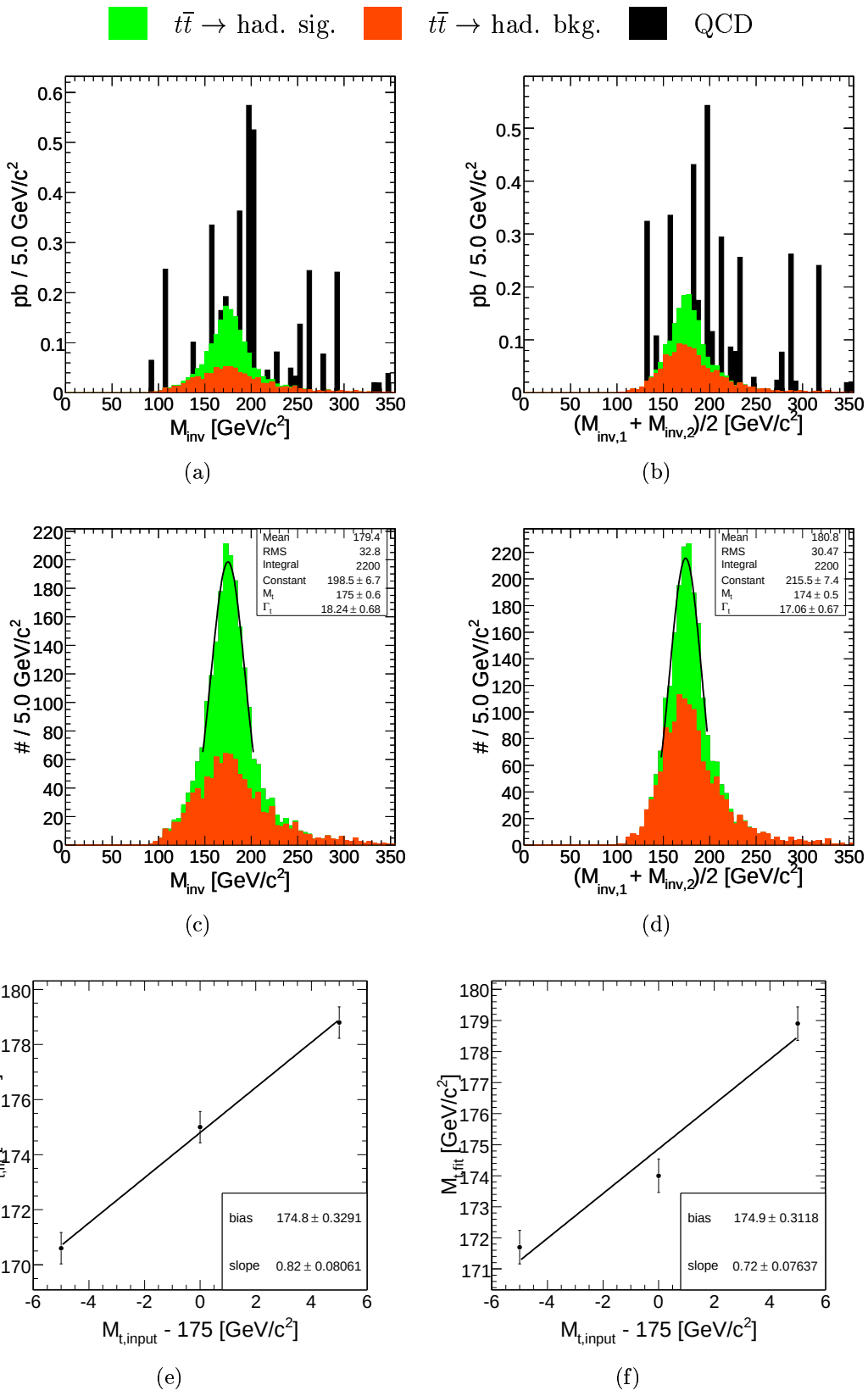

Figure 55. Invariant mass distribution of the reconstructed and rescaled top(s), on the left for the chosen top, and on the right for the average of both tops. (a), (b): for selected background and both signal classes, (c), (d): for both signal classes with Gaussian fit to the peak, (e), (f): linearity of the mass estimator.

5. Summary and Conclusion

The selection of $t\bar{t}$ events with the CMS experiment at the LHC has been presented. In all $t\bar{t}$ decay modes considered, di-lepton, semi-leptonic and fully hadronic, the signal can be established with high significance, allowing to measure the $t\bar{t}$ production cross section with an accuracy of about 10%. The selected event samples allow an accurate determination of the mass of the top quark, at the level of 1 GeV/c^2 accuracy, and set the stage for precision determinations of its other properties.

References

[1] W. Bernreuther, A. Brandenburg, Z. G. Si, P. Uwer, *'Top quark pair production and decay at hadron colliders'*, Nucl.Phys. B690 (2004) 81-137.

[2] C. Weiser. A Combined Secondary Vertex Based B-Tagging Algorithm in CMS. *CMS Note*, 2006/014, 2006.

[3] P. Bartalini, R. Chierici, and A. De Roeck. Guidelines for the Estimation of Theoretical Uncertainties at the LHC. *CMS Note*, 2005-013, 2005.

[4] CMS Collaboration. CMS Physics TDR Volume 1. *CERN/LHCC*, 2006-001, 2006.

[5] S. Gennai et al. Tau jet reconstruction and tagging at High Level Trigger and off-line. *CMS Note*, 2006/028, 2006.

[6] J.Heyninck, J.D'Hondt, S.Lowette, *Top quark mass measurement in single-leptonic $t\bar{t}$ events'*, CMS Note 2006/066.

[7] The D0 Collaboration, *'Measurement of the $t\bar{t}$ cross section in $p\bar{p}$ collisions at $\sqrt{s}$=1.96 TeV using kinematic characteristics of lepton plus jets events'*, Phys. Lett. **B**626 (2005) 45.

[8] T.Sjöstrand, P.Edén, C.Friberg, L.Lönnblad, G.Miu, S.Mrenna and E.Norrbin, *'High-Energy-Physics Event Generation with PYTHIA 6.1'*, Computer Phys. Commun. 135 (2001) 238 (LU TP 00-30, hep-ph/0010017).

[9] S.Agostinelli *et al.*, *'GEANT4: A Simulation Toolkit'*, NIM **A** 506 (2003), 250-303.

[10] CMS webpage of the OSCAR program, Object oriented Simulation for CMS Analysis and Reconstruction, `http://cmsdoc.cern.ch/oscar/` .

[11] CMS webpage of the ORCA program, Object-oriented Reconstruction for CMS Analysis, `http://cmsdoc.cern.ch/orca/` .

[12] CMS webpage of the FAMOS program, CMS Fast Simulation, `http://cmsdoc.cern.ch/famos` .

[13] J.D'Hondt, J.Heyninck, S.Lowette, *'Lepton reconstruction in single-leptonic $t\bar{t}$ events'*, CMS Note 2006-024.

[14] J.D'Hondt *et al.*, *'Fitting of Event Topologies with External Kinematic Constraints in CMS'*, CMS Note 2006-023.

[15] J.D'Hondt, S.Lowette, J.Heyninck, S.Kasselmann, *'Light quark jet energy scale calibration using the W mass constraint in single-leptonic* $t\bar{t}$ *events'*, CMS Note 2006-025.

[16] G.Altarelli and G.Parisi, *'Asymptotic freedom in parton language'*, Nucl.Phys. **B126** (1977) 298.

[17] P.Bartalini, R.Chierici, A.De Roeck, *'Guidelines for the estimation of theoretical uncertainties at the LHC'*, CMS Note 2005-013.

[18] DELPHI Collaboration, *'Tuning and Test of Fragmentation Models Based on Identified Particles and Precision Event Shape Data'*, Zeit. Phys. C73 (1996) 11.

[19] B.Andersson, *'The Lund Model'*, Cambridge University Press (2005).

[20] S.Lowette, J.D'Hondt, J.Heyninck, P.Vanlaer, *'Offline Calibration of b-jet Identification Efficiency'*, CMS Note 2006-013.

[21] G.Altarelli, M.L.Mangano, *'Proceedings of the Workshop on Standard Model Physics (and more) at the LHC'*, CERN Yellow Report 2000-004.

[22] CMS Collaboration. The TriDAS Project Technical Design Report, Volume 2: Data Acquisition and High-Level Trigger. *CERN/LHCC*, 2002-26, 2002. CMS TDR 6.2.

[23] CMS Collaboration, *'The CMS high level trigger'*, Eur. Phys. J. C 46 (2006) 605.

[24] M. Vos and F. Palla. B-tagging in the High Level Trigger. *CMS Note*, 2006/030, 2006.

[25] CDF Collaboration and D0 Collaboration (Daniel Wicke for the collaboration). Top Pair production cross-section measurement in the all-hadronic channel at CDF and D0. *Int. J. Mod. Phys. A*, 20:3183–3186, 2005.

[26] A. et al. Heister. Measurement of Jets with the CMS Detector at the LHC, 2006. CMS Note 2006/036.

[27] R. Brun and F. Rademakers. ROOT - An Object Oriented Data Analysis Framework. In *AIHENP'96 Workshop*, volume Phys. Res. A 389, pages 81–86, Lausanne, Switzerland, September, 1996 1997.

[28] CDF webpage, `http://www-cdf.fnal.gov/physics/new/top/top.html` .

[29] D0 webpage, `http://www-d0.fnal.gov/Run2Physics/WWW/results/top.htm` .

[30] V.Konoplianikov, O.Kodolova, A.Ulyanov, *'Jet Calibration using γ+jet Events in the CMS Detector'*, CMS Note-2006/042.

[31] C. Weiser, *'A Combined Secondary Vertex Based B-Tagging Algorithm in CMS'*, CMS Note 2006/014.

[32] The DELPHI Collaboration, *'Measurement of the Mass and Width of the W Boson in e^+e^- Collisions at $\sqrt{s}$ = 189 GeV'*, Phys. Lett. **B**511 (2001) 159.

[33] The D0 Collaboration, *''*, Phys. Lett. **B**626 (2005) 35.
The CDF Collaboration, *''*, Phys. Rev. **D** 71, 072005.

[34] Abe, F. and others. First observation of the all hadronic decay of t anti-t pairs. *Phys. Rev. Lett.*, 79:1992–1997, 1997.

[35] Group, Tevatron Electroweak Working. Combination of CDF and D0 results on the mass of the top quark. 2006.